Hypoxia-induced *microRNA-210* regulation of kidney development

by

Shelby Lynn Hemker

B.S., Michigan State University, 2014

Submitted to the Graduate Faculty of the

School of Medicine in partial fulfillment

of the requirements for the degree of

Doctor of Philosophy

University of Pittsburgh

2020

UNIVERSITY OF PITTSBURGH

SCHOOL OF MEDICINE

This dissertation was presented

by

Shelby Lynn Hemker

It was defended on

March 2, 2020

and approved by

Sunder Sims-Lucas, PhD, Assistant Professor, Department of Pediatrics

Donna Beer Stolz, PhD, Associate Professor, Department of Cell Biology

Michael Butterworth, PhD, Associate Professor, Department of Cell Biology

Neil Hukriede, PhD, Professor, Department of Developmental Biology

Dissertation Director: Jacqueline Ho, MD, Assistant Professor, Department of Pediatrics

Hypoxia-induced *microRNA-210* regulation of kidney development

Shelby L. Hemker, PhD

University of Pittsburgh, 2020

Intrauterine growth restriction is a common pregnancy complication that is thought to arise from fetal hypoxia and results in reduced nephron number. This decrease in the total amount of nephrons (which are the functional unit of the kidney) increases an affected individual's lifelong risk for developing disease, such as hypertension and chronic kidney disease. However, the mechanisms by which fetal hypoxia affects kidney development are poorly understood. To address this, an unbiased RNA sequencing approach was utilized to identify miRNAs induced by hypoxia during kidney development, of which *miR-210* was identified as the top hypoxia-induced miRNA. To further understand the functional role that *miR-210* plays in regulating kidney development, a transgenic mouse line with a global *miR-210* deletion was investigated. Interestingly, deletion of *miR-210* resulted in a male-specific decrease in nephron number, which appears to be due to a combination of increased expression of lymphoid enhancer-binding factor-1 (an effector of Wingless-related integration site/β-catenin signaling) and caspase-8 associated protein 2 (effector of Fas cell surface death receptor-mediated apoptosis signaling). To understand how deletion of *miR-210* affects kidney development in the setting of fetal hypoxia, embryonic mice were exposed to moderate intrauterine hypoxia. Embryos with the *miR-210* deletion did not exhibit many differences to their wildtype littermates also exposed to hypoxia, except that they may have decreased ureteric bud branching. Further investigation into the mechanisms by which hypoxia-induced *miR-210* impacts kidney development during normal and hypoxic kidney development would expand our understanding of how hypoxic signaling impacts fetal development and risk for developing kidney disease.

Table of Contents

List of Tables

List of Figures

1.0 Introduction

1.1 Kidney disease is linked to low nephron number

1.1.1 Kidney disease is prevalent and debilitating

Chronic kidney disease (CKD) affects about 15% of American adults (1). CKD is defined by five stages of disease progression, each characterized by increasingly reduced kidney function (2). There is no cure and an individual will eventually develop end stage kidney disease (ESKD), at which point the kidneys are non-functional (2). Dialysis and medications can be used to replace kidney function long-term, but kidney transplant is currently the best treatment (3, 4). Unfortunately, kidney transplant still carries significant morbidity with the required long-term immunosuppression (5). In America, about 83% of people on the national organ donor waiting list are waiting for a kidney (the other 17% account for those waiting for all other organs), but only 20% of them receive a kidney transplant (6). As the population continues to age and people are living longer, the number of people on the organ donor wait list is increasing but the number of donors is stagnant (6). In order to address this public health crisis, more needs to be understood about the causes and risk factors of CKD, especially since 90% of those with CKD (particularly in its early stages) are unaware they have it (1).

There are many risk factors for the development of CKD, including diabetes, hypertension, genetic sex, and developmental abnormalities such as low nephron number (2, 7, 8). Hypertension is one of the most common causes of CKD (9) and about 29% of American adults have hypertension (1); thus, a significant portion of our population is at an increased risk for developing CKD. Kidneys play an important role in regulating blood pressure, and inadequate kidney function contributes to the development of hypertension (10-12). Thus, hypertension and CKD and intimately linked in their etiology, making it difficult to study their cause-effect relationship.

Congenital anomalies of the kidney and urinary tract (CAKUT) are one of the most common congenital defects, with an occurrence of 3-6 per 1000 live births (13, 14). CAKUTs comprise a spectrum of malformations that occur in the kidney (e.g. hypoplasia, dysplasia),

collecting system (e.g. hydronephrosis, megaureter), bladder (e.g. ureterocele, vesicoureteral reflux), or urethra (e.g. posterior urethral valves) (15, 16). Many genes have been linked to CAKUT, but much is still unknown about the genetic causes (13, 15-17). CAKUTs are responsible for causing 34-59% of CKD and 31% of ESKD in children in the United States (13). Children with ESKD require renal replacement therapy, have a high risk of developing hypertension, and have a survival rate about 30 times lower than that of healthy children (13, 18, 19). Thus, CAKUTs pose a significant health risk, and a greater understanding of kidney development is essential for understanding the mechanisms underlying the pathophysiology of CAKUTs.

1.1.2 The nephron is the functional unit of the kidney

The kidney is responsible for salt and water homeostasis, waste excretion, drug metabolism, blood pressure regulation, and signaling for red blood cell production. The nephron begins at the glomerulus, where the fenestrated glomerular capillaries are surrounded by podocytes, which allow small molecules (e.g. protein <70kDa, amino acids, sugar, ions) to pass through into the proximal convoluted tubule. The proximal tubule is the workhorse of the nephron, performing most of the ion and protein reabsorption, which are then transported to the basal side of the polarized proximal tubule epithelial cells and exported to the peritubular capillaries. The filtrate then passes through the loop of Henle and the distal convoluted tubule, both responsible for more water and salt reabsorption. The filtrate then goes through its final step of concentration in the collecting duct, which then transports the urine through the papilla to the ureter and, finally, to the bladder for excretion. **Figure 1** shows an overview of gross kidney and nephron structure.

Humans develop, on average, 1 million nephrons, but the actual number that form may range from 100,000 to 1.5 million (20-22). Nephron number is established during development, thus no new nephrons form after nephrogenesis has ended (23). Healthy human kidneys lose about half their functional nephrons between their 20s and 70s (24). Since the average human is born with an excess of nephrons, this loss often does not result in any significant pathology (25). However, humans with less nephron endowment are at an increased risk for developing pathology with aging (24), and for developing disease in general (e.g. cardiovascular, metabolic, and kidney) (20, 26). Kidneys have the capacity to raise their filtration rate in response to stimuli, termed the

renal reserve (27). The hyperfiltration theory states that a low nephron number results in hypertrophy of the remaining glomeruli to compensate for fewer glomeruli and to maintain normal kidney function (28, 29). Overtime, this hypertrophy becomes unsustainable and results in nephron loss and leads to the development of disease (29-31).

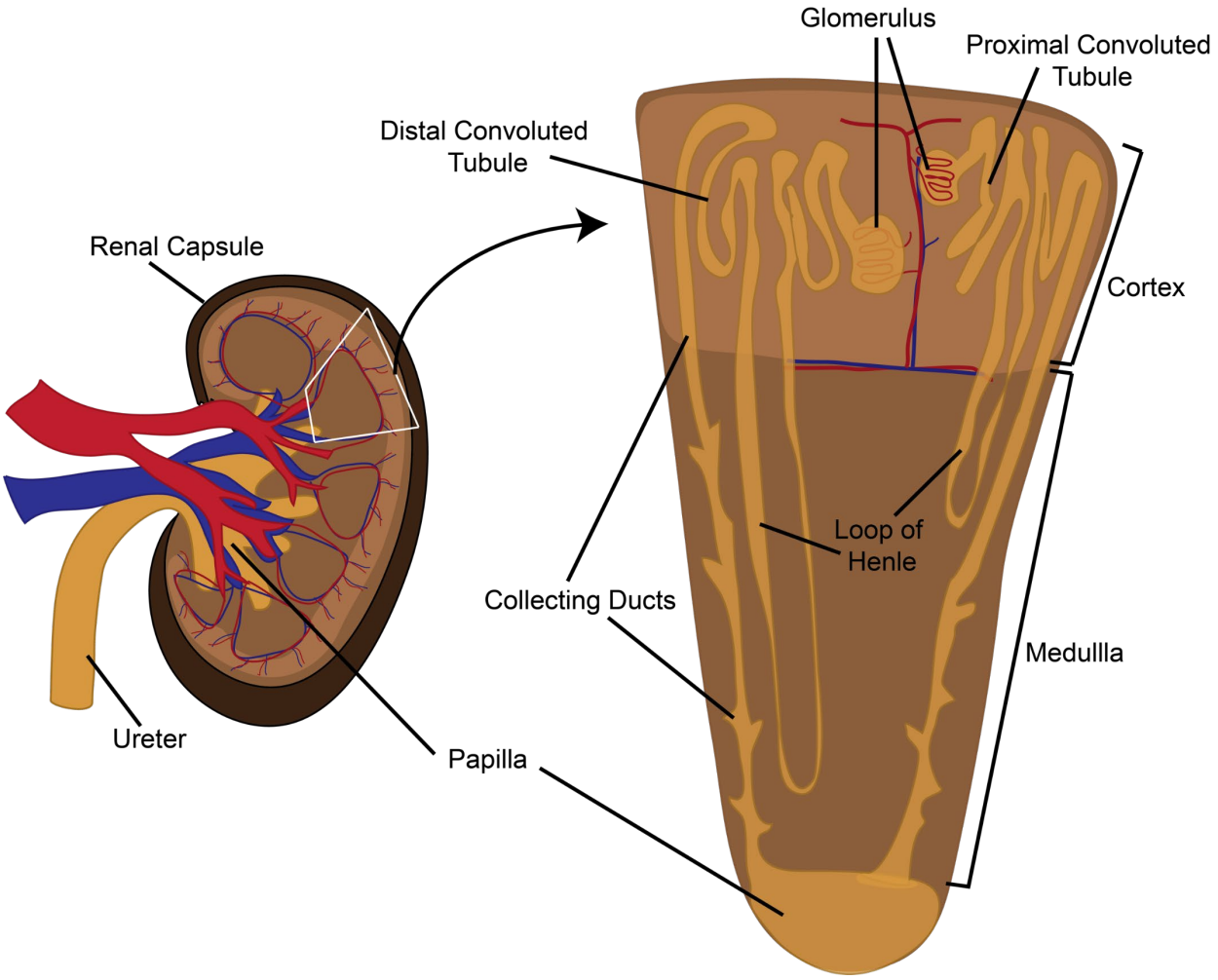

Figure 1: Overview of the kidney and nephron

The functional unit of the adult kidney (left) is the nephron (right). The renal capsule is the fibrous outer layer of the kidney providing a tough barrier and resistance to trauma. The large renal artery enters near the papilla and then branches to form smaller arteries and capillaries (both glomerular and peritubular). The glomerulus is where the blood is filtered for waste and small molecules to pass through the proximal tubule, loop of Henle, distal convoluted tubule, and the collecting duct, where concentrated urine is transported to the papilla, ureter, and then the bladder for excretion. Most nephrons are in the cortex, with short loops of Henle, but there are also juxtamedullary nephrons with longer loops of Henle.

1.1.3 Overview of kidney development

Mammalian kidney development occurs in a process defined by three stages: the pronephros, mesonephros, and metanephros. In mammals, the pronephros and mesonephros are transient structures and the metanephros is the final structure, forming the final adult kidney (32). Kidney development starts at embryonic day 8.0 (E8.0) in mice and gestational day 22 (GD22) in humans, when the non-functional pronephros—which is the first kidney structure to form—forms from the intermediate mesoderm (33). A portion of intermediate mesoderm cells form a short rod of cells that grow caudally and undergo a mesenchymal-to-epithelial transition (MET) to form the pronephric duct (a.k.a. nephric duct) (34). Soon after forming, the cranial end of the nephric duct undergoes apoptosis and the caudal end is used for development of the mesonephros (35, 36).

The mesonephros—the second kidney to form—forms at E9.0 in mice (GD24 in humans) and contains about 18 pairs of tubules that are split into distinct cranial and caudal sets (34, 37, 38). The cranial nephrons are believed to develop as outgrowths from the nephric duct and form rudimentary glomeruli and branched tubules that connect to the nephric duct at 4-6 sites (39). The caudal nephrons form at E9.0 from condensed nephrogenic cord cells that undergo MET to form a renal vesicle that elongates into a S-shaped body (37, 40). The caudal pairs make up the bulk of the mesonephros and are made of primitive unbranched tubules that do not connect to the nephric duct (34). At E14.5, the mesonephros begins degenerating in a caudal to cranial direction, and by 24 hours almost all of the tubules have undergone apoptosis (39, 40). Males retain some cranial tubules for development of the epididymal ducts of the testis (37).

In mice, the metanephric kidney—the final form of the kidney—will begin forming around E10.5, progress through birth at E18.5, and continue until postnatal day 3 (P3) (34, 41). While in humans, the metanephric kidney begins forming around GD 36 and its development ends before birth, around 36 weeks of gestation (32, 38). Metanephric kidney development begins when signals from the ureteric bud, which buds from the caudal nephric duct, stimulate condensing of the metanephric mesenchyme into a “cap” of nephron progenitors around the ureteric bud tips (42, 43). Concurrently, signals from the metanephric mesenchyme induce branching of the ureteric bud to generate the collecting duct system (44, 45). Nephron progenitors have the capacity to self-renew or differentiate, undergoing a mesenchymal to epithelial transition (MET) to form the renal vesicle (46). The renal vesicles sequentially develop to form comma- and S-shaped body structures

as nephrogenesis proceeds (46). The proximal end of the developing nephron becomes the glomerulus, while the distal end fuses with the collecting duct, to form the functional nephron (46). Nephron number is partly determined by the balance of nephron progenitor self-renewal versus differentiation, thus no new nephrons are formed after the nephron progenitor pool has been depleted (41, 47). The amount of ureteric branching also contributes to determining nephron number (48, 49). Branching morphogenesis is an exponential growth process (50). Since kidney development proceeds exponentially, the majority of nephrons are formed in later stages of kidney development, which in mice is postnatally from P1 to P3 (41, 51).

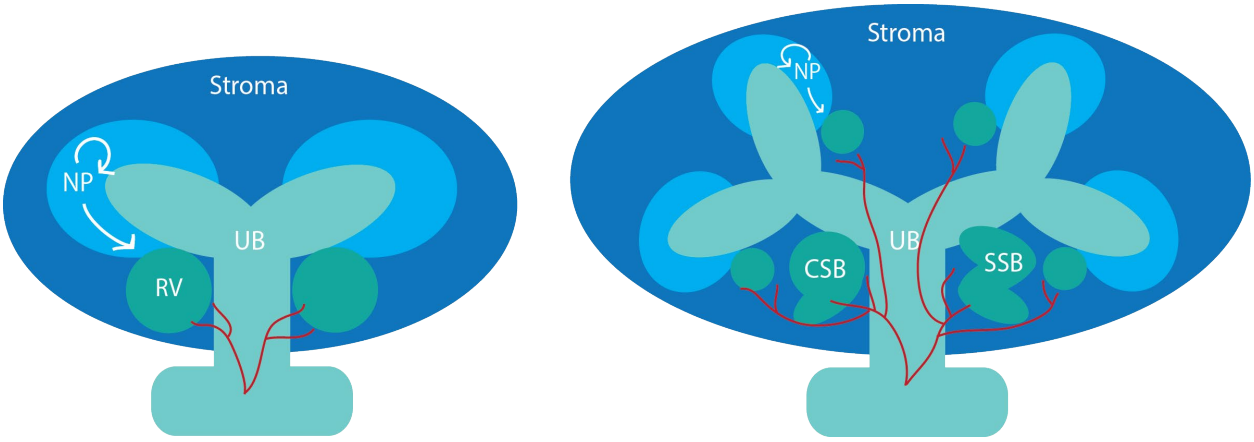

Figure 2: Overview of metanephric kidney development

The metanephric kidney forms when the ureteric bud (UB) protrudes out from the mesonephric duct into the metanephric mesenchyme. Some of this mesenchyme condenses around UB tips (light green), forming a cap of nephron progenitors (NP; light blue). These cells can either self-renew or undergo a mesenchymal to epithelial transition, forming the pretubular aggregate, which differentiates into the renal vesicle (RV; dark green), the first epithelial nephron structure. This RV will further develop into the comma-shaped body (CSB; dark green), S-shaped body (SSB; dark green), and finally the mature nephron. Meanwhile, reciprocal interactions between the NP and UB signal for UB branching to form the collecting duct system of the mature kidney. The uncondensed mesenchyme makes up the stroma (dark blue) of the kidney and gives rise to a variety of cells surrounding the nephron. The renal vasculature (red) develops in conjunction with nephron development, with perfused vessels starting near the UB induction site and extending to the RV.

1.1.4 Hypoxia is an important factor during kidney development

Kidney development normally occurs in a relatively hypoxic environment (physiological hypoxia) (52-55). However, pathological hypoxia (lower than normal oxygen concentration or prolonged hypoxia) is detrimental to development (52, 53, 56). Intrauterine hypoxia is caused by a variety of factors, which can be maternal (e.g. smoking, environmental pollutants, diet), placental (e.g. placental insufficiency), or fetal (e.g. anemia, cardiac defects) in origin (56). Indeed, placental insufficiency is a common pregnancy complication that results in pathological fetal hypoxia, and subsequent intrauterine growth restriction (IUGR) (57, 58). Fetal hypoxia results in abnormal kidney development, including aberrant protein expression, nephron deficit, and abnormal collecting duct patterning (59-63).

IUGR results in low nephron number (64), and is associated with an increased life-long risk for developing disease (65). One explanation is the "developmental origins of adult disease"—also known as the "Barker hypothesis"—which proposes that the increased risk for disease is due to fetal adaptations for survival under malnourishment (66). However, the nephron deficit is not the only cause for development of renal-related disease. For example, IUGR is also thought to increase the risk for hypertension due to dysregulation by the sympathetic nervous system, and thus, the observed hypertension may not necessarily be due to the nephron number deficit (67, 68).

Nephron progenitors reside in physiological hypoxia, and their differentiation is linked with renal blood flow and oxygenation (69). Hypoxia inducible factors (HIFs)—which govern the main cellular responses to hypoxia to promote survival—are expressed throughout kidney development (54, 70). HIFs are a family of transcription factors that bind to hypoxia-responsive elements (HREs) in the promoters of target genes (56, 71). HIFs are heterodimers, composed of an oxygen-sensitive α-subunit, of which there are three (Hif1α, Hif2α, and Hif3α), and a constitutively expressed β-subunit, known as Hif1β, thus, HIFs are referred to by their α-subunit number (56). Little is known about Hif3α, and the current consensus is that is largely acts as a negative regulator of the other Hifα-subunits (52). Hif1α has increased expression in nephron progenitors and plays more of a role in their development than Hif2α (72). In HEK293 cells Hif1α, but not Hif2α, stimulates glycolytic gene expression (73). Glycolysis is an important regulator of nephron progenitor cell fate, with a high glycolytic flux promoting self-renewal and inhibition of

glycolysis promoting differentiation (74). Deletion of the endogenous HIF inhibitor, Von Hippel-Lindau protein (VHL), from nephron progenitors results in a nephron deficit that is caused by impaired nephron progenitor differentiation due to dysregulation of metabolism (75). Together, these data support a mechanistic link between fetal hypoxia and low nephron number.

1.1.5 Sexual dimorphism in kidney development and disease

In humans, females have about 15% fewer nephrons than males (21, 76). A similar difference is observed in mice (60, 77). Gene expression analysis of adult mouse and human normal and diseased kidneys show that there are distinct differences between the sexes (78-80). Analysis of adult rat kidneys also shows differential estrogen receptor expression (81). Despite the mild decrease in nephron number, females are protected from most kidney injuries and diseases for unclear reasons (79, 82-84). However, once reproductive senescence is reached, females lose the protective effect of estrogen (85, 86). Thus, nephron number may not be an accurate predictor of risk for kidney and cardiovascular disease in pre-menopausal females (60, 82, 87). The renal sympathetic nervous system has been implicated as a mechanistic link between IUGR and risk for developing hypertension in males and females (88, 89). Interestingly, androgen receptor blockade differentially regulates blood pressure in growth-restricted versus ovarian-deficient female rats (90). Thus, our understanding of sex-specific differences in prenatal programming of hypertension and kidney disease is increasing, but much still has yet to be investigated (91).

There are also sex-specific differences in kidney development in response to intrauterine hypoxia. In mice, male and female offspring exposed to moderate prenatal hypoxia and (untreated females) had about 25% fewer nephrons than untreated males, suggesting a male-specific reduction in nephrons after prenatal hypoxia (60). Both hypoxia-exposed males and females were more susceptible to salt-induced cardiac fibrosis, but renal fibrosis was exacerbated by high salt in only the male offspring (60). Further, prenatal hypoxia resulted in a male-specific disruption of collecting duct patterning, resulting in a urine concentrating defect (61). Other insults during kidney development have also been found to result in sex-specific effects on kidney development and risk for disease. One study investigated the adverse effects of angiotensin II blockade during kidney development in rats (84). Both male and female rats exhibited an increase in blood pressure

and decrease in nephron number, but only the males showed an increase in renal pathology (84). Maternal corticosterone exposure during murine kidney development resulted in male-specific adverse renal outcomes (92). The mechanisms regulating these sex-specific differences in kidney development are poorly understood.

1.2 Genetic regulation of kidney development

1.2.1 Genetic markers of nephron progenitor cells

Nephron progenitor cells surround the ureteric bud tips and have the capacity to self-renew or differentiate to form the nephron. Several genes have been found to play a role in regulating the development and activity of these cells. In early metanephric development, Spalt like transcription factor 1 (Sall1) is expressed in the metanephric mesenchyme surrounding the ureteric bud and is required for ureteric bud invasion (93). Similarly, Odd-skipped related transcription factor 1 (Osr1) demarcates a multi-potent population of intermediate mesoderm that undergoes progressive restriction to an Osr1-dependent nephron progenitor compartment (94). Osr1 acts downstream of and interacts synergistically with Sine oculis homeobox homolog 2 (Six2) to maintain nephron progenitor cells during kidney organogenesis (95). Six2 is a transcription factor that is specifically expressed in nephron progenitors in the kidney and regulates their capacity to self-renew (43, 96). Six2 is expressed in all nephron progenitor cells and is downregulated as they are induced to begin the differentiation process (97). Eyes absent homolog 1 (Eya1) is expressed in the condensing mesenchymal cells around the ureteric bud, serving as a marker for all nephron progenitor cells (98, 99). Eya1 is required for both kidney formation and Six2 expression (100). Further, Eya1 interacts with Six2 and Proto-oncogene c-Myc (c-Myc) to regulate expansion of the nephron progenitor pool during nephrogenesis (101); and c-Myc plays a role in maintaining nephron progenitor self-renewal (102).

Some of the identified genetic markers also identify subsets of nephron progenitor cell types. Cbp/p300 interacting transactivator with Glu/Asp rich carboxy-terminal domain 1 (Cited1) is a transcriptional co-activator that is specifically expressed in the self-renewing portion of

nephron progenitors (103). There is a clear distinction between Cited1+ and Cited1- cells that discriminates between non-induced and induced nephron progenitors, respectively (97). Thus, Cited1+ nephron progenitors are considered self-renewing, while Cited1- nephron progenitors are considered to be primed for differentiation. Double PHD fingers 3 (Dpf3) and Mesenchyme homeobox 1 (Meox1) mark a subset of nephron progenitors that are both Cited1+ and Six2+, but does not overlap with all of the Cited1+ nephron progenitors (97). Dpf3 and Meox1 mark a subset of nephron progenitors that do not have as much proliferative capacity—since the Cited1+ cells closest to the fork of the ureteric bud tips are the most naïve—but are not yet primed for differentiation, providing further insight into the role of compartmentalization of the nephron progenitor cells (104).

1.2.2 Wnt/β-catenin signaling pathway

The canonical Wingless-related integration site (Wnt)/β-catenin pathway signaling is important at multiple steps for nephrogenesis. In brief, secretion of Wnt-protein ligands leads to activation of β-catenin. Activated β-catenin translocates to the nucleus, where it complexes with the Lymphoid enhancer-binding factor 1 / Transcription factor (Lef1/Tcf) family proteins to upregulate expression of target genes which mediate the downstream effects of active Wnt/β-catenin signaling.

Canonical Wnt/β-catenin signaling is both necessary and sufficient for initiating and maintaining nephron progenitor induction (105). Wnt family member 9b (Wnt9b) is expressed in the ureteric bud to induce nephron progenitors to undergo MET (106). The induced nephron progenitor cells initiate Wnt family member 4 (Wnt4) expression, leading to formation of the pretubular aggregate (107, 108). Wnt4 induces Lef1 expression, making Lef1 a readout for canonical Wnt signaling activation (104). Upon activation, β-catenin complexes with Lef1 and Tcf to induce nephron progenitor differentiation (109). Low levels of β-catenin signaling promote nephron progenitor renewal, while high levels promote their differentiation (110). Interestingly, sustained β-catenin activation also blocks MET (105). Thus, β-catenin activation must be carefully controlled to promote proper nephrogenesis.

After MET and formation of the renal vesicle, Wnt9b also induces expression of Fibroblast growth factor 8 (Fgf8) (106), which is required in nascent nephrons (111). When Fgf8 is deleted, the nascent nephrons do not express Wnt4 and Lim homeobox 1 (Lhx1; which marks the distal renal vesicle (112)) and nephrogenesis does not progress to the S-shaped body phase (111, 113). Thus, Lhx1 expression is downstream of Wnt4 and Fgf8.

Canonical Wnt/β-catenin signaling is also required for ureteric branching (114). Suppression of β-catenin signaling inhibits ureteric branching (115). Wnt family member 11 (Wnt11)-mediated signaling cooperates with Ret proto-oncogene / Glial derived neurotrophic factor (Ret/Gdnf) signaling to regulate ureteric branching (116).

1.2.3 Notch signaling pathway

The Notch signaling pathway is required for the formation of all nephron segments and primes nephron progenitors for differentiation (117). In brief, the ligands and receptors are expressed on the surface of neighboring cells and upon ligand binding, the receptor undergoes a series of proteolytic cleavages, releasing its intracellular domain, which translocates to the nucleus to upregulate expression of Notch target genes. In mammals, there are four receptors (Notch1-4) and five ligands (Delta like (Dll) 1, 3, and 4; and Jagged (Jag) 1 and 2). Notch1 and Notch2 are both involved in regulating kidney development, but Notch2 is the major receptor responsible for nascent nephron development (118). Jagged1 is one of the major Notch receptor ligands important in kidney development and is expressed by nascent nephron structures, particularly in the cells closest to the ureteric bud tip (109, 112, 118). Dll1 is the other major ligand involved in kidney development and is also expressed in the differentiated nephron structures (119).

Notch signaling promotes nephrogenesis by downregulating Six2 (120). Notch regulates nephron segmentation, and is particularly important for formation of the S-shaped body (119). Hes related family bHLH transcription factor with YRPW motif 1 (Hey1) is a downstream marker of Notch signaling, is expressed in all nascent nephron structures (121), and is required for proximal nephron (glomerulus and proximal tubule) formation (122). Several studies show there is crosstalk between Wnt and Notch signaling pathways and they often act synergistically (123). Notch

pathway activation can replace the requirement for Wnt4 and Wnt9b in regulating the MET of nephron progenitors (124).

1.3 *microRNA-210* is induced in hypoxia

1.3.1 miRNA biogenesis and function

microRNAs (miRNAs) are short (~22 nucleotide) non-coding RNA molecules that fine-tune gene expression. miRNA genes can be intragenic (intronic) or intergenic (mono- or poly-cistronic) and are transcribed by RNA Polymerase II (RNAPII) into primary miRNA (pri-miRNA). This pri-miRNA is processed in the nucleus by the Microprocessor complex, which is made up of Drosha ribonuclease type III (Drosha) and its cofactor DiGeorge syndrome critical region 8 (Dgcr8), into stem-loop precursor miRNA (pre-miRNA). Pre-miRNA is then exported to the cytoplasm by Exportin-5. In the cytoplasm, Dicer1 ribonuclease type II (Dicer1) then processes pre-miRNA into a small miRNA duplex, made of the mature guide and the complementary passenger miRNA strands, which can be either the 5p or 3p strands. The duplex is then loaded onto an Argonaute protein to form the RNA-induced silencing complex (RISC) and the passenger strand quickly dissociates and is often degraded. RISC scans mRNAs for complementary matches to the miRNA 6-8 nucleotide seed sequence (which are usually in the 3' untranslated region (UTR)) and will either repress translation of the mRNA target or cause it to degrade. This is summarized in **Figure 3**.

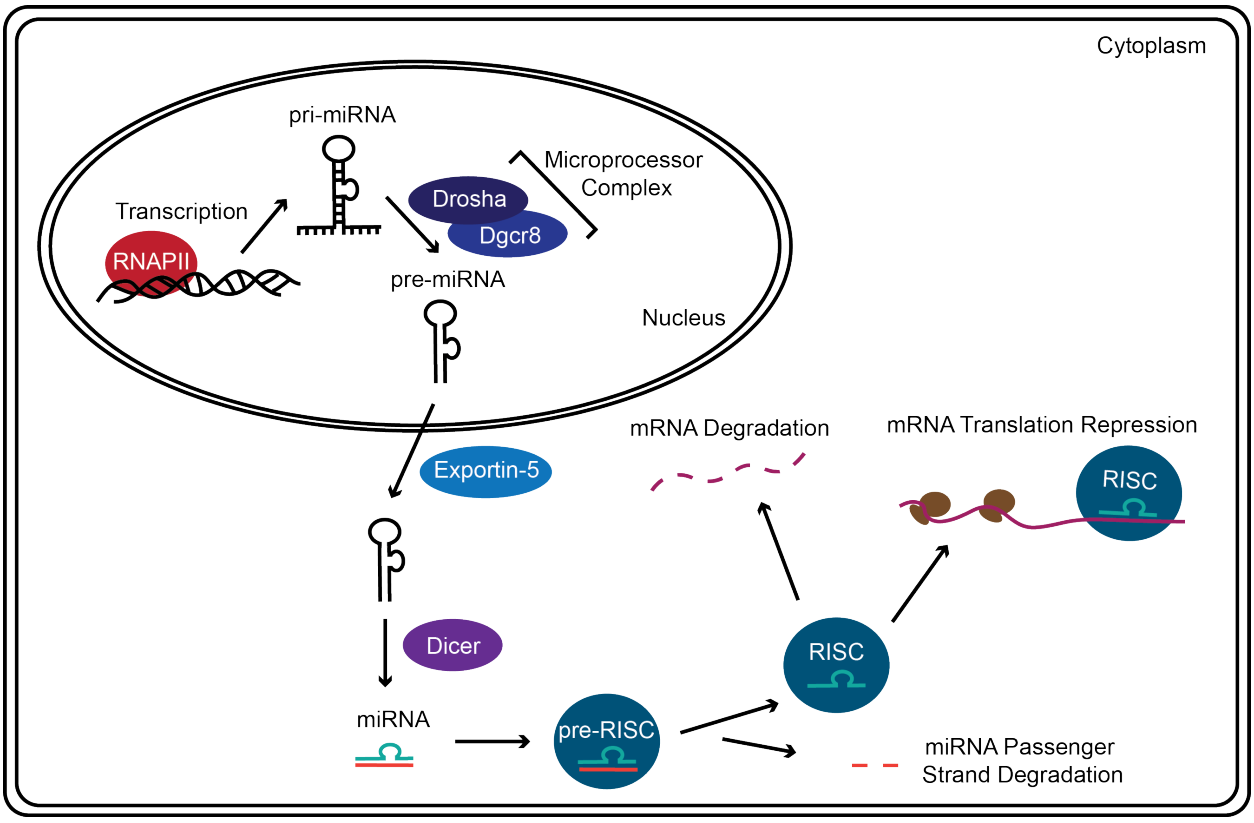

Figure 3: microRNA biogenesis and function

RNA Polymerase II (RNAPII) transcribes microRNA (miRNA) genes into primary miRNA (pri-miRNA). Then the Microprocessor complex (Drosha/Dgcr8) makes pre-miRNA, which is then exported to the cytoplasm. Dicer processing makes the miRNA duplex of guide and passenger strands, which are then loaded into RNA-induced silencing complex (RISC). The passenger strand dissociates and degrades, leaving RISC to scan mRNAs for complementary matches to the guide miRNA seed sequence and will either lead to mRNA degradation or translation repression.

1.3.2 miRNAs in kidney development

Developing embryonic tissues have different miRNA expression profiles (125, 126), and recently our laboratory identified miRNAs expressed in E15.5 mouse nephron progenitors (127). Several studies have implicated various miRNAs in the development of CAKUTs (128, 129). In order to determine the roles of miRNAs in kidney development, several groups have created cell-type specific deletions of *Dicer*, which is responsible for creating the mature miRNA molecule. Conditional *Dicer* deletions have been created for nephron progenitors, renal stroma, ureteric

epithelium, podocytes, proximal tubules, and juxtaglomerular cells (130-140). *Dicer* deletion in mouse nephron progenitor cells results in their premature depletion due to increased apoptosis (138). Loss of *Dicer* in the renal stroma results in impairment of nephron progenitor differentiation as well as vascular development (133, 137). Ureteric bud deletion of *Dicer* results in marked renal cysts, and hypoplasia appearing to result from early termination of branching morphogenesis (132, 139). Further, *Drosha* and *Dgcr8* knockout models also show that loss of miRNAs results in abnormal kidney development (141, 142). Deletion of specific miRNAs has also been found to induce a kidney development phenotype. For example, deletion of the *miR-17~92* cluster in nephron progenitors resulted in a decrease in nephron number and renal function in adult mice (143, 144). Together, these data show that miRNAs are important for multiple aspects of kidney development.

1.3.3 *miR-210* regulation

MicroRNA-210 (*miR-210*) is the most consistently induced miRNA in hypoxia and is often referred to as the "master hypoxamir" (145-147). *miR-210-3p*, the dominant strand, has been found to regulate a variety of genes involved in cell cycle progression, angiogenesis, metabolism, DNA damage response, and apoptosis (148). Several of its targets have functions related to processes important in kidney development, such as the angiogenesis inhibitor *Ephrin a3* (*Efna3*) (149-152); the pro-apoptotic *Caspase-8 associated protein 2* (*Casp8ap2*) (153, 154); the pro-proliferation and renal vesicle marker *Fibroblast growth factor receptor-like 1* (*Fgfrl1*) (152, 155-157); and the Wnt/β-catenin signaling transcription factor *Transcription factor 7-like 2* (*Tcf7l2*) (158). In addition to its inhibition of *Tcf7l2*, *miR-210* has also been shown to inhibit β-catenin expression of which it has a potential binding site in the transcript's 3'UTR (159). *miR-210* has also been implicated in activation of Notch signaling pathway (160), however the mechanism of this regulation is unknown. In the setting of ovarian cancer, *miR-210* inhibition promotes EMT (161), which has interesting implications for nephrogenesis, where nephron progenitors undergo the opposite process, MET.

Both HIF1 and HIF2 bind to the hypoxia response element (HRE) in the *miR-210* promoter to upregulate its expression in hypoxia (152, 162-164). HIF-dependent regulation of *miR-210* is

the most studied, but a few other transcription factors have been implicated in regulating *miR-210* expression. In hypoxic cardiomyocytes, *miR-210* is upregulated through Akt- and p53-dependent pathways to exert cytoprotective effects (165). *miR-210* is induced by Nuclear factor kappa b subunit 1 (Nfκb1) in female, but not male placentas, due to increased tumor-necrosis factor-alpha (TNFα) (166). Further, there is evidence from CHiP-seq data that Six2 binds upstream of *miR-210* in mouse E16.5 nephron progenitors (167).

1.3.4 *miR-210* in kidney

Most of the studies investigating *miR-210* in kidney have focused on renal cell carcinomas (RCCs), which are commonly caused by deleterious mutations in *VHL* (168). *miR-210* expression is promoted in clear cell RCCs (ccRCCs) due to both increased hypoxia, which is a common feature of tumors, and inactivation of VHL (168-170). The hypoxic environment of renal cancer tumors induces Hif1 and Hif2 up-regulation, which then increase *miR-210* expression (164). Expression of *miR-210* is linked to centrosome amplification in RCCs, which contributes to the development of aneuploidy, and suggests that *miR-210* plays a role in the early stages of tumorigenesis (171). Increased *miR-210* levels are linked to poor prognosis of ccRCC, suggesting that it may be a useful prognostic biomarker (172).

In addition to its potential role as a biomarker in RCCs, *miR-210* may be a biomarker for other kidney-related diseases. High plasma levels of *miR-210* after acute kidney injury is associated with mortality (173). Low *miR-210* levels in urine are associated with acute rejection of kidney transplants (174). Additionally, *miR-210* is a potential biomarker for fetal hypoxia (which is detrimental for kidney development) from pregnancies with pre-eclampsia and during labor (175-177).

There are a few studies looking specifically at *miR-210* in the kidney. *miR-210* expression is increased in rat models of both systemic and kidney hypoxia and protects against hypoxia-induced apoptosis in HK-2 cells by targeting Hif1α (178). Upregulation of *miR-210* promotes VEGF signaling pathway-mediated renal angiogenesis under *in vivo* and *in vitro* ischemia/perfusion injury (179). Further, overexpression of *miR-210* in proximal tubule cells damages them and promotes a metabolic shift from oxidative phosphorylation to anaerobic

glycolysis (180). In regards to kidney development, our group recently published that expression of *miR-210-3p* is increased in E15.5 mouse nephron progenitors compared to whole kidney (127). Together, these data show that *miR-210* is induced in hypoxia and is implicated in kidney development and disease.

2.0 Transcriptome of Hypoxic Kidney Development

2.1 Introduction

Embryonic development occurs in a "physiological hypoxia" of 1-10% O_2, with the desired physiological oxygen concentration varying depending on tissue type and developmental stage (53). Several studies have found that ~5% O_2 is the best culturing condition for developing embryos and tissue cultures (53, 181, 182). Kidney explant organ cultures have been used for several decades to study the mechanisms regulating kidney development as an *ex vivo* model for kidney development. In this model, embryonic kidneys are dissected and transferred to a filter that is suspended over culture medium and can be kept in a cell culture incubator for several days (183); however, the majority of these studies have been conducted in 21% O_2 culturing conditions. Recently, studies have shown that kidney explants should be cultured at 5% O_2 to better mimic the *in vivo* conditions of kidney development (53, 181, 182). Oxygen levels around 1% are considered more optimal for stem and progenitor cells, but oxygen levels below 1% are considered "pathologically hypoxic" for stem and progenitor cells (53). While 1% O_2 is beneficial for stem cells, it is considered as pathological hypoxia for differentiated cells of the developing tissue (53).

Kidney development normally occurs in a hypoxic environment, but the exact levels of oxygen in different spatial locations of the developing tissue have not been identified (55, 69, 72). Little is known about how different levels of oxygen affect gene expression in the developing kidney. To investigate the role of hypoxia on gene expression in an unbiased fashion in early kidney development, RNA sequencing was used to analyze both mRNA and miRNA gene expression in mouse kidney explants cultured in different oxygen levels: pathological hypoxia (1% O_2), physiological hypoxia (5% O_2), and hyperoxia (21% O_2).

2.2 Methods

2.2.1 Mouse strains

All animals were housed in the vivarium at the Rangos Research Center at the UPMC Children's Hospital of Pittsburgh (Pittsburgh, PA, USA) and all animal experiments were carried out in accordance with the policies of the Institutional Animal Care and Use Committee at the University of Pittsburgh. CD1 time-mated pregnant females were ordered from Charles River Laboratories, Inc (Wilmington, MA, USA). The day of the plug was considered embryonic day 0.5 (E0.5).

2.2.2 Model of *ex vivo* kidney development in different oxygen conditions

Embryos from wildtype CD1 time-mated pregnant females were collected on embryonic day 12.5 (E12.5). Embryos were placed in cold HyClone™ Dulbecco's Phosphate Buffered Saline, Modified (PBS) under a Leica S6E dissection microscope and L2 light source (Buffalo Grove, IL, USA). Their kidneys were then dissected and placed on cell culture inserts (0.4μm pore membrane; Corning) in MULTIWELL™ 12 well plates, notched (Becton Dickinson and Company). For each embryo, one kidney was placed in one well plate and the contralateral kidney was placed in a separate plate. 9-12 embryonic kidneys were placed on each membrane and suspended over 500μL of media composed of Advanced Dulbecco's Modified Eagle Medium (DMEM; Thermo Fisher Scientific, Grand Island, NY, USA) with 10% fetal calf serum and 1:10,000 penicillin and streptomycin. 2 kidneys were placed on a separate membrane for immunostaining (see below).

Each well plate was then cultured at 37ºC with 5% CO_2 in either 1% or 21% O_2 for 3 days. This process was repeated to culture embryonic kidneys in 5% and 21% O_2. A hypoxia chamber (hypoxic glovebox, model AC100 CO_2 controller, oxygen controller, and humidified incubation box; Coy Laboratory Products, Inc., Grass Lake, MI, USA) was used to culture kidneys in 1% and 5% O_2 while a Forma™ Series II Water Jacketed CO_2 Incubator (Thermo Fisher Scientific) was used to culture kidneys in 21% O_2.

After the 3-day organ culture incubation, the culture media was removed and replaced with PBS to rinse the kidney explants. Forceps were used to transfer the kidney explants into 150μL Qiazol Lysis Reagent (Qiagen, Hilden, Germany) for storage at -80ºC. The tissues were

homogenized using the Fisherbrand™ Disposable Pestle System (Thermo Fisher Scientific) and the Qiagen miRNeasy Mini Kit was then used to purify RNA. RNA purity and concentration were determined with the NanoDrop® ND-1000 Spectrophotometer (Thermo Fisher Scientific).

An overview of this protocol is depicted in **Figure 4**.

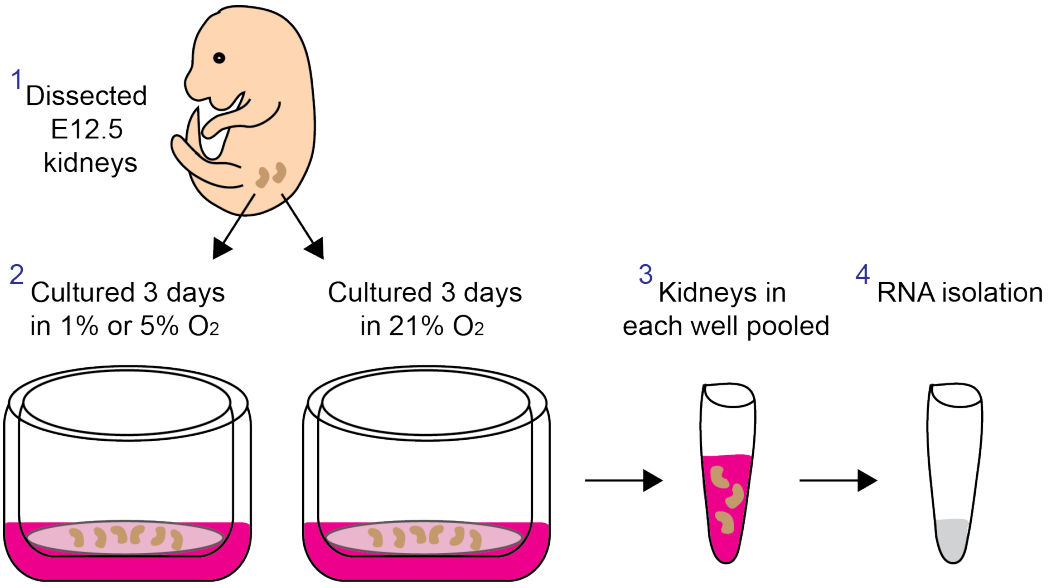

Figure 4: Overview of kidney explant organ culture in different oxygen conditions

First, kidneys were dissected from E12.5 embryos, placing one kidney for culturing in either 1% or 5% O_2 and the other for culturing in 21% O_2. Kidneys were suspended above media using transwell inserts and cultured for 3 days in 1%, 5%, or 21% O_2. All kidneys from each well (approximately 9) were pooled and transferred to Qiazol for RNA isolation. $N \geq 5$ pooled kidney explant samples per oxygen condition.

2.2.3 Immunostaining of kidney explants

After the 3-day organ culture incubation (as described above), the culture media was removed and replaced with PBS to rinse the kidney explants. A scalpel was used to cut the membrane with the kidney explants and the membrane was placed in a clean well of a 24-well plate and fixed with 100% ice cold methanol for 10min at -20ºC. Methanol was removed and the explants were rinsed with PBS. Explants were then permeabilized with PBS-T (PBS + 0.1% Tween-20) and blocked with 1% BSA (bovine serum albumin) / PBS-T. Explants were then incubated with primary antibodies (1:200 Rabbit α-Six2 (Proteintech, Rosemont, IL, USA) and

1:50 Monoclonal Mouse α-pan-cytokeratin (pCK) (Sigma Aldrich, St. Louis, MO, USA)) overnight at 4°C. Primary antibodies were rinsed with PBS-T and then incubated with secondary antibodies (1:200 anti-rabbit-594 and 1:200 anti-mouse-488 (both Jackson ImmunoResearch Laboratories, West Grove, PA, USA)) overnight at 4°C. Secondary antibodies were rinsed with PBS-T and were then mounted on Leica Biosystems Surgipath® X-tra® pre-cleaned micro slides and ProLong™ Gold antifade reagent with DAPI (Invitrogen, Carlsbad, CA, USA). The sections were then imaged using a Leica DM 2500 microscope (Buffalo Grove, IL, USA) and Qcam Fast 1394 camera (Teledyne Qimaging, Surrey, BC, Canada) and the images were analyzed and prepared using Adobe Photoshop (San Jose, CA, USA).

2.2.4 qPCR analysis of mRNA expression in kidney explants

Total RNA was isolated using the Qiagen miRNeasy Mini Kit, as per the manufacturer's instructions. cDNA was synthesized from total RNA using Superscript^{TM} III First-Strand Synthesis System (Thermo Fisher Scientific), as per the manufacturer's instructions. qPCR was performed in a 96 well C100 Thermal Cycler (Bio-Rad, Hercules, CA, USA) using Sso Advanced SYBR Green Master Mix (Thermo Fisher Scientific). The list of primers used in these experiments is shown in **Table 1**. Expression levels were normalized to the endogenous control (*Rn18S*) and analyzed using the $2^{-\Delta\Delta C}{}_T$ method (184).

Table 1: Primers used for qPCR

Gene	Forward	Reverse	Product Size (bp)
Cited1	GTCTCCAGGTCTTACCACCGA	GCAGAGATGGCCACGTGTAT	155
Eya1	GGAATGCTATTATGAGGTAGAA	ATCCTTGTTGACACTTGAC	158
Fgf8	GCTAATTGCCAAGAGCAACG	GGTAGTTGAGGAACTCGAAGC	245
Fgfrl1	TCAACTACACTCTCATCATCA	GGTCTGGTCATCCTTCAT	242
Lef1	AGCTTGTTGAAACCCCAGAC	TTTTTGGAAGTCGGCGCTTG	160
Ldha	TGTCTCCAGCAAAGACTACTGT	GACTGTACTTGACAATGTTGGGA	155
Meox1	CACACCGTTGAGTTGAAG	TCAGAGTCCTTGGAGAAC	150
c-Myc	CAGCGACTCTGAAGAAGAGCAAG	GGGTTTGCCTCTTCTCCACAG	71
Rn18S	GACAGGATTGACAGATTGATAG	CCAGAGTCTCGTTCGTTA	114
Slc2a1	ACTTCATTGTGGGCATGTGC	TCGGGTGTCTTGTCACTTTG	196
Six2	GCAGGACTCCATACTCAA	GATACCGAGCAGACCATT	215
Vegfa	AGCAGATGTGAATGCAGACCA	CACAGTGAACGCTCCAGGAT	127
Wnt4	TGGGAAGGTGGTGACACAAG	TGACCACTGGAAGCCCTGT	166

2.2.5 Statistical analysis

2-way ANOVA with Tukey correction was used to determine statistical significance of qPCR results: $*P \leq 0.05$ and $**P \leq 0.01$. All statistical analyses were performed using Prism 8 software package (GraphPad Software, Inc., La Jolla, CA, USA).

2.2.6 mRNA-sequencing

mRNA sequencing (mRNA-seq) was performed by TUCF Genomics (Tufts University, Boston, MA) using the Illumina HiSeq 2500 System rapid run mode. The mRNA library was prepared using polyA selection with the Ovation® RNA-Seq System (NuGEN Technologies, Inc.). mRNA-seq was then performed using 150bp paired end sequencing with 40-50 million reads per sample.

mRNA-seq quality control assessment, read alignment, and differential expression analysis was then performed by Andrew Clugston (Dr. Dennis Kostka Laboratory, Department of Developmental Biology and Dr. Jacqueline Ho Laboratory, Department of Pediatrics, University of Pittsburgh, PA). mRNA-seq sample read quality was assessed using FastQC (v0.11.4) (185). The mRNA-seq data files were trimmed using Trim Galore (v0.4.0) (186). Paired-end read

alignment of transcripts to the *Mus musculus* genome assembly MGSCv37 (mm9) (187) was performed using the STAR software package (188). Reads were annotated using the GenomicAlignments (189) R package with annotations from the Ensembl database (190). Differential expression of mRNA transcript between the different oxygen culturing conditions was performed using the DESeq2 R package (191). An FDR of 0.05 was used to determine significantly differentially expressed genes of interest. An overview of this pipeline is outlined in **Figure 5**.

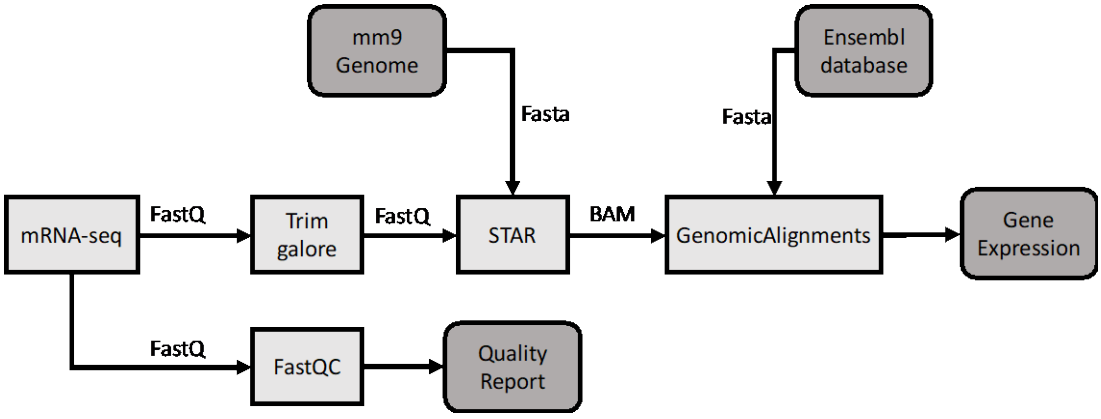

Figure 5: mRNA-seq analysis pipeline

The mRNA-seq FastQ data files were analyzed for their read quality using FastQC. The FastQ files were trimmed using Trim Galore and mapped to the mm9 genome using STAR. The mapped reads were annotated using GenomicAlignments with the Ensembl database. Differential gene expression was then determined using DESeq2. Data and figure prepared by Andrew Clugston (Dr. Dennis Kostka, Department of Developmental Biology; Dr. Jacqueline Ho Laboratory, Department of Pediatrics, University of Pittsburgh, Pittsburgh, PA).

2.2.7 smRNA-sequencing

small-RNA sequencing (smRNA-seq) was performed by TUCF Genomics using the TruSeq Nano DNA Library Prep Kit (Illumina). smRNA-seq was then performed using 50bp single end sequencing with 10-15 million reads per sample.

smRNA-seq quality control assessment, read alignment, and differential expression analysis was then performed by Andrew Clugston (Dr. Dennis Kostka Laboratory, Department of Developmental Biology, and Dr. Jacqueline Ho Laboratory, Department of Pediatrics, University of Pittsburgh, PA). smRNA-seq sample read quality was assessed using FastQC (v0.11.4) (185).

The smRNA-seq data files were trimmed using Cutadapt (v1.1) (192) and aligned to the *Mus musculus* genome assembly MGSCv37 (mm9) (187) using Bowtie (v1.1.2) (1). Identification and quantification of known and potential novel miRNAs was performed using miRDeep2 (v2.0.0.7) (6) and known miRNA sequences were downloaded from the miRbase database (193). Differential expression of miRNA transcript between the different oxygen culturing conditions was performed using the DESeq2 R package (191). An FDR of 0.05 was used to determine significantly differentially expressed miRNAs of interest. An overview of this pipeline is outlined in **Figure 6**.

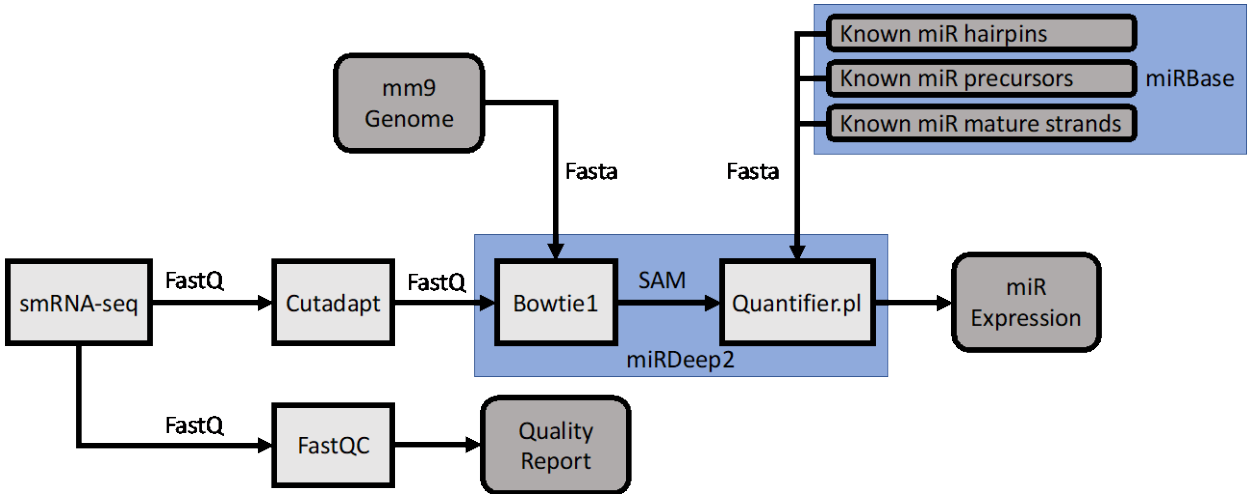

Figure 6: smRNA-seq analysis pipeline

The smRNA-seq FastQ data files were analyzed for their read quality using FastQC. The FastQ files were trimmed using Cutadapt and mapped to the mm9 genome using miRDeep2, which used Bowtie1. The mapped reads were annotated using miRDeep2, which used Quantifier using miRbase for known miRNA information. Differential gene expression was then determined using DESeq2. Data and figure prepared by Andrew Clugston (Dr. Dennis Kostka, Department of Developmental Biology; Dr. Jacqueline Ho Laboratory, Department of Pediatrics, University of Pittsburgh, Pittsburgh, PA).

2.3 Results

2.3.1 Kidney explant organ cultures in varying oxygen levels

In order to further understand the role hypoxia plays in regulating kidney development, kidneys were cultured in different oxygen concentrations: 1% (pathological hypoxia), 5% (physiological hypoxia), and 21% (hyperoxia). E12.5 kidneys from CD-1 wildtype embryos were dissected and one kidney was cultured in either 1% or 5% O_2 and the other kidney in 21% O_2 for three days (**Figure 4**). To validate the *ex vivo* kidney explant model, two kidneys per litter and oxygen condition were stained for the nephron progenitor marker Six2 and the ureteric bud marker pCK (194) and showed that the explants' nephron progenitors differed between oxygen conditions (**Figure 7**). In 1% O_2, the nephron progenitor cells are loosely organized into caps around the ureteric bud tips (**Figure 7A**). As the oxygen levels increase, the nephron progenitor cells are organized more tightly in caps around the ureteric bud tips in 5% (**Figure 7B**) and 21% O_2 (**Figure 7C**).

To further validate the model, qPCR analysis of expression of various markers was performed (**Figure 8**). Six2 expression was increased in kidneys cultured in 1% O_2, compared to 21% O_2 (**Figure 8A**). Expression of other nephron progenitor markers (*Cited1, Meox1,* and *Eya1*) was not different between oxygen conditions (**Figure 8A**). Analysis of expression of various markers for differentiation of developing nephron structures (*Wnt4, Lef1, Fgf8,* and *Fgfrl1*) showed no differences between kidneys cultured in different oxygen conditions (**Figure 8B**). Analysis of expression of various genes induced in hypoxia (*c-Myc, Ldha, Slc2a1,* and *Vegfa*) showed increased expression of *Ldha, Slc2a1,* and *Vegfa* in kidneys cultured in 1% compared to 21% O_2 as well as increased expression of *Ldha* and *Vegfa* in 1% compared to 5% O_2 cultures (**Figure 8C**).

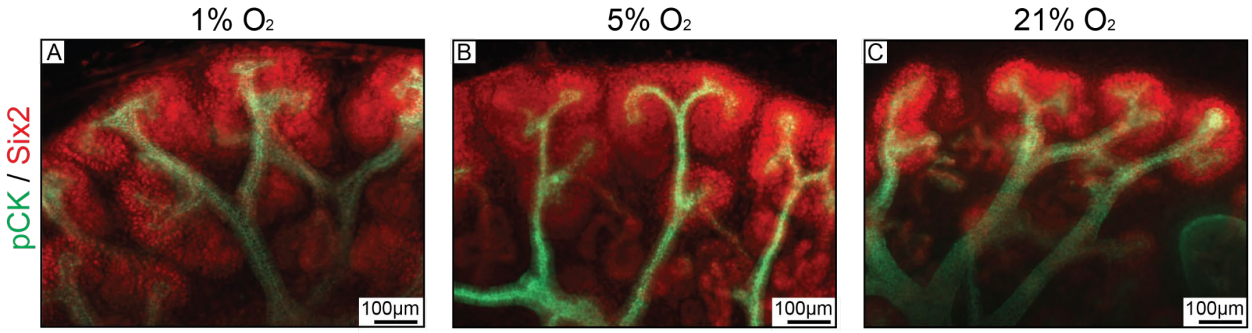

Figure 7: Immunostaining shows differing cap mesenchyme structure between different oxygen conditions

(A-C) Immunostaining for nephron progenitor marker Six2 (red) and ureteric bud marker pCK (green) in E12.5 kidneys explants cultured for three days in (A) 1%, (B) 5%, and (C) 21% O_2. $N \geq 5$ kidney explants per oxygen condition.

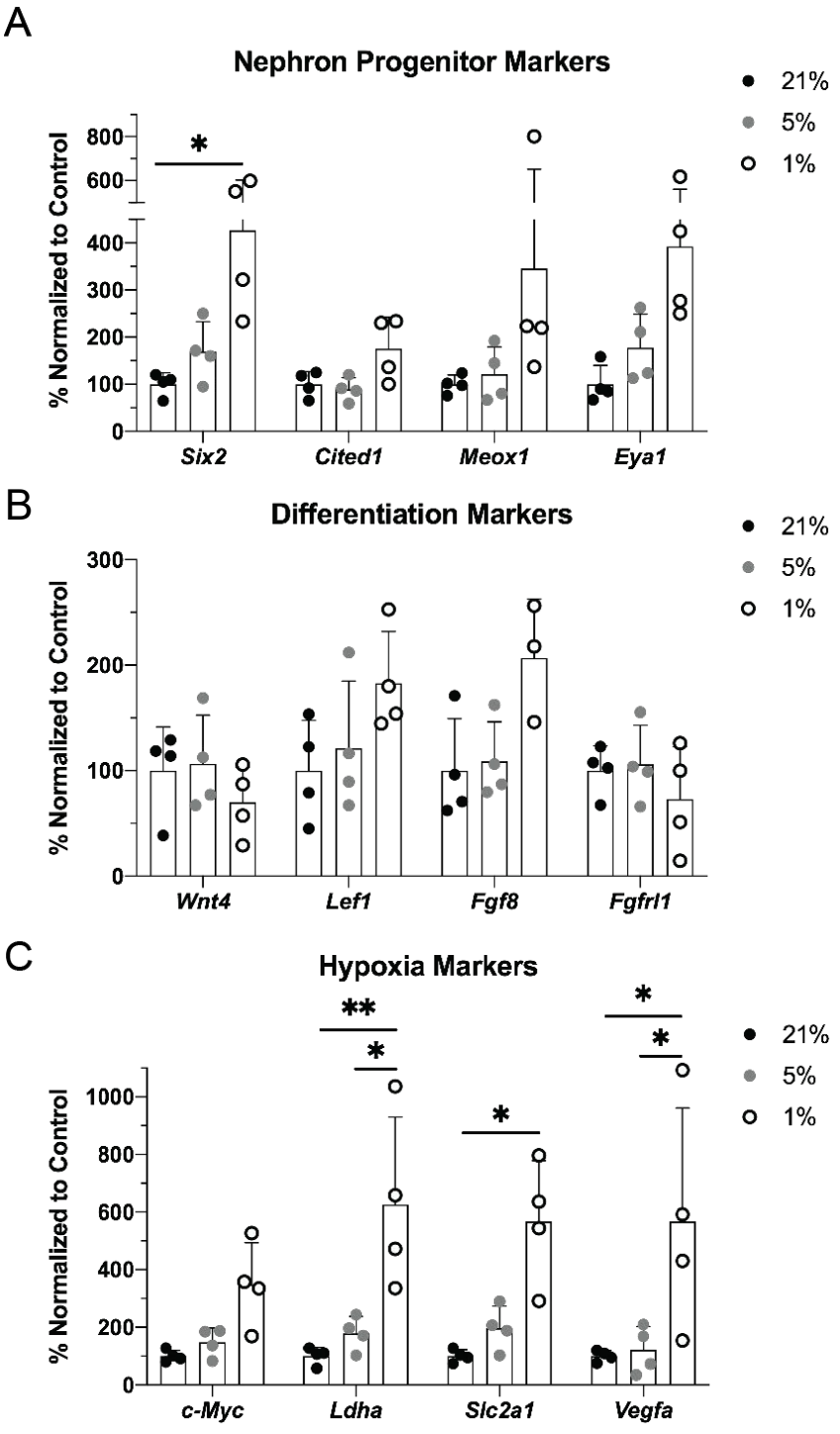

Figure 8: qPCR validation of hypoxia model

(A-C) qPCR analysis of expression of (A) nephron progenitor, (B) differentiation, and (C) hypoxia markers in kidney explants cultured in 1%, 5%, and 21% O_2. RNA expression was normalized to *Rn18S*. Error bars ± SEM, **P*<0.05, ***P*<0.01, 2-way ANOVA with Tukey correction, $N \geq 4$ pooled kidney explant samples per oxygen condition.

2.3.2 mRNA sequencing sample analysis

Principal component analysis (PCA) plots, which cluster samples according to inherent variations stemming from differences in sequence counts between samples, showed one of the low O_2 samples (specifically "1% 7/13B") is an outlier (**Figure 9A**). The PCA plot with the outlier sample omitted showed expected distribution between samples (**Figure 9B**). All analysis of the kidney explants was then performed without the outlier sample.

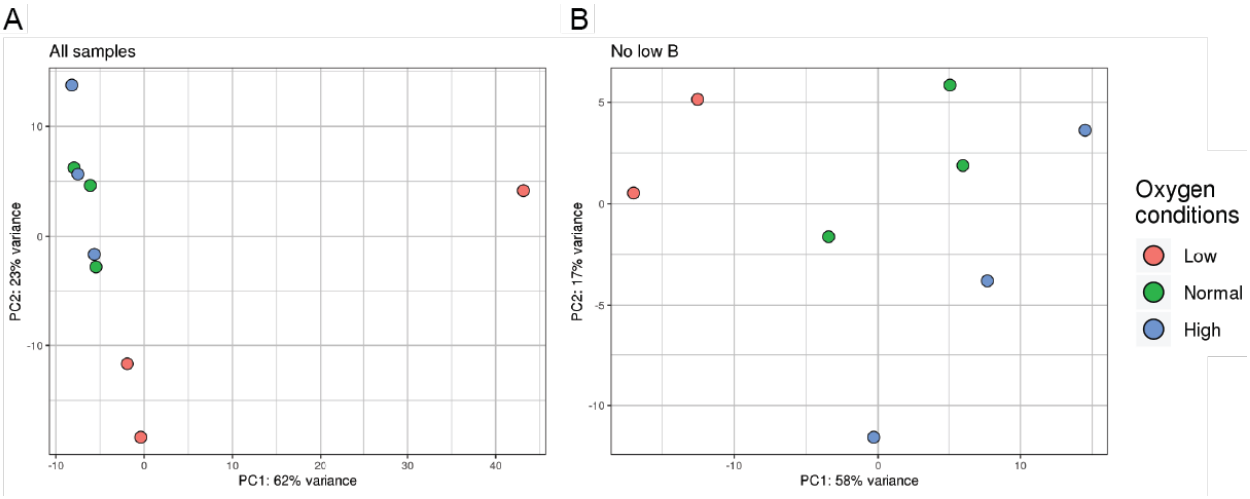

Figure 9: PCA shows outlier sample

(A) PCA plot of mRNA-seq samples of kidney explants cultured in low (1%; red), normal (5%; green), and high (21%; blue) O_2. (B) PCA plot of mRNA-seq samples of kidney explants cultured in low, normal, and high O_2 with outlier sample omitted. $N \geq 3$ pooled kidney explant samples per oxygen condition. Data and graphs prepared by Andrew Clugston (Dr. Dennis Kostka, Department of Developmental Biology; Dr. Jacqueline Ho Laboratory, Department of Pediatrics, University of Pittsburgh, Pittsburgh, PA).

The normalized library sizes of the mRNA-seq reads from the kidney explants cultured in different oxygen conditions showed at least 12 million reads per sample (**Figure 10A**). The sample distance heatmap—which depicts how different samples are to each other—showed proper segregation of the samples based on their different culturing conditions (**Figure 10B**). The minus average plots—which are used to visualize the intensity-dependent ratio of raw gene expression data—depicted the amount of significantly differentially expressed genes in red (**Figure 10C-E**). Note that there are minimal differences of gene expression when comparing the 5% and 21% O_2

culture conditions (**Figure 10E**); however the transcriptional differences are greater when comparing 1% and 5% O_2 (**Figure 10C**) and even higher when comparing 1% and 21% O_2 (**Figure 10D**) cultures. Since the 5% O_2 cultures are physiologically hypoxic, all further analysis was conducted with the 1% to 5% O_2 comparison to exclude potential effects of presumed hyperoxia.

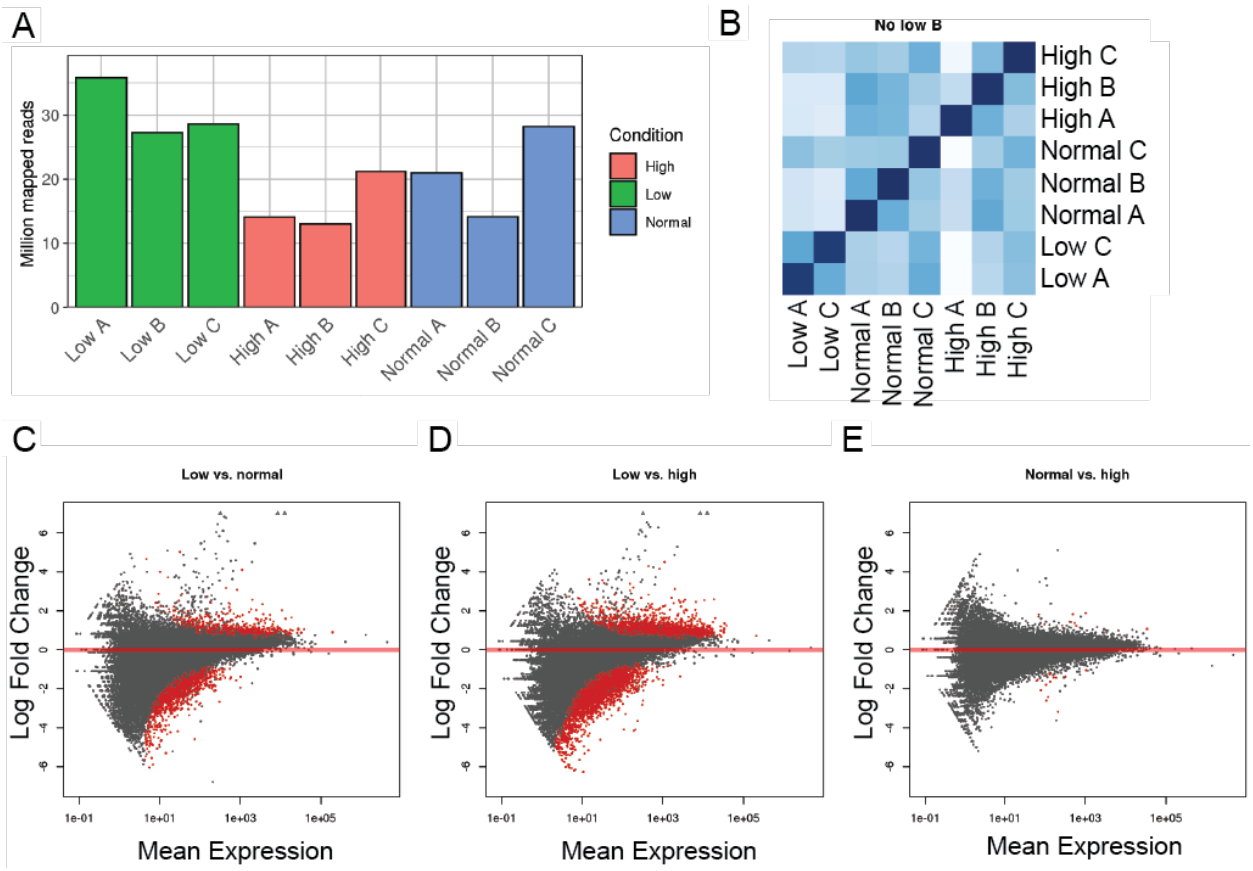

Figure 10: mRNA-seq read anlysis

(A) Normalized library size of each kidney explant sample. (B) The number of differences in normalized counts between each sample is shown as a shade of blue, where darker hues indicate similarity and lighter hues indicate differences. Note outlier sample has been removed from analysis. (C-E) Scatter plots showing the total number of counts of each gene (x-axis) versus the fold change in its expression between (C) low (1%) and normal (5%), (D) low (1%) and high (21%), and (E) normal (5%) and high (21%) O_2 samples. Genes with an FDR ≤ 0.05 are shown in red. $N \geq 2$ pooled kidney explant samples per oxygen condition. Data and graphs prepared by Andrew Clugston (Dr. Dennis Kostka, Department of Developmental Biology; Dr. Jacqueline Ho Laboratory, Department of Pediatrics, University of Pittsburgh, Pittsburgh, PA).

2.3.3 mRNA sequencing analysis of differential gene expression

The heatmap of the top 100 differentially expressed genes showed a clear difference in expression levels in kidney explants from 1% O_2 cultures compared to the ones from 5% and 21% O_2 cultures (**Figure 11A**). Looking at the top 20 genes, there was up-regulation of several genes involved in the hypoxia response: genes involved in 1) metabolism (*Slc2a3, Pdk1, Pgk1, Ppp1r3c, Slc2a1, Ak4, Pfkf3b, Slc16a3,* and *Hk2*); 2) HIF regulation (*Ero1l, P4ha1,* and *Wsb1*); 3) apoptosis (*Bnip3*); and 4) kidney development (*Igfbp2*) (**Figure 11B**).

Analysis of the full gene list (of top differentially expressed genes when comparing 1% and 5% O_2 cultures with an FDR ≤ 0.05) using Ingenuity Pathway Analysis (Qiagen) showed that that top five pathways activated in 1% O_2 kidney cultures were glycolysis, gluconeogenesis, sucrose degradation, atherosclerosis signaling, and HIF1 signaling. The up-regulation of genes involved in anaerobic energy production was expected (74) and upregulated cholesterol signaling fits with the recent finding of its role in regulating nephron progenitor self-renewal and differentiation (Saifudeen ASN Kidney Week 2019, unpublished). The observed HIF1 signaling up-regulation serves as a nice internal control (56).

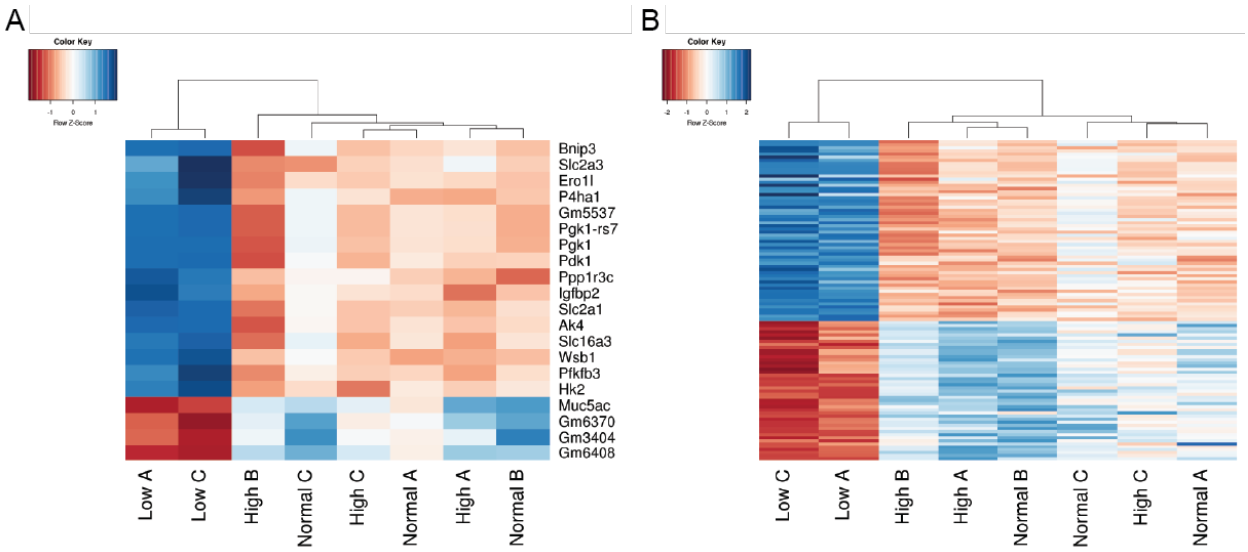

Figure 11: Top differentially expressed genes in kidneys cultures in 1%, 5%, and 21% O_2

(A) Heatmap of top 100 differentially expressed genes in kidney explants cultured in low (1%), normal (5%), and high (21%) O_2. (B) Heatmap of top 20 differentially expressed genes, with gene names noted on the left. Blue is up-regulation and orange is down-regulation. $N \geq 2$ pooled kidney explant samples per oxygen condition. Data and heatmaps prepared by Andrew Clugston (Dr. Dennis Kostka, Department of Developmental Biology; Dr. Jacqueline Ho Laboratory, Department of Pediatrics, University of Pittsburgh, Pittsburgh, PA).

2.3.4 small-RNA sequencing sample analysis

The PCA plot of the smRNA-seq data with the outlier sample (determined in the mRNA-seq analysis) omitted showed expected distribution between samples (**Figure 12A**). The normalized library sizes of the smRNA-seq reads from the kidney explants cultured in different oxygen conditions showed at least 7 million reads per sample (**Figure 12B**). The sample distance heatmap showed proper segregation of the samples based on their different culturing conditions (**Figure 12C**). Thus, analysis of the smRNA-seq was then performed without the outlier sample. The minus average plots depicted the amount of significantly differentially expressed genes in red (**Figure 12D-F**). Unlike the mRNA-seq, the smRNA-seq analysis showed notable differences of gene expression when comparing the 5% and 21% O_2 culture conditions (**Figure 12F**), however the transcriptional differences were still greater when comparing 1% and 5% O_2 (**Figure 12D**) and 1% and 21% O_2 (**Figure 12E**) cultures.

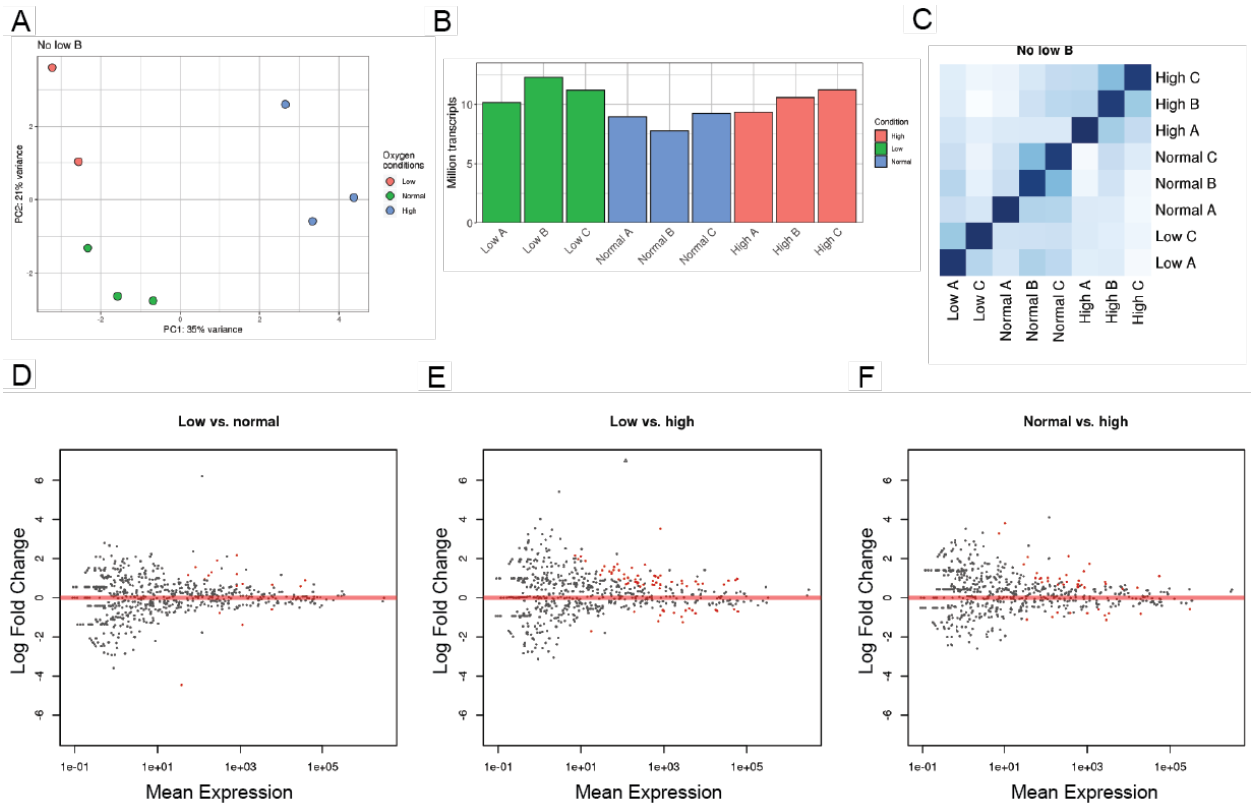

Figure 12: smRNA-seq read analysis

(A) PCA plot of smRNA-seq samples of kidney explants cultured in low (1%; red), normal (5%; green), and high (21%; blue) O_2 with outlier sample omitted. (B) Normalized library size of each kidney explant sample. (C) The number of differences in normalized counts between each sample is shown as a shade of blue, where darker hues indicate similarity and lighter hues indicate differences. (D-F) Scatter plots showing the total number of counts of each gene (x-axis) versus the fold change in its expression between (D) low (1%) and normal (5%), (E) low (1%) and high (21%), and (F) normal (5%) and high (21%) O_2 samples. Genes with an FDR ≤ 0.05 are shown in red. $N \geq 2$ pooled kidney explant samples per oxygen condition. Data and graphs prepared by Andrew Clugston (Dr. Dennis Kostka, Department of Developmental Biology; Dr. Jacqueline Ho Laboratory, Department of Pediatrics, University of Pittsburgh, Pittsburgh, PA).

2.3.5 smRNA sequencing analysis of differential expression

When using DESeq2 to compare differential expression between the 1% and 5% O_2 cultures, there were 13 differentially expressed miRNAs with an FDR ≤ 0.05 (**Figure 13A**). Notably, *miR-210*, the master hypoxamir (147), was the top up-regulated miRNA in 1% O_2 cultures. Surprisingly *miR-210-5p*, which is the passenger strand, is reported instead of the guide strand *miR-210-3p*. Further analysis of this result suggested that miRDeep2 reported both strands of *miRNA-210* as the same strand (-5p), instead of reporting the -3p and -5p strands separately (**Figure 14A-C**). This result occurred using several different settings for running the miRDeep2 program. To confirm that *miR-210-3p* was being expressed in these samples, the analysis of miRNA reads was performed using an alternative method that relies on the Rsubread package for alignment (195) (instead of miRDeep2), which identified miRNA transcripts by counting how many align to their footprint in the genome (**Figure 14D**). Then, the *miR-210* read results were analyzed using DESeq2, which show that both *miR-210-5p* and *miR-210-3p* were increased in the 1% O_2 cultures compared to the 5% and 21% O_2 cultures, with *miR-210-3p* exhibiting much higher expression, as expected (**Figure 14E**). Analysis of the heatmap comparing low and normal oxygen culture miRNA expression produced using the Rsubread analysis places both *miR-210-3p* and *miR-210-5p* as the top differentially expressed miRNAs (**Figure 13C**) and lists many of the same miRNAs as those in (**Figure 13A**).

The number of significantly differentially expressed miRNAs increased greatly when comparing 1% and 21% O_2 cultures (**Figure 13B**). The top differentially expressed miRNAs from these conditions were also compared using the Rsubread analysis and produced a similarly long list (**Figure 13D**). Since the 5% O_2 cultures are physiologically hypoxic, further analysis was conducted with the miRNAs from the 1% to 5% O_2 comparison to produce more stringent results.

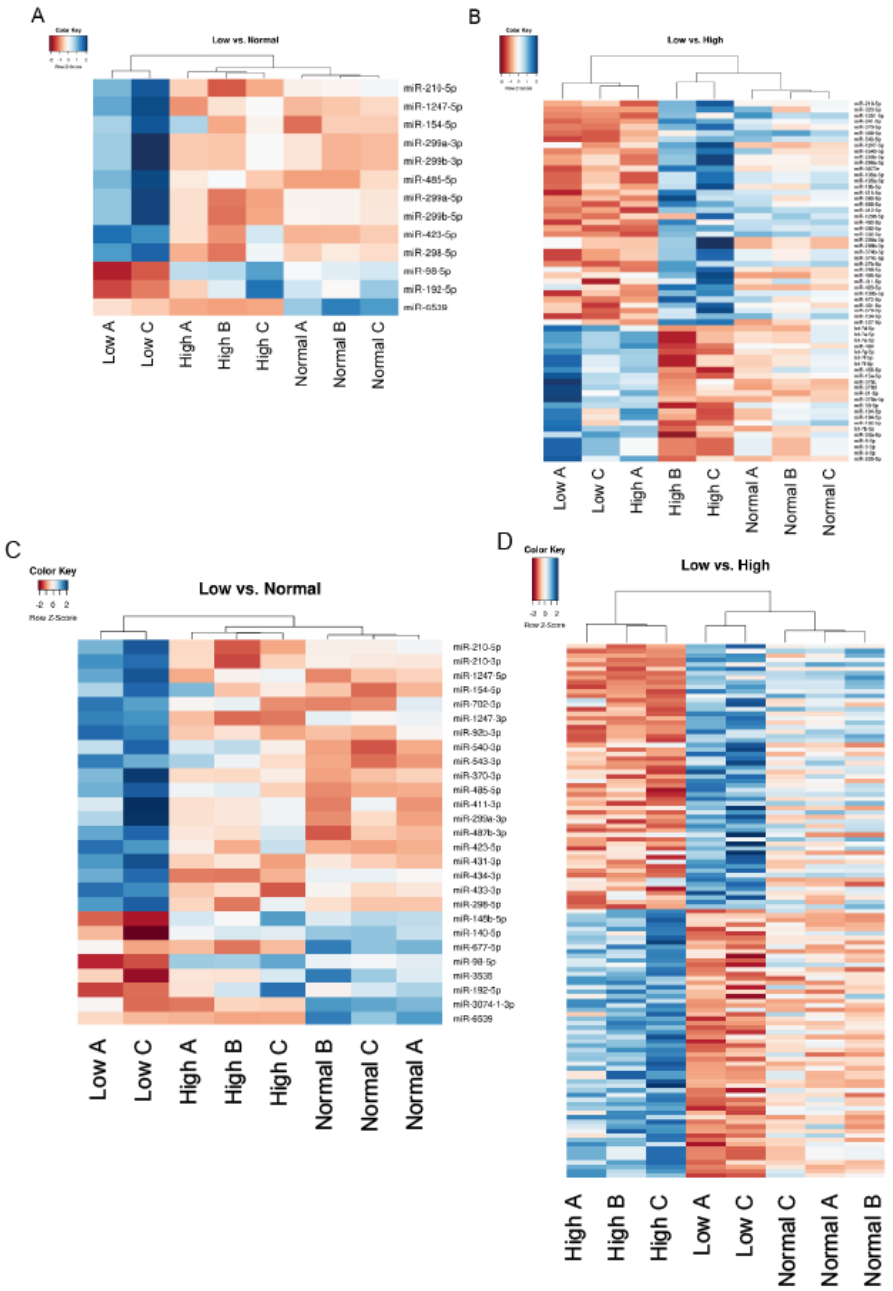

Figure 13: Top differentially expressed miRNAs in kidneys cultured in 1%, 5%, and 21% O_2

(A-B) Heatmap of top differentially expressed miRNAs (identified using miRDeep2; FDR ≤ 0.05) in kidney explants cultured in low (1%), normal (5%), and high (21%) O_2, when differential expression analysis is done comparing (A) low and normal and (B) low and high oxygen cultures. (C-D) Heatmap of top differentially expressed miRNAs (identified using Rsubread; FDR ≤ 0.05) in kidney explants cultured in low, normal, and high oxygen, when comparing (C) low and normal and (D) low and high oxygen cultures. Gene names noted on the left. Blue is up-regulation and orange is down-regulation. $N \geq 2$ pooled kidney explant samples per oxygen condition. Data and heatmaps prepared by Andrew Clugston (Dr. Dennis Kostka, Department of Developmental Biology; Dr. Jacqueline Ho Laboratory, Department of Pediatrics, University of Pittsburgh, Pittsburgh, PA).

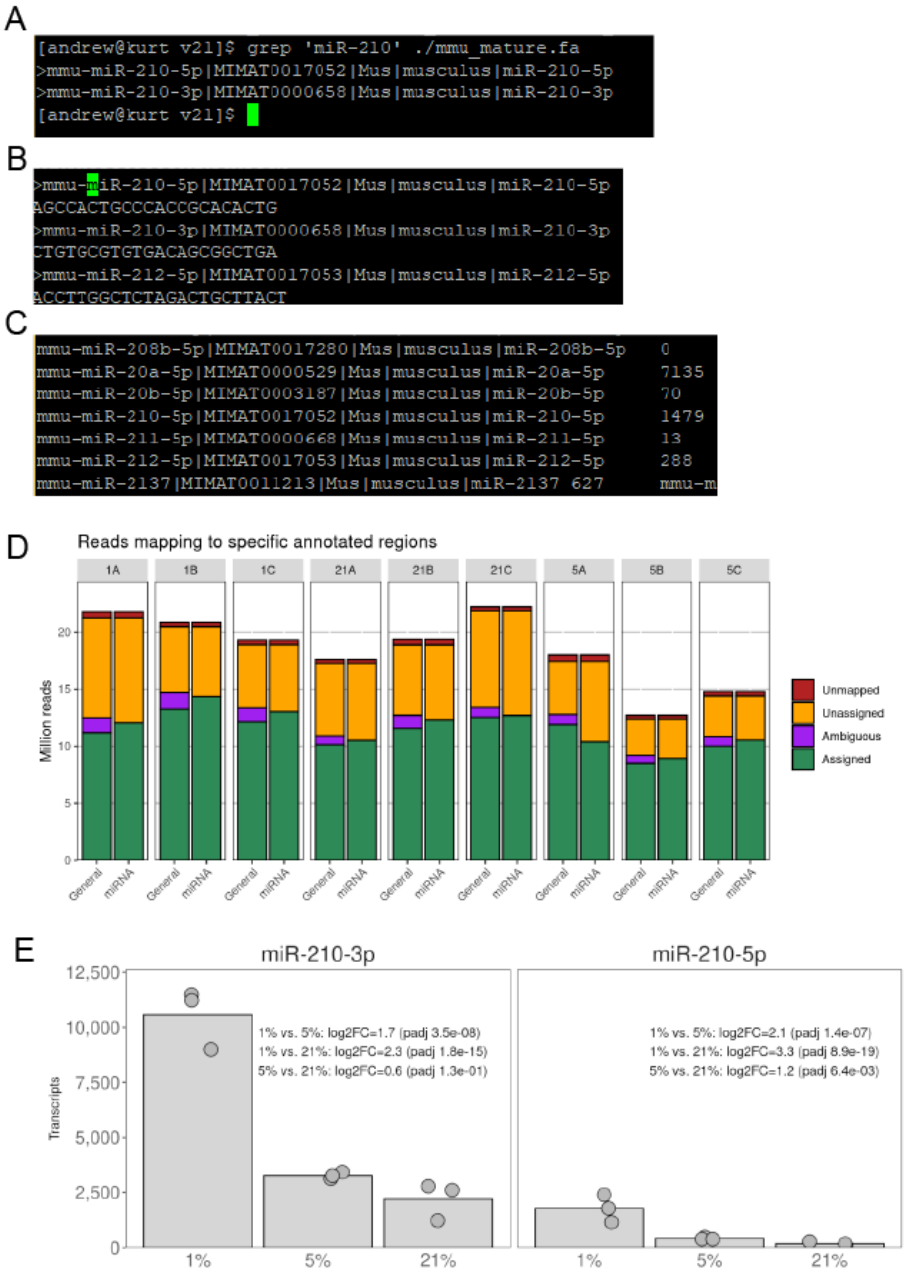

Figure 14: Analysis of *miR-210* guide versis passenger strand expression

(A-C) Line code for the miRDeep2 analysis showing that (A) miRDeep2 was instructed to look for both *miR-210* strands and that (B) reads aligned for both sequences, but (C) the reads were reported as only *miR-210-5p*. (D) The miRNA transcripts from 1%, 5%, and 21% O_2 cultures were aligned using Rsubread to their footprints in the genome in order to differentiate between the miRNA strands. (E) DESeq2 analysis of both *miR-210* strands showed very little *miR-210-5p* expression in the samples and significantly higher *miR-210-3p* expression in 1% O_2 cultures. $N \geq 2$ pooled kidney explant samples per oxygen condition. Data and Figures prepared by Andrew Clugston (Dr. Dennis Kostka, Department of Developmental Biology; Dr. Jacqueline Ho Laboratory, Department of Pediatrics, University of Pittsburgh, Pittsburgh, PA).

2.3.6 miRNA-mRNA target pair analysis

Ingenuity Pathway Analysis was used to compare the list of differentially expressed mRNAs with the list of differentially expressed miRNAs between the kidneys cultured in 1% and 5% O_2, producing a list of miRNA-mRNA target pairs. There was little overlap of genes being targeted by multiple miRNAs with differential expression, suggesting that these miRNAs play distinct roles in regulating hypoxic gene expression. This list of paired genes was then analyzed using DAVID (196) to identify common themes for hypoxia-specific transcriptional changes. The top ten GO terms (i.e. most common functional roles of genes regulated by miRNAs in hypoxic kidney development) are listed in **Table 2**. Not surprisingly, the top gene functions of these miRNA-mRNA pairs included those involved in signaling, substrate transport, and development. The top ten KEGG Pathways involved in the miRNA-mRNA pairs affected by hypoxia are listed in **Table 3**. There is a clear representation of genes involved in metabolism, which makes sense since cells need to be able to quickly change their metabolism to meet the different energy demands of a hypoxic environment.

Table 2: GO term analysis of miRNA-mRNA target pairs in hypoxic kidney development

GO Term	# of Genes	*P*-Value
Transcription, DNA-templated	47	0.0079
Transport	46	0.0070
Multicellular organ development	31	0.0030
Ion transport	23	0.00045
Transmembrane transport	15	0.0040
Sodium ion transport	9	0.0013
Liver development	8	0.0012
Cation transport	6	0.0081
Response to glucose	6	0.011
Regulation of macrophage activation	3	0.0076

Table 3: KEGG pathway analysis of miRNA-mRNA target pairs in hypoxic kidney development

KEGG Pathway	# of Genes	*P*-Value
AMPK signaling pathway	10	0.0006
Biosynthesis of antibiotics	10	0.019
Ras signaling pathway	10	0.028
Lysosome	7	0.027
Central carbon metabolism in cancer	6	0.0067
Glucagon signaling pathway	6	0.040
Glycolysis / Gluconeogenesis	5	0.035
Circadian rhythm	4	0.020
Fructose and mannose metabolism	4	0.025
Glycine, serine and threonine metabolism	4	0.038

2.4 Conclusion

Ex vivo analysis of gene expression during early nephrogenesis in different oxygen conditions revealed stark differences. Pathological hypoxia promoted gene expression consistent with that of nephron progenitors (i.e. Hif1α-mediated hypoxia response and anaerobic glycolysis). Nephron progenitors utilize glycolysis, promoting self-renewal, while switching to oxidative phosphorylation promotes their differentiation (74). Further, these findings are consistent with a genetic mouse model of pathological hypoxic gene expression, where Hif1α is constitutively expressed in nephron progenitors, resulting in increased glycolysis and inhibited differentiation (75). The metabolic gene expression changes observed in the pathological hypoxia organ cultures are consistent with an inhibition of nephrogenesis (197); however few significant changes in differentiation markers were observed in the 1% O_2 cultures, suggesting that the phenotype of inhibition of differentiation may take a few more days of hypoxic insult to manifest.

These data show that while not many miRNAs respond to pathological hypoxia in kidney development, the few that do have a significant effect on regulating expression. Consistent with other studies, *miR-210* was the top miRNA upregulated in hypoxia (147). When looking at the miRNA-mRNA target pairs, these data suggest that the developing kidney uses a handful of miRNAs to regulate signaling and metabolic pathways important in survival under pathological hypoxia. The developing kidney's limited energy capacity under hypoxic conditions could help

explain how IUGR and fetal hypoxia contribute to the development of a smaller kidney with fewer nephrons.

Most studies investigating miRNAs in hypoxia focus on cancer and ischemia-reperfusion injury (163, 169, 198-201). While some of these studies are performed in kidney, renal cancer and renal injury have expression profiles that are very different from the genes expressed during development. Few of the miRNAs identified in these studies were also identified in the developing kidney cultures. Thus, this panel of hypoxia-induced miRNAs during kidney development provide a platform for future work investigating each miRNA's role in pathologically hypoxic kidney development. This study lends novel insight into the mechanisms regulating impaired nephron formation from intrauterine hypoxia during kidney development.

3.0 *miR-210* in Kidney Development

3.1 Introduction

Kidney development takes place in a physiologically hypoxic environment (55, 69, 72). Pathological hypoxia during kidney development impairs kidney development (56), but the mechanisms regulating this are poorly understood. *miR-210* is the top miRNA induced in pathologically hypoxic kidney development (**Figure 13**) and has been shown to be the most consistently induced miRNA in hypoxia (147). *miR-210* expression at E15.5 is higher in nephron progenitors compared to whole kidney (127). However, the expression pattern and functional role of *miR-210* during kidney development is unknown.

Thus, to piece together the puzzle of how hypoxic expression changes affect kidney development, looking at the top upregulated miRNA in hypoxia is an intriguing first step. Mice with a global deletion of *miR-210* were assayed for a kidney development defect in order to investigate the role of *miR-210* during kidney development.

3.2 Methods

3.2.1 Mouse strains

CD-1 time-mated pregnant females were ordered from Charles River Laboratories, Inc. Global *miR-210* knockout males (202, 203) were crossed to female C57Bl/6J wildtype mice from The Jackson Laboratory (Bar Harbor, ME, USA) to generate heterozygous mice. These heterozygous breeding pairs produced wildtype (control) and *miR-210* knockout littermates for analysis. Animals were genotyped using genomic DNA isolated from tail clipping by PCR with the following primers: 0.5μM F1 5'-AGACAGGCCTGCTTGTAGGA-3'; 0.5μM R 5'-TCAGGAGGTGGGTCCTGTAG-3'; and 1μM F2 5'-GGTCACTGCCAGGACTACGT-3'

(wildtype PCR product is 250bp and knockout product is 500bp). *miR-210 HRE* heterozygous mice (knockout mouse model, unpublished, obtained from our collaborator Xin Huang, formerly of the Department of Obstetrics, Gynecology, and Reproductive Sciences, University of Pittsburgh, Pittsburgh, PA) were generated in the same way and offspring were genotyped using the following primers: 0.5μM F1 (for knockout) 5'-CGCGTTCCTTTCGGCTT-3'; 0.5μM F2 (for wildtype) 5'-CACCGCGCGTTCCTTTCTGCACGT-3'; and 0.5μM R 5'-TGCCTGGAGAGT TATGAGTTCC-3'. All animals were housed in the vivarium at the Rangos Research Center at the UPMC Children's Hospital of Pittsburgh and all animal experiments were carried out in accordance with the policies of the Institutional Animal Care and Use Committee at the University of Pittsburgh.

3.2.2 Isolation of nephron progenitors using positive-selection MACS

Nephron progenitors were isolated from E14.5 and P0 kidneys using magnetic-activated cell sorting (MACS) as previously published (167, 204). Briefly, up to 24 CD-1 mouse kidneys were dissected and pooled from an individual litter, then the outer layers of cortical cells were digested into a single cell suspension using a mixture of collagenase A and pancreatin. Cell suspensions were then mixed with magnetic beads biotinylated to α-Itgα8 antibodies (a cell surface protein expressed on nephron progenitors (167) (R&D Systems, Minneapolis, MN, USA)) using the DSB-X Biotin Protein Labeling Kit (Thermo Fisher Scientific). Bead-bound nephron progenitor cells were immobilized by a DynaMagTM-2 Magnet (Thermo Fisher Scientific) then washed, released, and resuspended. Total RNA was isolated from a fraction containing approximately 400,000 cells using the Qiagen miRNeasy Mini Kit, as per the manufacturer's instructions. Enrichment of nephron progenitors relative to surrounding cell types was confirmed in each sample by real-time quantitative PCR (qPCR) (see below).

3.2.3 qPCR for miRNA expression analysis

Total RNA was isolated from flash-frozen kidneys using the Qiagen miRNeasy Mini Kit, as per the manufacturer's instructions. *U6* snRNA (RT001973), *miRNA-210-3p* (RT00512), and

miRNA-210-5p (RT462444) cDNAs were generated with the TaqMan® MicroRNA Reverse Transcription Kit (Thermo Fisher Scientific) according to the manufacturer's instructions. Expression of mature miRNA was detected by qPCR performed in a 96 well C100 Thermal cycler (Bio-Rad) using FAM1 TaqMan® Universal PCR Master Mix with no AmpErase® UNG (Applied Biosystems, Foster City, CA, USA). Expression levels were normalized to the endogenous control (*U6* snRNA) and analyzed using the $2^{-\Delta\Delta C}{}_T$ method (184).

3.2.4 Size measurements

At the time of sacrifice, kidneys were photographed with a scale bar using a Qimaging QICAM Fast 1394 camera coupled to a Leica M165FC Stereo Microscope, using QCapture software. ImageJ software (https://imagej.nih.gov/ij/) was utilized to determine kidney length in each digital image. Kidney and mouse body masses were measured using a digital platform scale (Summit Series Analytical Balance SI-234, Denver Instrument, Bohemia, NY, USA).

3.2.5 Paraffin-embedding of kidneys

Kidneys were dissected and fixed in 4% PFA/PBS for 1-4hr at 25ºC or overnight at 4ºC. The kidneys were then transferred to Biopsy Tru-Tek® cassettes (Thermo Fisher Scientific) and submerged in 70% ethanol (Decon Labs., Inc., King of Prussia, PA, USA). The kidneys were then paraffinized using a Tissue-Tek® VIP® tissue processor (Sakura Finetek, Torrance, CA, USA). In short, the program first dehydrates the kidneys using an increasing ethanol gradient, followed by treatment with xylene (Thermo Fisher Scientific), and lastly treatment with Leica Surgipath® Blue Ribbon paraffin. See **Table 4** for timing of protocol steps for paraffin embedding for embryonic (i.e. E16-P4 kidneys) and adult (i.e. P30 and 3-month). These paraffinized kidneys were then embedded in blocks for sectioning using the Leica EG 1160.

Table 4: Tissue processing protocols

		Time (min)	
Step	**Solution**	**Embryonic**	**Adult**
1	70% Ethanol	5	20
2	95% Ethanol	3	10
3	95% Ethanol	5	10
4	100% Ethanol	5	10
5	100% Ethanol	5	10
6	100% Ethanol	5	10
7	Xylene	10	30
8	Xylene	10	30
9	Paraffin	5	30
10	Paraffin	5	30
11	Paraffin	10	30

3.2.6 Hematoxylin and eosin staining

Paraffin-embedded kidneys were sectioned at 4μm using a Microm HM 325 microtome (Waldorf, Germany) and placed on Surgipath® X-tra® Pre-cleaned micro slides (Leica). To stain the sections, first, excess paraffin was removed with xylene and washed with 100% ethanol. The sections were then rehydrated with water and stained with Hematoxylin 1 (Richard-Allan Scientific, San Diego, CA, USA), to mark nuclei. The sections were then washed with water, treated with Clarifier™ (Thermo Fisher Scientific) to reduce background hematoxylin staining, followed by another wash, and then treatment with Shandon™ Bluing Reagent (Thermo Fisher Scientific), to increase the blue staining of hematoxylin. The sections were again washed with water, followed by dehydration with 95% ethanol, and then were placed in Eosin-Y (Richard-Allan Scientific), to stain the cytoplasm. The eosin was then washed with 100% ethanol and then xylene. Dry, stained sections were then mounted in Cytoseal™ 280 (Richard-Allan Scientific) with a FisherFinest® Premium cover glass slip (Fisher Scientific, Hampton, NH, USA). The sections were then imaged using a Leica DM 2500 microscope and Qimaging Qcam Fast 1394 camera and the images were analyzed and prepared using Adobe Photoshop.

3.2.7 Nephron number estimation at P30

Kidneys were harvested from mice at postnatal day 30 (P30), fixed in 4% paraformaldehyde in PBS (PFA/PBS) and serially sectioned at 4µm. Slides every 100µm (26 sections) were stained with hematoxylin and eosin. A pair of consecutive sections out of every 26 sections was analyzed using a Walcom drawing tablet (Walcom, Portland, OR, USA) and Stereoinvestigator version 9.04 software, using a physical fractionator probe (MBF Bioscience, Williston, VT, USA). The total glomerular number (N_{glom}) was calculated using the following equation:

$$N_{glom} = \frac{\Sigma Q^{-}}{2} x \frac{A}{a} \; x \frac{1}{ASF}$$

where N_{glom} is the total of glomeruli in the entire kidney, ΣQ^{-} is the total number of glomeruli appearing and disappearing between two consecutive sections, A is the grid size (1000x1000), a is the counting frame size (800x800), and $1/ASF$ is the reciprocal of the section-sampling fraction (the number of sections advanced between section pairs; 26). This was performed as described in (205).

3.2.8 Histopathological analysis of 3-month kidneys

3-month-old kidneys were fixed in 4% PFA/PBS and embedded in paraffin (see above). For morphological analysis, the Rangos Histology Core at UPMC Children's Hospital of Pittsburgh sectioned kidneys at 4µm and performed H&E, Period Acid Schiff, and Trichrome staining. The sections were then imaged using a Leica DM 2500 microscope and Qimaging Qcam Fast 1394 camera and the images were analyzed and prepared using Adobe Photoshop.

3.2.9 Renal function analysis at 3-months

3-month-old mice were placed in metabolic cages overnight to collect urine. Blood was collected via cardiac puncture at the time of sacrifice into Microtainer® SSTTM tubes (BD Biosciences). The blood

collection tubes were centrifuged to separate out serum. Frozen serum was sent to the Kansas State Veterinary Diagnostic Laboratory (Manhattan, KS, USA) to assay blood urea nitrogen and creatinine levels. Urine albumin/creatinine ratio was assayed using the Exocell Albuwell M and Creatinine Companion kits (Philadelphia, PA, USA) as per manufacturer's instructions. Sample absorbance was measured using the SpectraMax® i3 plate reader (Molecular Devices, San Jose, CA, USA).

3.2.10 Immunofluorescent staining of kidney sections

Paraffin-embedded kidneys were sectioned at 4μm using a Microm HM 325 microtome and placed on Leica Surgipath® X-tra® Pre-cleaned micro slides. Sections were then deparaffinized using xylene, rehydrated through decreasing ethanol concentrations (i.e. 100%, 70%, 50%), and permeabilized in PBS-T. Then antigen retrieval was performed by boiling in 10mM sodium citrate pH 6.0 buffer or Trilogy (Cell Marque, Rocklin, CA, USA). Sections to be stained using the Tyramide Signal Amplification Kit (PerkinElmer, Waltham, Ma, USA) were treated with 3% H_2O_2 to inhibit endogenous peroxidase activity. Sections were then blocked with either 3% bovine serum albumin (BSA) or 5% normal donkey serum (NDS) in PBS-T. Sections were incubated overnight with primary antibody, washed with PBS-T, incubated with secondary antibody, washed again with PBS-T, incubated with 1:5000 4′,6-diamidino-2-phenylindole, washed with PBS-T, and then mounted in Fluoro Gel with DABCO^{TM} (Electron Microscopy Science, Hatfield, PA, USA). Primary antibodies were visualized either by staining with fluorescence-conjugated secondary antibodies or by horseradish peroxidase-conjugated antibodies followed by TSA-Plus Cyanine 5 or Fluorescein antibodies, as per the manufacturer's instructions. Some sections were co-stained with fluorescein- or rhodamine-labeled Dolichos Biflorus Agglutinin (DBA; 1:100), both purchased from Vector Laboratories (Burlingame, CA, USA), to visualize the ureteric bud epithelium / collecting duct system. Immunostaining was visualized with a Leica DM2500 microscope and photographed with a Leica DFC 7000T camera using LAS X software. The list of antibodies and their dilutions used is shown in **Table 5**.

Table 5: Antibodies used for immunofluorescent staining

Target	Dilution	Company	Animal Source
Primary Antibodies			
α-c-Casp3	1:100	Cell Signaling Technologies	Rabbit
α-β-Cat Active	1:100	Cell Signaling Technologies	Rabbit
α-β-Cat Total	1:80	Cell Signaling Technologies	Rabbit
α-Emcn	1:50	Santa Cruz Biotechnology	Monoclonal Rat
α-Jag1	1:100	Cell Signaling Technologies	Rabbit
α-Lef1	1:100	Cell Signaling Technologies	Rabbit
α-Ncam1	1:100	Sigma Aldrich	Monoclonal Mouse
α-pHH3	1:100	Sigma Aldrich	Rabbit
α-Six2	1:100	Proteintech	Rabbit
α-Wt1	1:100	Thermo Fisher Scientific	Rabbit
Secondary Antibodies			
α-Mouse-488	1:100	Jackson ImmunoResearch Laboratories	Donkey
α-Mouse-594	1:100	Jackson ImmunoResearch Laboratories	Donkey
α-Rabbit-488	1:100	Jackson ImmunoResearch Laboratories	Donkey
α-Rabbit-594	1:100	Jackson ImmunoResearch Laboratories	Donkey
α-Rabbit-HRP	1:100	Sigma Aldrich	Goat

*Note: Cell Signaling Technologies, Danvers, MA, USA; Santa Cruz Biotechnology, Dallas, TX, USA

3.2.11 qPCR for mRNA expression analysis

As described in Chapter 2, except that *Actb* was used as the endogenous control. Primers used in these experiments are shown in **Table 1** and **Table 6**.

Table 6: Primers used for qPCR (2)

Gene	Forward	Reverse	Product Size (bp)
Actb	GGCTGTATTCCCCTCCATCG	CCAGTTGGTAACAATGCCATGT	154
Casp3	TGACTTCCTGTATGCTTACT	TTGCCACCTTCCTGTTAA	161
Casp8ap2	GAGCTTCCGTCTCAGGACAAA	GCCGTAATGTTTCACGTCATTC	135
Cited1	GTCTCCAGGTCTTACCACCGA	GCAGAGATGGCCACGTGTAT	155
Efna3	GTTCACCATGTACAGCACGTA	GGAACAGCTCCAATCAGCA	143
Fgf8	GCTAATTGCCAAGAGCAACG	GGTAGTTGAGGAACTCGAAGC	245
Hey1	AAGTCGCCAGTAAGTCAG	GTTCGTAATCACTACCTCAATT	174
Jag1	GTCTCCAGGTCTTACCACCGA	GCAGAGATGGCCACGTGTAT	144
Lef1	AGCTTGTTGAAACCCCAGAC	TTTTTGGAAGTCGGCGCTTG	160
Lhx1	CTACATCATAGACGAGAACAAG	TCATTACTACCACCTTCCTTAT	198
Ret	ACACTCAGCACTCCTCTA	AGCATTCTCAGCCACATAA	224
Six2	GCAGGACTCCATACTCAA	GATACCGAGCAGACCATT	215
Sox9	AAGGAAGGAAGGAAGGAAG	AGGCACAGTGAATGTTCTA	201
Vegfr2	GAGAGGTGCTGCTTAGAT	GAGAGTAGAGTCAACACATTC	164
Wnt4	TGGGAAGGTGGTGACACAAG	TGACCACTGGAAGCCCTGT	166

3.2.12 Western blot analysis of protein expression

Kidneys were harvested from P0 or P2 pups and dissociated in RIPA buffer (20mM Tris-HCl pH7.5; 150 mM NaCl; 1% Triton X-100; 1% sodium deoxycholate, and 1% SDS) using the Sonic Dismembrator Model 100 (Fisher Scientific). The protein concentration of extracts was determined using the Pierce™ BCA Protein Assay Kit (Thermo Fisher Scientific), as per manufacturer's instructions, and the SpectraMax® i3 plate reader (Molecular Devices). 10µg, 20µg, or 40µg from each sample was run on a reducing 8%, 10%, or 12% SDS-PAGE gel or on a 4-20% Mini-PROTEAN® TGX™ Precast protein gel (Bio-Rad) and blotted to an ImmunoBlot polyvinylidene difluoride membrane (Bio-Rad) using a Trans-Blot SD Semi-Dry Transfer Cell (Bio-Rad). The list of antibodies used is shown in **Table 7**. The signals were developed on CL-Xposure™ Film (Thermo Fisher Scientific) using either the Pierce™ ECL Western Blotting Substrate (Thermo Fisher Scientific), Pierce™ ECL Plus Western Blotting Substrate (Thermo Fisher Scientific), or SuperSignal™ West Femto Maximum Sensitivity Substrate (Thermo Fisher Scientific). Densitometric analysis of bands was performed using Image J software.

Table 7: Antibodies used for Western blot

Target	Dilution	Company	Animal Source
Primary Antibodies			
α-β-Act	1:5000	Cell Signaling Technologies	Rabbit
α-c-Casp8 p18	1:1000	Santa Cruz Biotechnology	Rabbit
α-Hif-1α	1:250	Novus Biologicals	Monoclonal Mouse
α-Jag1	1:1000	Cell Signaling Technologies	Rabbit
α-Lef1	1:1000	Cell Signaling Technologies	Rabbit
α-Six2	1:1200	Proteintech	Rabbit
α-β-Tub	1:1000	Sigma Aldrich	Monoclonal Mouse
α-α/β-Tub	1:1000	Cell Signaling Technologies	Rabbit
Secondary Antibodies			
α-Mouse-HRP	1:3000	Cell Signaling Technologies	Horse
α-Rabbit-HRP	1:4000 or 1:8000 for α-Six2	Sigma Aldrich	Goat

*Note: Novus Biologicals, Centennial, CO, USA

3.2.13 MitoSOX analysis of mitochondrial function

Kidneys were dissected from P1 *miR-210* WT, HET, and KO mice. The kidneys were broken into small pieces with a razor and then placed in 500µL 0.3% collagenase in PBS. Kidneys were incubated with collagenase for 10min at 37ºC with agitation. The homogenized tissue was run through 18G then 25G needles to further break up tissue. The cell suspension was transferred to a 50mL tube with 5mL of 2% FBS (fetal bovine serum) in PBS and centrifuged for 5min at 500 g. The supernatant was removed and the cells were resuspended in 500µL 2% FBA/PBS. Cells were counted using a hemocytometer, resuspended to 1 x 10^6 cells, and stained with 5mM MitoSOX™ Red Mitochondrial Superoxide Indicator (Thermo Fisher Scientific) for 15 minutes at 37ºC per manufacturer's guidelines. Cells were analyzed on a BD LSRFORTESSA cell analyzer (BD Biosciences, San Jose, Ca, USA) through the Flow Cytometry Core at the Rangos Research Center located at the UPMC Children's Hospital of Pittsburgh. Mean fluorescent intensity was determined using FlowJo software (v10.1; Becton, Dickinson and Company, Franklin Lakes, NJ, USA).

3.2.14 qPCR analysis of mitochondrial number

DNA from P0 kidneys was isolated using Qiagen DNA Easy Blood and Tissue Kit, as per manufacturer instructions. To determine the amount of mitochondrial and nuclear DNA, *Co1* and *Ndufv1* expression levels were analyzed, respectively. qPCR was performed in a 96 well C100 Thermal Cycler (Bio-Rad) using Sso Advanced SYBR Green Master Mix (Thermo Fisher Scientific). Primers for mitochondrial DNA gene *Co1* (F 5'-TGCTAGCCGCAGGCATTAC-3' and R 5'-GGTGCCCAAAGAATCAGAAC-3') and nuclear gene *Ndufv1* (F 5'-CTCCCACTGGCCTCAAG-3' and R 5'-CCAAAACCCAGTGATCCAGC-3') were used. Expression levels were normalized to the endogenous control (*Actb*) and analyzed using the $2^{-\Delta\Delta C}{}_T$ method (184).

3.2.15 *in situ* hybridization analysis of RNA expression

Kidneys were harvested from P2 pups and fixed in 4% PFA/PBS overnight at 4ºC. The kidneys were rinsed with PBS, incubated with 30% sucrose/PBS overnight at 4ºC, embedded in optimal cutting temperature compound (OCT) (Scigen Scientific Inc., Carson, CA, USA), and stored at -80 ºC. The OCT-embedded kidneys were sectioned at 10-12mm using the Microm HM 550 cryo-tome (Thermo Fisher Scientific) and affixed to Fisherbrand® Superfrost Plus Microscope Slides, Precleaned (Thermo Fischer Scientific). The sections were fixed in fresh 4% PFA/PBS for 10min, rinsed with PBS, and permeabilized with 15µg/mL Proteinase K for 10min. The sections were rinsed with PBS and refixed with 4% PFA/PBS for 5min. The sections were acetylated for 10min in a solution of 1.5% Triethanolamine, 0.02M hydrochloric acid, and 0.375% acetic anhydride. The sections were rinsed with PBS and blocked with hybridization buffer (50% formamide, 1.3X standard saline citrate (SSC) pH 4.5, 5mM EDTA pH 8.0, 50mg/mL yeast tRNA, 0.2% Tween-20, 0.5% CHAPS, 100mg/mL Heparin) for 2hr. The *Wnt9b* Digoxigenin-labelled probe (prepared as in (144) with forward primer 5'-GTCTTTGCCAAGTCTGCCTC-3' and reverse primer 5'-CGATGTTAATACGACTCACTATAGGGGC-3') was diluted 1:250 in hybridization buffer and heated at 80ºC for 5min, before incubating the sections with the probe solution at 68ºC overnight. The sections were rinsed with 0.2X SSC and NTT (0.15M NaCl, 0.1M

Tris pH 7.5, 0.1% Tween-20) and then blocked with 5% heat inactivated sheep serum in 2% blocking reagent (Roche, Basel, Switzerland)/NTT for 2hr. Sections were then incubated with 1:2500 anti-Digoxigenin-AP antibody (Roche) in 1% heat inactivated sheep serum in 2% blocking reagent/NTT at 4ºC overnight. Sections were rinsed with NTT and NTTML (0.15M NaCl, 0.1M Tris pH 9.5, 0.1% Tween-20, 50mM $MgCl_2$, and 2mM Levamisole) then incubated with BM Purple (Roche) at room temperature until color developed (~48hrs). The sections were rinsed with PBS, fixed with 4%PFA/PBS with 0.2% glutaraldehyde for 1hr, rinsed, and mounted in Cytoseal™ 280 (Richard-Allan Scientific, San Diego, CA, USA). The sections were visualized with a Leica DM2500 microscope and photographed with a Leica DFC 7000T camera using LAS X software.

3.2.16 Semi-quantitative analysis of differentiation

To estimate the number of Lef1 and Jag1 staining for differentiating structures, kidney sections stained with Lef1 or Jag1 were imaged around the whole kidney section (9-14 images per section) and the number of Lef1- or Jag1-positive differentiating structures was quantified per image using Image J. This semi-quantitative analysis was performed in a blinded manner.

3.2.17 Nephron number estimation at P2

Kidneys were harvested from mice at P2, fixed in 4% PFA/PBS and serially sectioned at 4µm. Slides every 40µm (10 sections) were stained with an antibody for Wilms tumor 1 (Wt1), which marks glomeruli (206), using the Vector® DAB kit (Vector Laboratories, Burlingame, CA, USA) as per manufacturer's instructions. A pair of consecutive sections out of every 10 sections was analyzed using a Walcom drawing tablet (Walcom, Portland, OR, USA) and Stereoinvestigator version 9.04 software, using a physical fractionator probe (MBF Bioscience, Williston, VT, USA). The total glomerular number (N_{glom}) was calculated using the following equation:

$$N_{glom} = \frac{\Sigma Q^-}{2} x \frac{A}{a} \; x \frac{1}{ASF}$$

where N_{glom} is the total of glomeruli in the entire kidney, ΣQ^- is the total number of glomeruli appearing and disappearing between two consecutive sections, A is the grid size (600x600), a is the counting frame size (400x400), and $1/ASF$ is the reciprocal of the section-sampling fraction (the number of sections advanced between section pairs; 10). This was performed as described in (205, 207).

3.2.18 Semi-quantitative analysis of ureteric branching

To estimate the number of ureteric branch tips, kidney sections stained with DBA were imaged around the whole kidney section (9-14 images per section) and the number of DBA-positive ureteric tips was quantified per image using Image J. This semi-quantitative analysis was performed in a blinded manner.

3.2.19 Semi-quantitative analysis of proliferating nephron progenitors

To estimate the number of proliferating cells, kidney sections were stained for pHH3 expression. Nephron progenitors were visualized by co-staining with α-Six2 antibodies. Stained sections were imaged around the whole kidney section (9-14 images per section) and the percentage of pHH3-positive nephron progenitor cells per image was quantified using ImageJ. This semi-quantitative analysis was performed in a blinded manner.

3.2.20 Semi-quantitative analysis of apoptotic cells

To estimate the number of apoptotic cells, kidney sections were stained for cleaved Caspase-3 (c-Casp3) expression. Nephron progenitors were visualized by co-staining with α-Six2 antibody. Differentiated developing nephron structures were visualized by co-staining with α-Jag1 antibody. Stained sections were imaged around the whole kidney section (9-14 images per section) and the percentage of c-Casp3-positive nephron progenitor cells or developing nephron structure

cells per image was quantified using ImageJ. This semi-quantitative analysis was performed in a blinded manner.

3.2.21 Statistical analysis

All experiments were performed with at least three biological replicates collected from multiple litters. Mann-Whitney U test and two-way ANOVA with Tukey correction were used to determine statistical significance where applicable: $*P \leq 0.05$; $**P \leq 0.01$; and $***P \leq 0.001$. All statistical analyses were performed using Prism 8 software package (GraphPad Software, Inc.).

3.3 Results

3.3.1 *miR-210* expression throughout kidney development

To determine if there is differential expression of *miR-210* during kidney development, its expression was measured in early (E14.5), mid (P0), and late (P2) nephrogenesis. Kidneys from CD-1 wildtype mice were dissected and all from one litter were pooled and nephron progenitors from the pooled kidney homogenates were isolated using MACS with magnetic beads conjugated to streptavidin and biotinylated α-Itgα8 antibodies. RNA expression was analyzed in whole kidney and isolated nephron progenitors using qPCR. *miR-210-3p* expression in whole kidney was low in E14.5 kidneys but increased about 5-fold by P0 (**Figure 15A**). While not statistically significant, a similar trend of increased *miR-210-3p* expression in isolated nephron progenitors was observed (**Figure 15B**). *miR-210-3p* expression was only significantly increased from E14.5 to P0 when comparing expression in whole kidney, suggesting that its expression increases in multiple cell compartments during kidney development. Unfortunately, assessment of the localized pattern of *miR-210* expression in developing kidney tissue was using *in situ* hybridization was not possible (data not shown). As expected, since it is the passenger strand and readily degraded, *miR-210-5p* expression was undetectable (data not shown). To investigate expression in another mouse strain,

kidneys from P0 and P2 C57Bl/6 male and female mice (strain more commonly used for kidney development research) were analyzed for *miR-210-3p* expression. There were no significant differences between male and female P0 and P2 kidneys, but there was highly variable expression at P0 that suggests higher expression than at P2 (**Figure 15C**). It is possible that *miR-210-3p* expression decreases from P0 to P2 due to further development of the renal vasculature, thus decreasing hypoxia-induced gene expression.

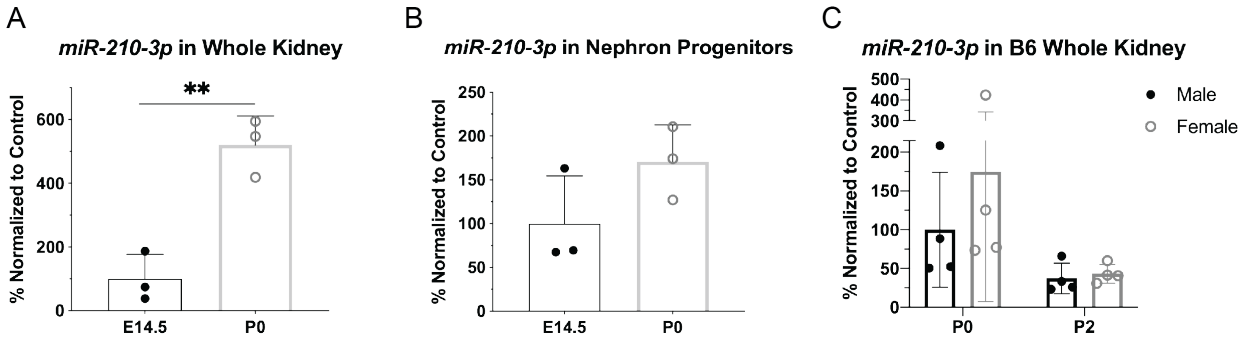

Figure 15: *miR-210* expression peaks at P0

(A) qPCR analysis of *miR-210-3p* expression in CD1 E14.5 and P0 kidneys. (B) qPCR analysis of *miR-210-3p* expression in CD1 E14.5 and P0 MACS-isolated nephron progenitors. (C) qPCR analysis of *miR-210-3p* expression in P0 and P2 WT male and female kidneys from *miR-210* HET matings. RNA expression was normalized to *U6* snRNA. Error bars ± SEM, $^{**}P<0.01$, (A-B) Mann-Whitney U test, (A) $N \geq 3$ kidneys per embryonic age, (B) $N \geq 3$ pooled kidneys from one litter per embryonic age, (C) 2-way ANOVA with Tukey correction, $N \geq 3$ kidneys per embryonic age. Samples in (A) and (B) prepared by Andrew Clugston (Dr. Dennis Kotska, Department of Developmental Biology; Dr. Jacqueline Ho Laboratory, Department of Pediatrics, University of Pittsburgh, Pittsburgh, PA) (208)

3.3.2 *miR-210* knockout mouse model

Then the function of *miR-210* in kidney development was investigated using a mouse knockout model. In collaboration with Dr. Yoel Sadovsky and Dr. Xin Huang (Department of Obstetrics, Gynecology, and Reproductive Sciences, University of Pittsburgh, Pittsburgh, PA), the global *miR-210* knockout (KO) model (202) was obtained and *miR-210* KO expression validated in P2 male and female kidneys (**Figure 16**).

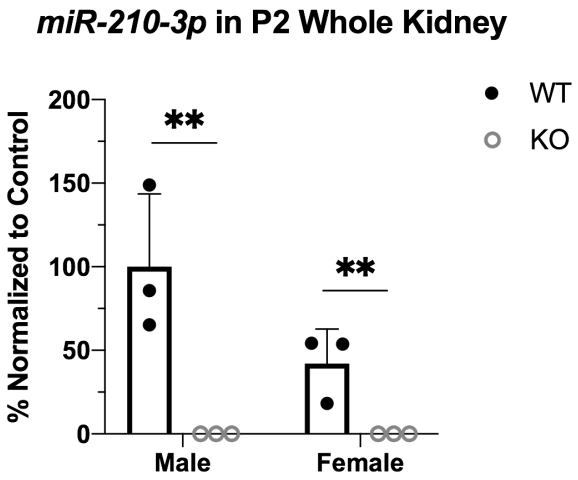

Figure 16: *miR-210* knockout model validation

qPCR analysis of *miR-210-3p* expression in P2 *miR-210* WT and KO male and female kidneys, normalized to *U6* snRNA expression. $^{**}P<0.01$, Error bars ± SEM, Mann-Whitney U test. $N \geq 3$ kidneys per embryonic age and genotype. (208)

3.3.3 *miR-210* KO sex-specific nephron deficit

Nephron number is determined during kidney development by a variety of factors, including the balance of nephron progenitor self-renewal versus differentiation. Thus, the major readout of determining if a gene mutation results in abnormal kidney development is an alteration in nephron number. *miR-210* is expressed in whole kidney and nephron progenitors throughout kidney development, thus it may play a role in regulating nephron number.

To test the overall effect of *miR-210* deletion on kidney development, the physical disector/fractionator combination method (205) was used to determine nephron number at postnatal day 30 (P30). Representative images of hematoxylin and eosin (H&E) staining of male (**Figure 17A-B**) and female (**Figure 17C-D**) paraffin-embedded kidneys showed no gross tissue pathology. Male *miR-210* KO mice had an approximately 35% reduction in nephron number compared to *miR-210* WT male mice (**Figure 17E**). There was an approximately 28% reduction in nephron number of both *miR-210* WT and KO female mice compared to *miR-210* WT male mice, but no difference between WT and KO females. This decrease in nephron number did not coincide with gross changes in glomerular size ((**Figure 17A-D**). The kidney:body mass ratio was not affected by global *miR-210* KO (**Figure 17F**), which suggests that the reduction in nephron

number is not due to an overall effect of the gene deletion on development. At P30, *miR-210* KO mice did not have reduced body mass, but female WT and KO mice did (**Figure 18A**). When comparing kidney mass and length, *miR-210* KO females had a decrease in both compared to male KO (**Figure 18B-C**).

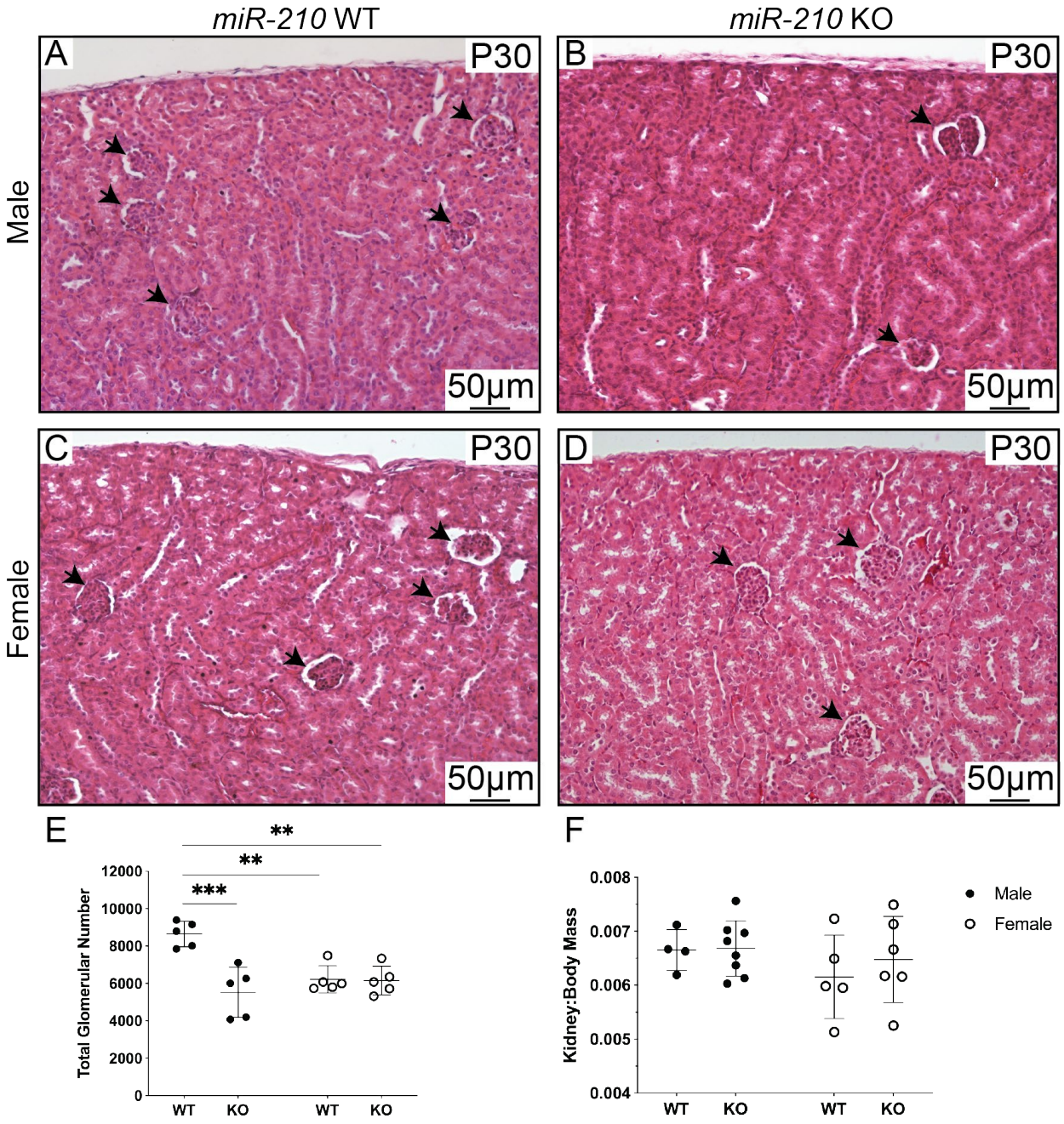

Figure 17: Decreased nephron number in *miR-210* KO mice

(A-D) Representative images of H&E stained sections for *miR-210* (A,C) WT and (B,D) KO (A-B) male and (C-D) female mice used for glomerular counting. Glomeruli are marked with black arrows. (E) Nephron number of male and female *miR-210* WT and KO mice at P30. (F) Kidney:body mass ratio for male and female *miR-210* WT and KO mice at P30. (E-F) Representative images of H&E stained sections for female miR-210 WT and KO mice. ***P*<0.01, ****P*<0.001, Error bars ± SEM, 2-way ANOVA with Tukey correction. $N \geq 4$ per genotype and sex. (208)

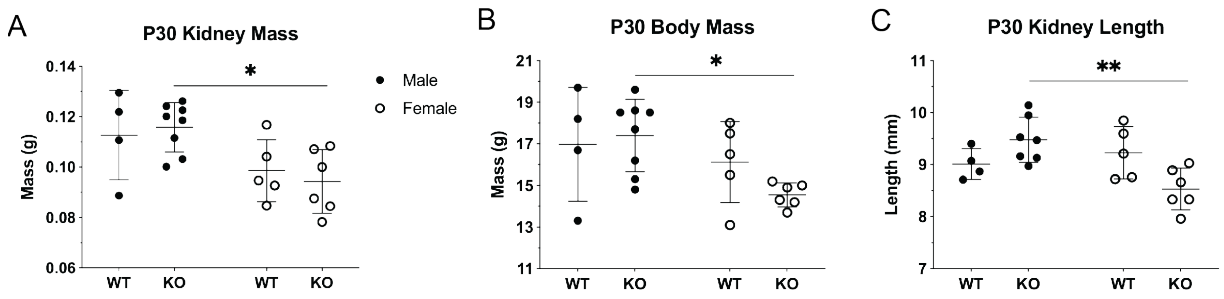

Figure 18: Gross phenotype of *miR-210* KO mice

(A) Kidney mass of *miR-210* WT and KO male and female mice at P30. (B) Body mass. (C) Kidney length. **P*<0.05, ***P*<0.01, Error bars ± SEM, 2-way ANOVA with Tukey correction. $N \geq 4$ per genotype and sex. (208)

3.3.4 Decrease in nephron number from *miR-210* deletion is not dependent on HIF during normoxic kidney development

Since both Six2 and HIF are important factors that regulate kidney development and bind the *miR-210* promoter, it is important to determine how much of the *miR-210*-mediated decrease in nephron number is due to HIF-dependent regulation of *miR-210*. Thus, a mouse model with a global deletion of the HRE in the *miR-210* promoter was obtained (*miR-210 HRE* KO mouse model, unpublished, provided by Xin Huang, formerly of the Department of Obstetrics, Gynecology, and Reproductive Sciences, University of Pittsburgh, Pittsburgh, PA). In this model, all regulation of *miR-210* at its promoter is preserved except for that performed by HIF. As with the *miR-210* knockout model, the physical disector/fractionator combination method (205) was used to determine nephron number in *miR-210 HRE* knockout model at postnatal day 30 (P30). Neither the male nor female *miR-210 HRE* KO mice had a nephron deficit (**Figure 19A**). Representative images of H&E staining of male (**Figure 19B-C**) and female (**Figure 19E-F**) P30 kidney sections showed no gross tissue pathology. However the kidney:body mass ratio was decreased in male KO mice, compared to WT (**Figure 19D**), which may be a result of several WT males with low body mass, but normal kidney size (**Figure 19G-I**). Thus, *miR-210* may be regulated by other transcription factors in addition to HIF during kidney development to ensure normal nephron number formation. It is also possible that these *miR-210 HRE* KO mice would be more susceptible to a nephron deficit when exposed to intrauterine hypoxia.

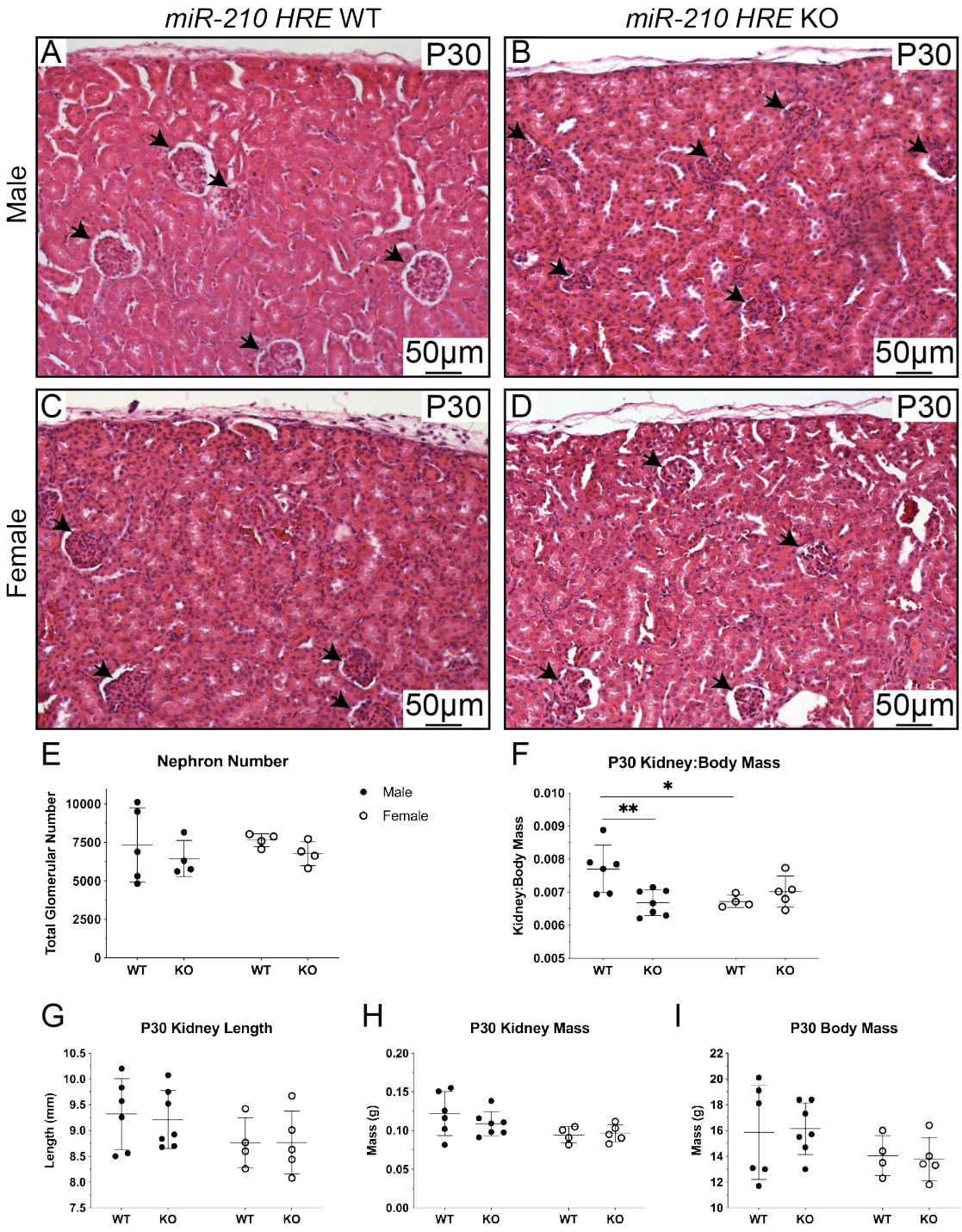

Figure 19: Nephron number in *miR-210 HRE* KO mice

(A-D) Representative images of H&E stained sections *miR-210 HRE* (A,C) WT and (B,D) KO (A-B) male and (C-D) female mice used for glomerular counting. Glomeruli are marked with black arrows. (E) Nephron number of male and female *miR-210 HRE* WT and KO mice at P30. (F) Kidney:body mass ratio. (G) Kidney length. (H) Kidney mass. (I) Body mass. *P<0.05, **P<0.01, Error bars ± SEM, 2-way ANOVA with Tukey correction. $N \geq 4$ per genotype and sex.

3.3.5 3-month miR-210 KO kidneys have normal function and histology

Since the *miR-210* KO mice had a 35% reduction in nephron number, kidney histology and function were assessed at 3-months of age to determine if the nephron deficit increased risk for development of renal pathology with age. Trichome and PAS staining of male and female *miR-210* WT and KO kidneys showed normal tissue histology (**Figure 20A-H**). That is, there is no increase in fibrosis in KO mice (**Figure 20A-D**) and the tubular lumens and basement membranes are intact (**Figure 20E-H**). As expected, WT and KO females had smaller body mass than WT and KO males (**Figure 20I**). However, there was no difference in kidney size nor the body to kidney mass ratio (**Figure 20J-K**). Serum analysis of kidney function, as measured by blood urea nitrogen and creatinine levels, showed no differences (**Figure 20L-M**). The urine albumin to creatinine ratio showed no difference in kidney function (**Figure 20N**). Together, this suggests that *miR-210* KO mice did not exhibit any signs of compromised kidney function or disease at 3-months of age. However, 3 months is still a young age and the 35% nephron deficit is relatively mild. Aging the mice further to 12-months-old or stressing the mice (e.g. high-salt diet, ischemia-reperfusion injury) might be required to determine if KO mice have a sex-specific increased risk for developing kidney disease.

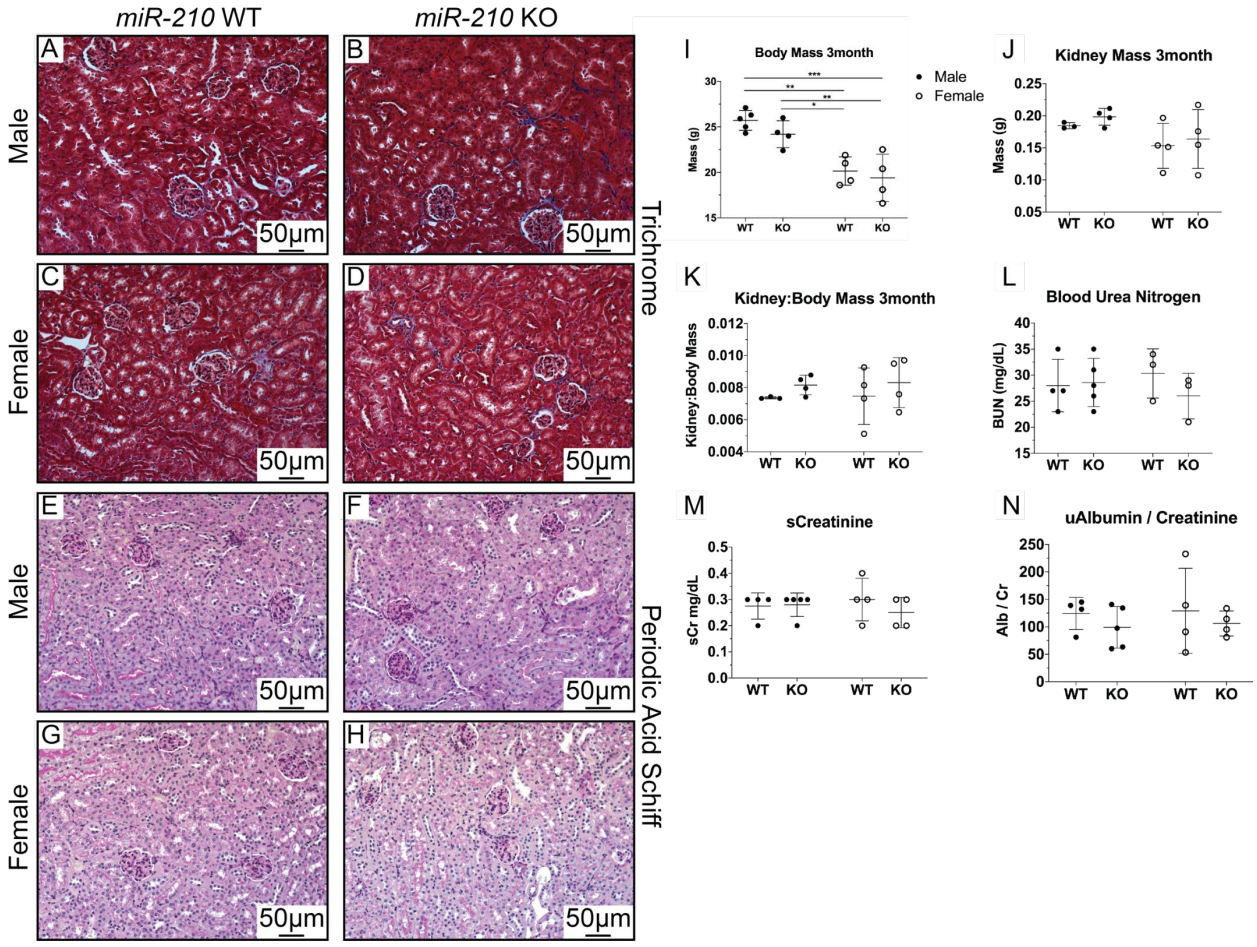

Figure 20: 3-month-old *miR-210* WT and KO kidney histology and renal function are normal

(A-D) Trichrome staining of 3-month-old (A-B) male and (C-D) female *miR-210* (A,C) WT and (B,D) KO mice. (E-H) PAS staining of (E-F) male and (G-H) female *miR-210* (E,G) WT and (F,H) KO mice. (I) Body mass. (J) Kidney mass. (K) Kidney:body mass ratio. (L) Blood urea nitrogen levels. (M) Serum creatinine levels. (N) Urine albumin/creatinine ratio. **P*<0.05,***P*<0.01, ****P*<0.001, Error bars ± SEM, 2-way ANOVA with Tukey correction. $N \geq 3$ per genotype and sex. (208)

3.3.6 Kidney development at E16 is unaffected by *miR-210* KO

Since *miR-210* expression peaks at P0, kidney development was first assessed at E16 (two days before). H&E staining showed no difference between WT and KO tissue histology in male and female kidneys (**Figure 21**). Immunostaining for nephron progenitor marker Six2 and nephron progenitor marker and developing nephron structure marker Ncam (209) showed similar expression patterns in male WT and KO kidneys (**Figure 22A-B**). Immunostaining for Six2 and the Notch ligand Jag1 (expressed in differentiated nephron structures) showed normal expression in male WT and KO kidneys (**Figure 22C-D**). Thus, kidney development appears unaffected by *miR-210* deletion at E16.

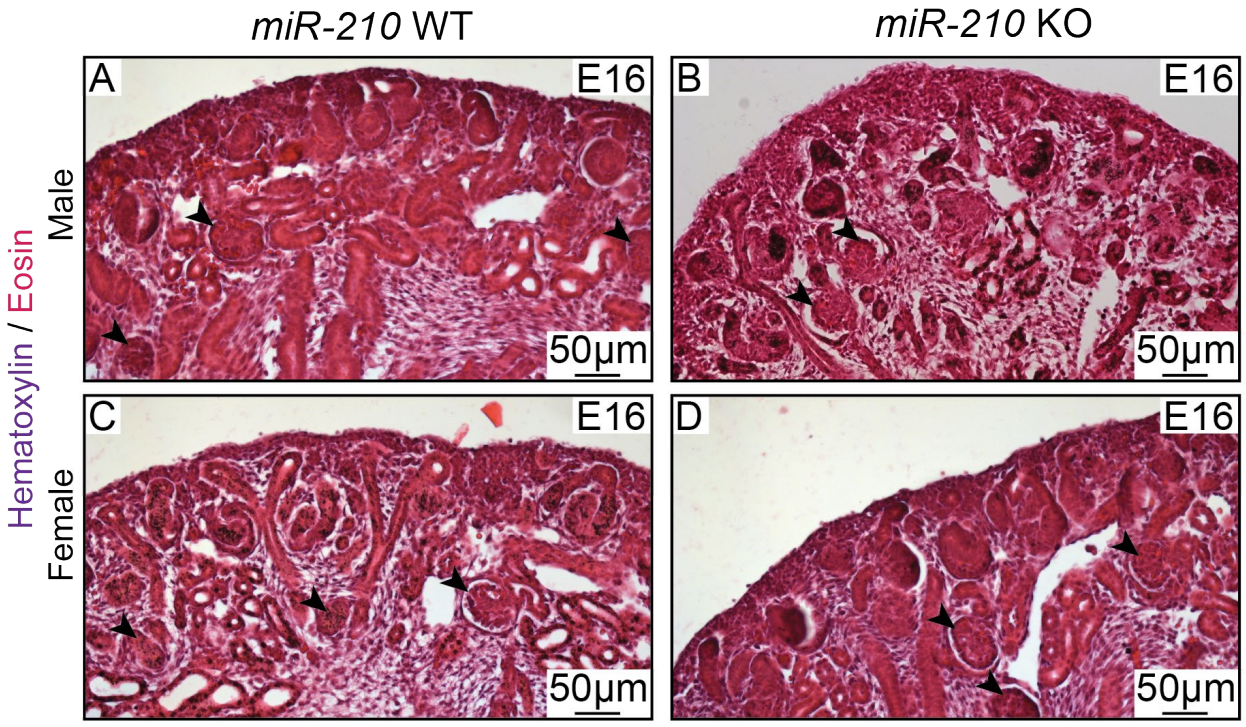

Figure 21: E16 *miR-210* KO kidneys have normal histology

(A-D) H&E staining of E16 (A-B) male and (C-D) female *miR-210* (A,C) WT and (B,D) KO kidneys. Glomeruli are marked with black arrows. $N \geq 2$ per genotype and sex.

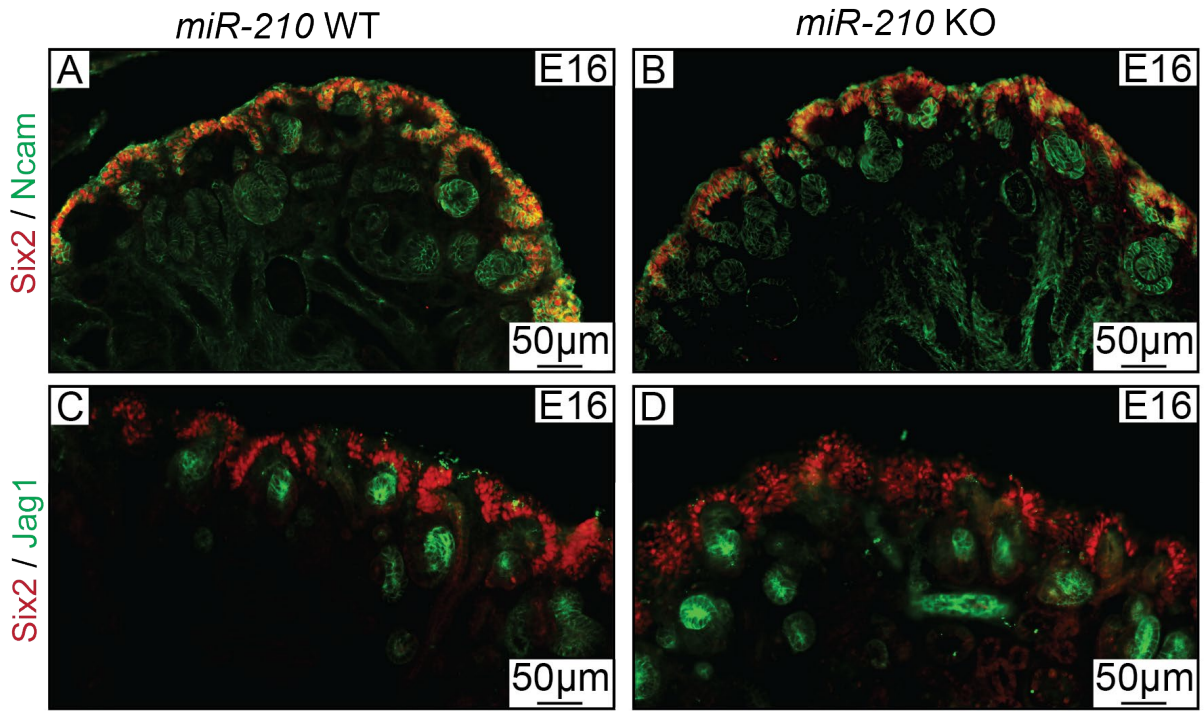

Figure 22: E16 male kidneys have normal expression of kidney development marker

(A-B) Immunofluorescent staining for nephron progenitor marker Six2 (red) and nephron progenitor and developing nephron structure marker Ncam (green) in E16 male (A) WT and (B) KO kidneys. (C-D) Immunofluorescent staining for Six2 (red) and developing nephron structure marker and Notch signaling ligand Jag1 (green) in E16 male (C) WT and (D) KO kidneys. $N \geq 2$ per genotype.

3.3.7 Kidney development appears normal at P0 in *miR-210* KO

To investigate the effect of *miR-210* deletion at the timepoint its expression increases during kidney development (i.e. P0), kidney development was assayed at P0. H&E staining showed normal histology in WT and KO male (**Figure 23A-B**) and female (**Figure 24A-B**) kidneys. Immunofluorescent staining for Six2 and Ncam showed a normal expression pattern in both WT and KO male (**Figure 23C-D**) and female (**Figure 24C-D**) kidneys. Further, Western blot analysis of Six2 expression in male kidneys showed no difference between WT and KO (**Figure 23I,K**). Analysis of Wnt/β-catenin signaling showed a normal expression pattern of its canonical downstream effector Lef1 (which is expressed in the differentiated nephron structures) in WT and KO male (**Figure 23E-F**) and female (**Figure 24E-F**) kidneys. Immunostaining for

Jag1 showed no expression differences between WT and KO male (**Figure 23G-H**) and female (**Figure 24G-H**) kidneys. Western blot analysis of Jag1 expression in male kidneys showed no differences between WT and KO (**Figure 23I-J**). Thus, kidney development appears unaffected by *miR-210* deletion at P0.

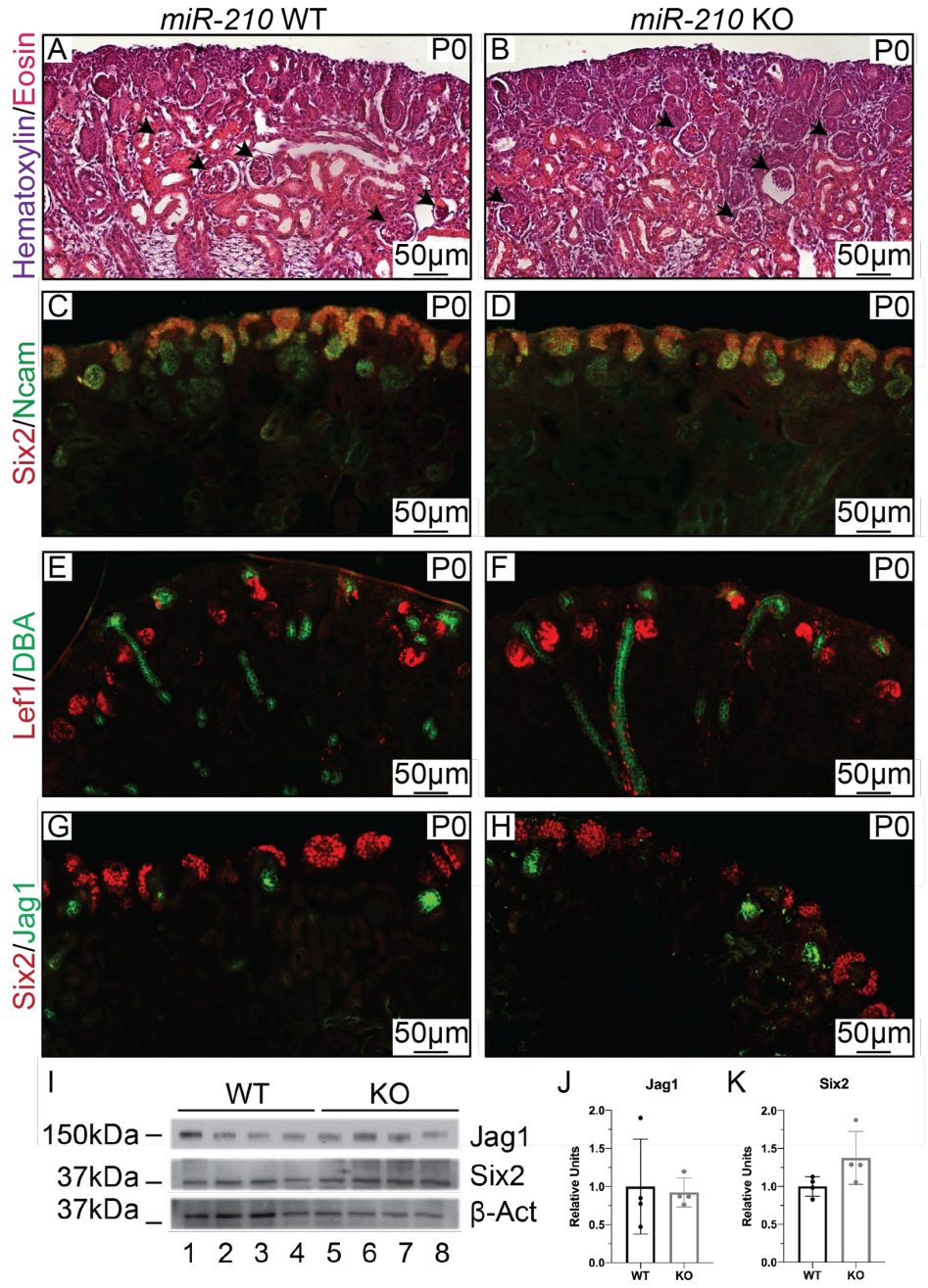

Figure 23: Kidney development is normal in P0 males

(A-B) H&E staining of P0 (A) WT and (KO) male kidneys. Glomeruli are marked with black arrows. (C-D) Immunofluorescent staining for nephron progenitor marker Six2 (red) and nephron progenitor and developing nephron structure marker Ncam (green) in (C) WT and (D) KO kidneys. (E-F) Immunofluorescent staining for Wnt/β-catenin signaling marker Lef1 (red) and ureteric bud marker DBA (green) in (E) WT and (F) KO kidneys. (G-H) Immunofluorescent staining for Six2 (red) and Notch signaling ligand Jag1 (green) in (G) WT and (H) KO kidneys. (I-K) Western blot analysis of (J) Jag1 and (K) Six2 expression, normalized to β-Act. Error bars ± SEM, Mann-Whitney U test. $N \geq 3$ per genotype. (208)

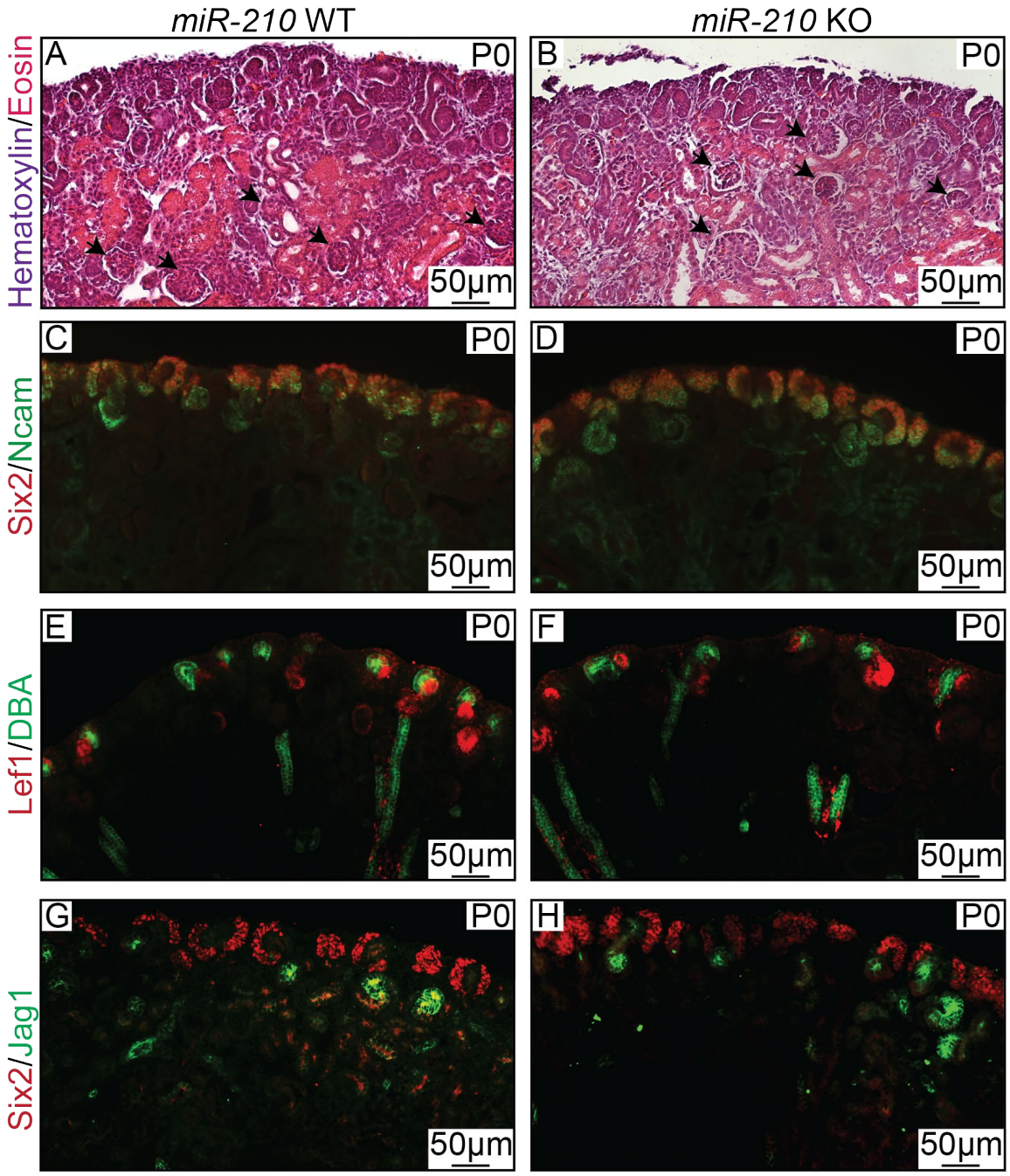

Figure 24: Kidney development is normal in P0 females

(A-B) H&E staining of P0 (A) WT and (KO) female kidneys. Glomeruli are marked with black arrows. (C-D) Immunofluorescent staining for nephron progenitor marker Six2 (red) and nephron progenitor and developing nephron structure marker Ncam (green) in (C) WT and (D) KO kidneys. (E-F) Immunofluorescent staining for Wnt/β-catenin signaling marker Lef1 (red) and ureteric bud marker DBA (green) in (E) WT and (F) KO kidneys. (G-H) Immunofluorescent staining for Six2 (red) and Notch signaling ligand Jag1 (green) in (G) WT and (H) KO kidneys. *N* ≥ 3 per genotype. (208)

3.3.8 HIF expression is unaffected in *miR-210* KO P0 kidneys

Since there is a regulatory feedback loop between HIF and *miR-210* (178, 210, 211), Hif1α expression could be perturbed by deletion of *miR-210* at the peak of *miR-210* expression during kidney development (i.e. P0). Western blot analysis of its expression in male and female WT and KO P0 kidneys showed no differences (**Figure 25**). Thus, deletion of *miR-210* had no significant effect on Hif1α expression.

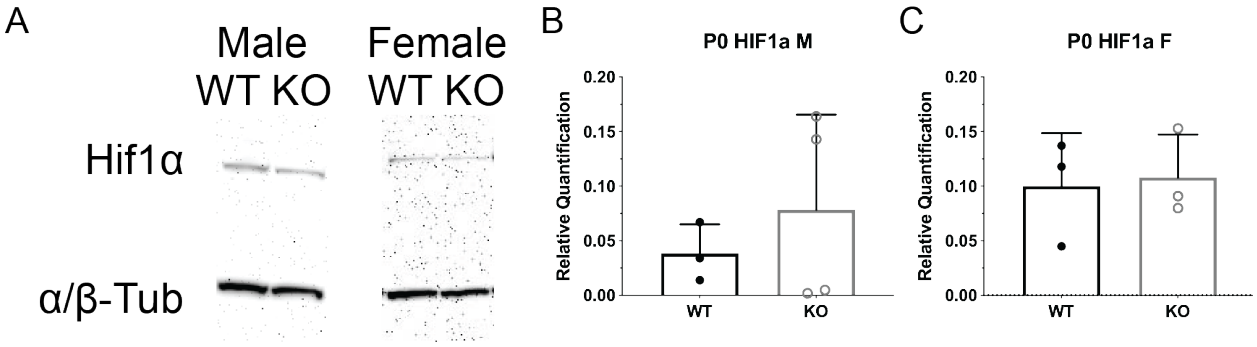

Figure 25: Hif1α expression is unaffected in P0 *miR-210* KO kidneys

(A) Representative images of Western blot for Hif1α and α/β-Tub in P0 *miR-210* WT and KO kidneys. (B-C) Quantification of expression of Hif1α normalized to α/β-Tub in (B) male and (C) female kidneys. Error bars ± SEM, Mann-Whitney U test. $N \geq 3$ per genotype and sex. Experiments performed by Dr. Kasey Cargill (formerly of Dr. Sunder Sims-Lucas Laboratory, Department of Pediatrics, University of Pittsburgh, Pittsburgh, PA).

3.3.9 Mitochondria are unaffected in *miR-210* KO in P0 and P1 kidneys

Since *miR-210* inhibits aerobic respiration by targeting several genes important for mitochondrial metabolism (148), mitochondria in *miR-210* KO kidneys were assayed. Mitochondrial function was unaffected in male and female *miR-210* KO P1 kidneys (**Figure 26A**). Further, analysis of mitochondrial number showed no difference between WT and KO male P0 kidneys (**Figure 26B**). Together, these data suggest that mitochondria number and function are unaffected by *miR-210* deletion.

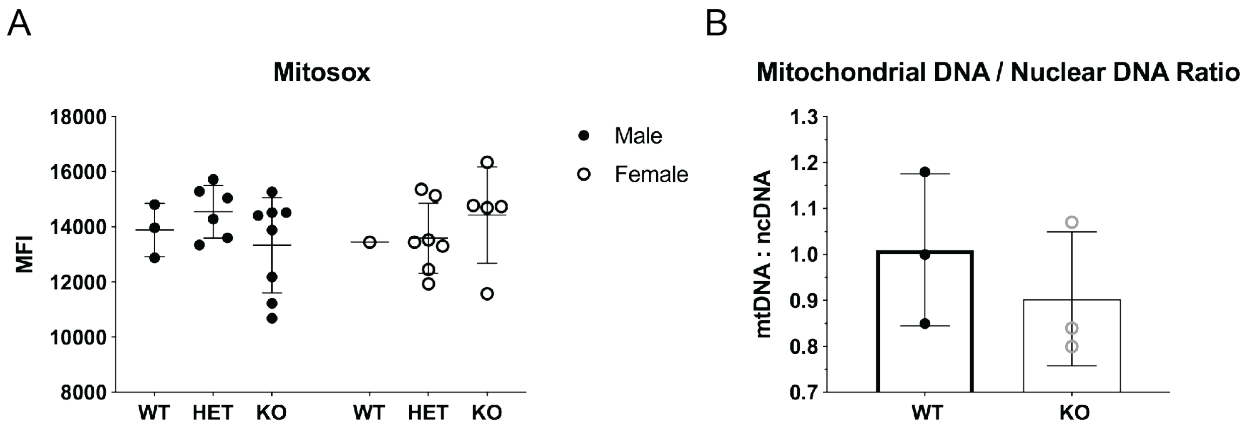

Figure 26: Metabolism is unaffcted by *miR-210* KO

(A) Mitosox analysis of mitochondrial function as measured by ROS production in P1 *miR-210* WT, HET, and KO kidneys. Error bars ± SEM, 2-way ANOVA with Tukey correction. (B) Assay of mitochondrial number through qPCR analysis of the mitochondrial DNA to nuclear DNA ration in male P0 WT and KO kidneys. Error bars ± SEM, Mann-Whitney U test. $N \geq 3$ per genotype and sex. Experiments performed by Dr. Kasey Cargill (formerly of Dr. Sunder Sims-Lucas Laboratory, Department of Pediatrics, University of Pittsburgh, Pittsburgh, PA).

3.3.10 Kidney development in P2 male kidneys is affected by *miR-210* KO

Since there was no apparent phenotype by P0 and about 50% of mouse nephrons form after birth (41, 51), kidney development was then assessed at P2. H&E staining showed normal histology of WT and KO male (**Figure 27A-B**) and female (**Figure 29A-B**) kidneys. Immunostaining for nephron progenitor markers Six2 and Ncam showed a normal expression pattern in both WT and KO male (**Figure 27C-D**) and female (**Figure 29C-D**) kidneys. qPCR analysis of expression of differentiation markers *Fgf8* and *Lhx1* suggested increased expression of the latter in KO male kidneys (**Figure 27I**). Interestingly, *Lhx1* is thought to function downstream of *Fgf8* as nephron progenitors form pre-tubular aggregates and then renal vesicles (46, 97, 212). Expression of these genes was not affected in KO female kidneys (**Figure 29I**).

Immunostaining for Wnt/β-catenin signaling marker Lef1 showed a normal expression pattern in both WT and KO male (**Figure 27E-F**) and female (**Figure 29E-F**) kidneys. Semi-quantitative analysis of the number of Lef1-positive developing nephron structures showed no significant difference between WT and KO male kidneys (**Figure 27N**). qPCR analysis showed no difference in *Wnt4* expression but did show increased expression of *Lef1* (**Figure 27I**). Note

that *Wnt4* is upstream of both *Lef1* and *Lhx1* (46, 97, 212), so their increase in expression occurs downstream of *Wnt4*. Western blot analysis of Lef1 protein expression corroborated this finding (**Figure 27J-K**). This increase in Lef1 expression does not appear to be due to increased expression in the peri-ureteric bud stroma (**Figure 31A-B**). Furthermore, *in situ* hybridization for *Wnt9b* (which is critical in inducing nephron formation) showed a normal ureteric bud tip expression pattern in both WT and KO male kidneys (**Figure 31C,D**), and immunostaining for total and active β-catenin showed no overt spatial differences in their expression patterns between male WT and KO kidneys (**Figure 28A-D**). qPCR analysis of female kidneys showed no difference in either *Wnt4* or *Lef1* (**Figure 29I**). Together, these data suggest that there is increased Wnt/β-catenin signaling in P2 KO male kidneys, which has been associated with impaired nephron formation (105, 213), although the spatial localization of components of this signaling pathway are preserved.

Since Notch signaling is required for priming nephron progenitors for differentiation (117), its activation in P2 kidneys was assayed. Immunostaining for Notch pathway ligand Jag1 showed a normal expression pattern in both WT and KO male (**Figure 27E-F**) and female (**Figure 29E-F**) kidneys. Semi-quantitative analysis of the number of Jag1-positive developing nephron structures showed no difference between WT and KO male kidneys (**Figure 27O**). qPCR analysis of *Jag1* and *Hey1* (the latter a downstream Notch signaling target) showed no difference between WT and KO in either male (**Figure 27I**) or female (**Figure 29I**) kidneys. Western blot analysis showed decreased Jag1 expression in male KO kidneys (**Figure 27L-M**). Together, these data suggest that while there is less Notch ligand expression in P2 male KO kidneys, the downstream activation of Notch signaling is not affected by deletion of *miR-210* in the whole kidney.

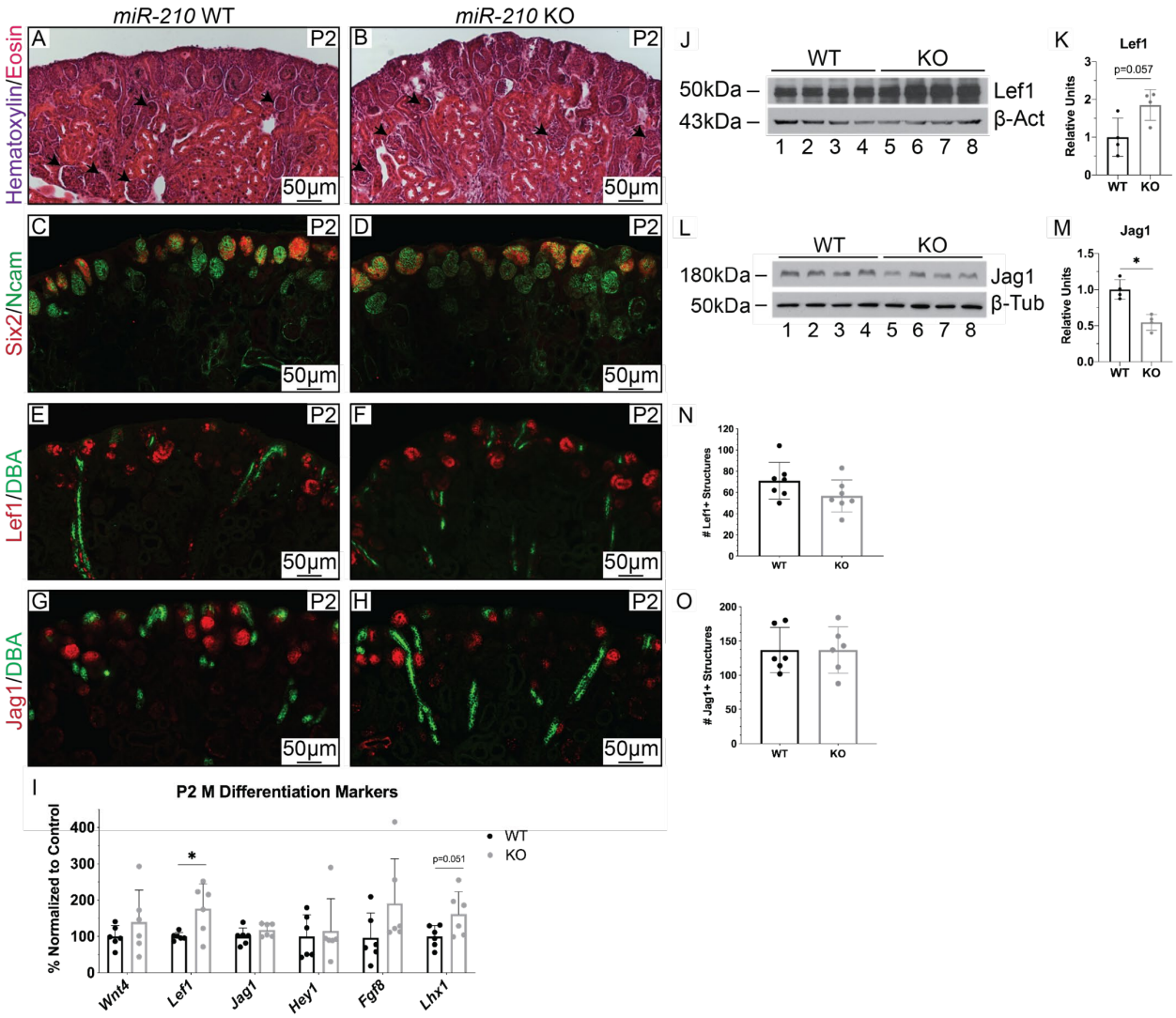

Figure 27: Dysregulation of differentiation markers in P2 male *miR-210* KO kidneys

(A-B) H&E staining of P2 (A) WT and (KO) male kidneys. Glomeruli are marked with black arrows. (C-D) Immunofluorescent staining for nephron progenitor marker Six2 (red) and developing nephron structure marker Ncam (green) in (C) WT and (D) KO kidneys. (E-F) Immunofluorescent staining for Wnt/β-catenin signaling marker Lef1 (red) and ureteric bud marker DBA (green) in (E) WT and (F) KO kidneys. (G-H) Immunofluorescent staining for Notch signaling ligand Jag1 (red) and DBA (green) in (G) WT and (H) KO kidneys. (I) qPCR analysis of expression of differentiation markers, normalized to *Actb* expression. (J-K) Western blot analysis of Lef1 expression, normalized to β-Act. (L-M) Western blot analysis of Jag1 expression, normalized to β-Tub. (N-O) Semiquantitative analysis of developing nephron structures that are positive for (N) Lef1 and (O) Jag1. *P<0.05, Error bars ± SEM, Mann-Whitney U test. $N \geq 3$ per genotype. (208)

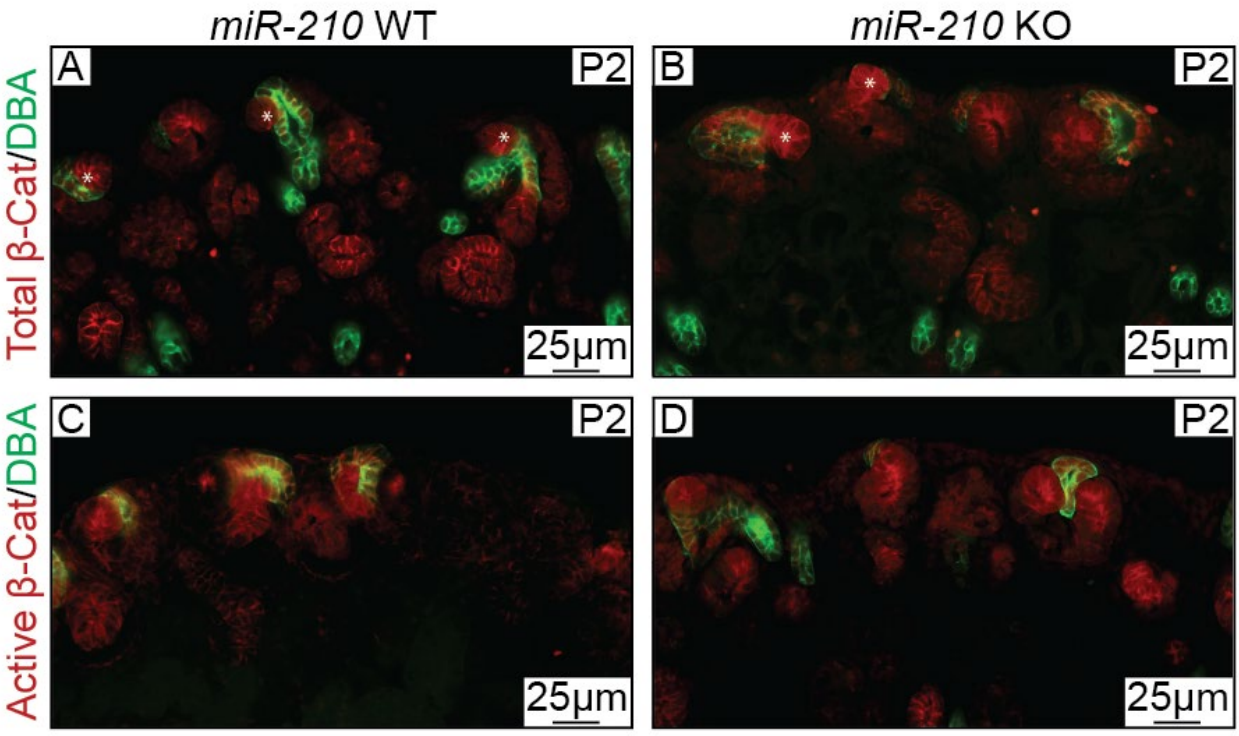

Figure 28: Expression of total and active β-catein in P2 male kidneys

(A-B) Immunofluorescent staining of total protein expression of Wnt/β-catenin signaling transducer β-catenin (red) and ureteric bud tip marker DBA (green) in P2 (A) WT and (B) KO male kidneys. White asterisks mark renal vesicles. (C-D) Immunofluorescent staining of active protein expression of Wnt/β-catenin signaling transducer β-catenin (red) and ureteric bud tip marker DBA (green) in P2 (C) WT and (D) KO male kidneys. $N \geq 3$ mice per genotype. (208)

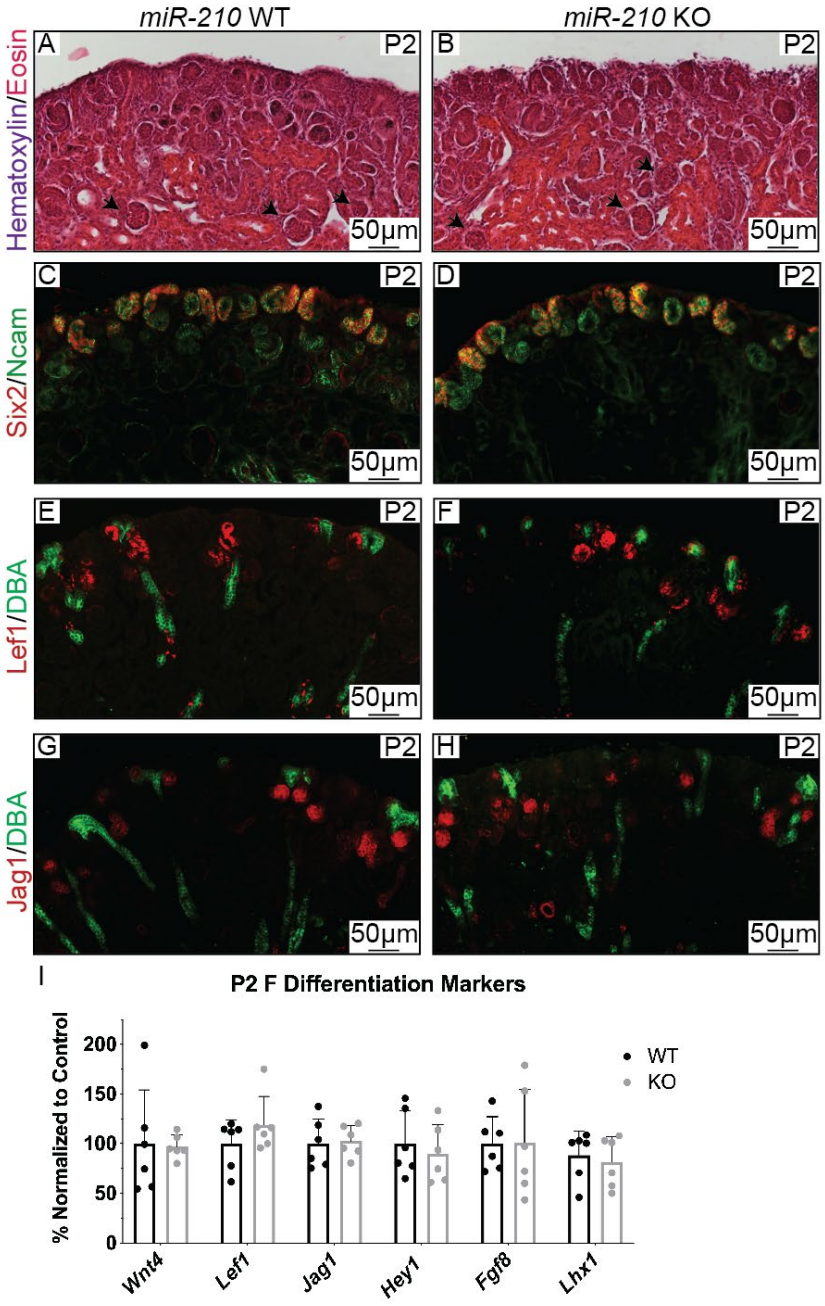

Figure 29: Expression of differentiation markers is normal in P2 females

(A-B) H&E staining of P2 (A) WT and (KO) female kidneys. Glomeruli are marked with black arrows. (C-D) Immunofluorescent staining for nephron progenitor marker Six2 (red) and developing nephron structure marker Ncam (green) in (C) WT and (D) KO kidneys. (E-F) Immunofluorescent staining for Wnt/β-catenin signaling marker Lef1 (red) and ureteric bud marker DBA (green) in (E) WT and (F) KO kidneys. (G-H) Immunofluorescent staining for Notch signaling ligand Jag1 (red) and DBA (green) in (G) WT and (H) KO kidneys. (I) qPCR analysis of expression of differentiation markers, normalized to *Actb* expression. Error bars ± SEM, Mann-Whitney U test. $N \geq 3$ per genotype. (208)

3.3.11 Nephron number not different at P2

Aberrant Wnt signaling results in impaired nephron progenitor differentiation (105) and was observed in male KO kidneys by P2. Thus, nephron number was examined at P2 to investigate the timing of the nephron deficit. Semi-quantitative analysis of the number of Lef1- and Jag1-positive developing nephron structures showed no significant differences between male WT and KO kidneys (**Figure 27N-O**). To perform a more robust analysis, the "gold standard" the physical disector/fractionator combination method (205) was used to quantify nephron number. No difference in Wt1-positive glomeruli was observed in WT and KO male and female P2 kidneys (**Figure 30**). Thus, the nephron deficit must not become apparent until after P2.

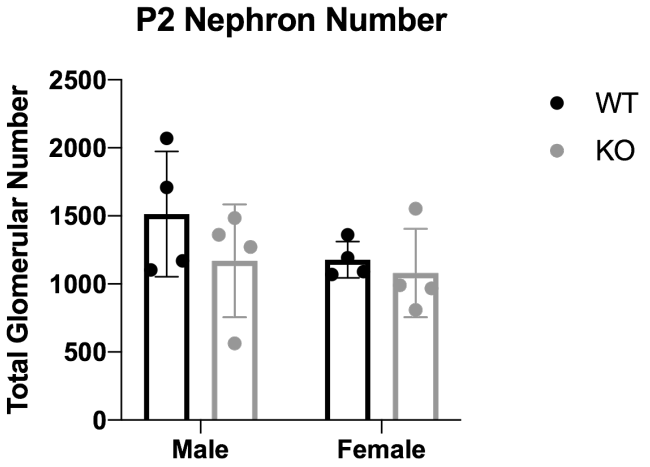

Figure 30: No difference in nephron number at P2

Nephron number of P2 male and female WT and KO kidneys. Error bars ± SEM, 2-way ANOVA with Tukey correction. $N \geq 4$ per genotype and sex. Experiment performed by Andrew J. Bodnar (Department of Pediatrics, University of Pittsburgh, Pittsburgh, PA).

3.3.12 Ureteric epithelium is normal at P2

Ureteric branching contributes to the determination of nephron number (214). Thus, altered ureteric epithelium development could contribute to the 35% nephron deficit observed in male KO kidneys. Analysis of expression of the Wnt/β-catenin signaling ligand expressed by the ureteric

bud tips *Wnt9b* showed no difference in expression between P2 WT and KO male kidneys (**Figure 31C-D**). qPCR analysis of the ureteric development makers *Ret* and *Sox9*, both of which mark the ureteric bud tips and are important for regulating ureteric branching (215) showed no difference in expression between WT and KO male (**Figure 31E**) and female (**Figure 31G**) P2 kidneys. Semi-quantitative analysis of the number of DBA-positive ureteric tips in P2 kidneys showed no difference between WT and KO male (**Figure 31F**) and female (**Figure 31H**) P2 kidneys. Together, these data suggest that *miR-210* deletion does not impact ureteric branching.

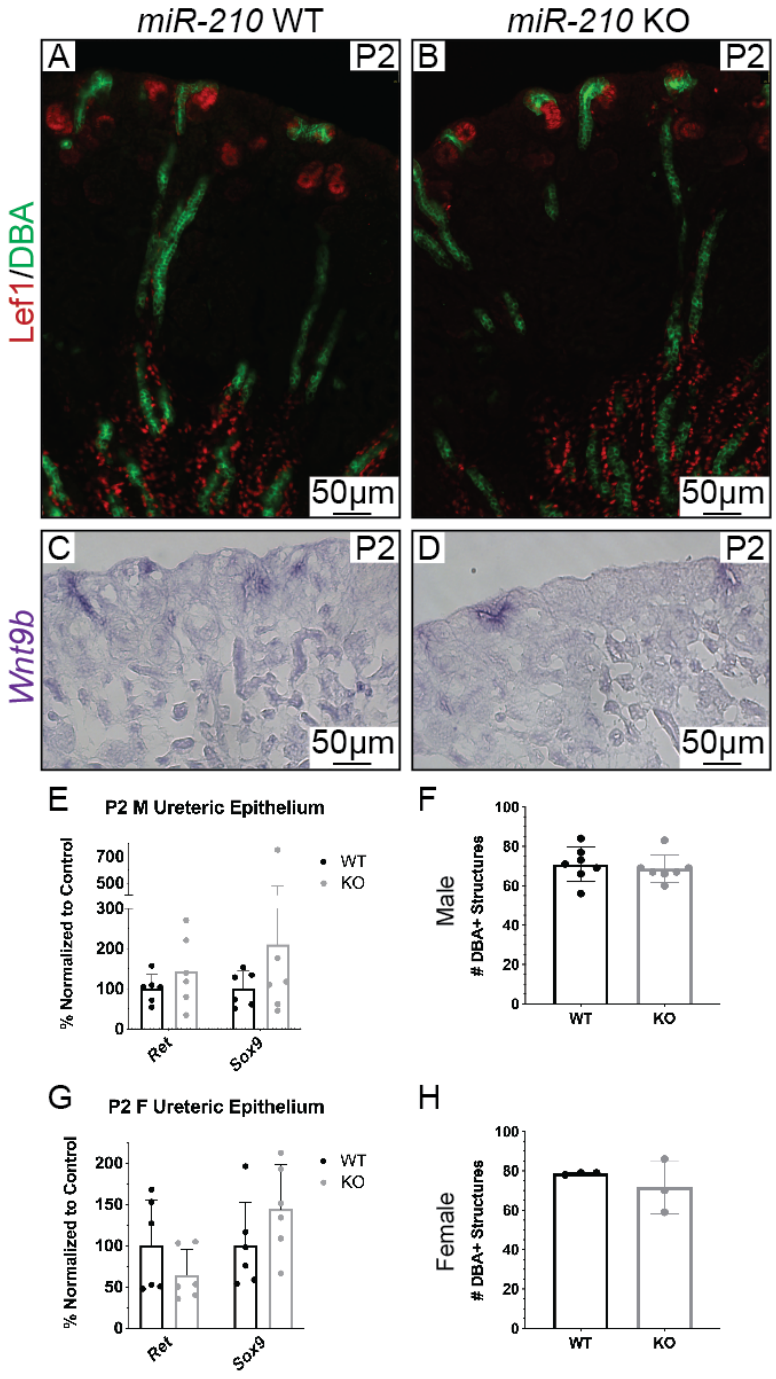

Figure 31: Ureteric development appears normal at P2

(A-B) Immunofluorescent staining for Wnt/β-catenin signaling marker Lef1 (red) and ureteric bud marker DBA (green) in P2 male (A) WT and (B) KO kidneys. (C-D) *in situ* hybridization for Wnt/β-catenin signaling ligand *Wnt9b* in P2 male (C) WT and (D) KO kidneys. (E,G) qPCR analysis of ureteric tip epithelium markers *Ret* and *Sox9,* normalized to *Actb* expression, in P2 WT and KO (E) male and (G) female kidneys. (F,H) Quantification of the number of DBA-positive ureteric bud tips in P2 WT and KO (F) male and (H) female kidneys. Error bars ± SEM, Mann-Whitney U test. $N \geq 3$ per genotype and sex. (208)

3.3.13 Renal vasculature is normal at P2

Since renal oxygenation contributes to regulating the balance of nephron progenitor self-renewal versus differentiation (69) and *miR-210* promotes angiogenesis, largely through inhibition of *Efna3*, an inhibitor of angiogenesis (149, 216, 217), deletion of *miR-210* could affect renal vasculature growth, and subsequently nephron number. Immunostaining for the vascular marker Emcn (218) and nephron progenitor and podocyte marker Wt1 (219) showed a normal expression pattern in WT and KO male (**Figure 32A-B,E-F**) and female (**Figure 32C-D,G-H)** P2 kidneys. Development of the glomerular vasculature also appeared normal (**Figure 32I-L**). qPCR analysis of vascular marker *Vegfr2* (220) and *Efna3* showed no differences between WT and KO male (**Figure 32M**) and female (**Figure 32N**) P2 kidneys. Thus, development of the renal vasculature does not appear to be affected by *miR-210* deletion.

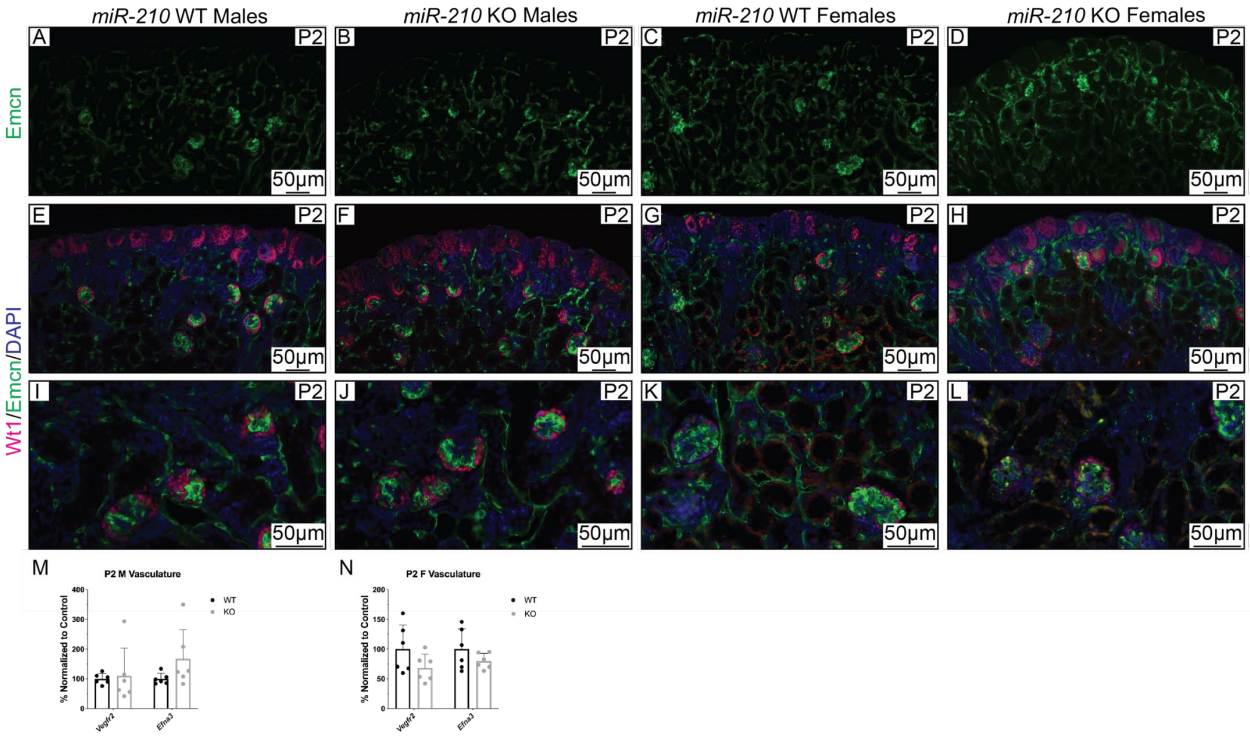

Figure 32: Renal vasculature development is normal at P2

(A-D) Immunofluorescent staining of endothelial marker Emcn (green) in P2 (A, C) WT and (B, D) KO (A-B) male and (C-D) female kidneys. (E-L) Immunofluorescent staining of nephron progenitor and podocyte makers Wt1 (red) in (E, G, I, K) WT and (F, H, J, L) KO (E-F, I-J) male and (G-H, K-L) female kidneys. (I-L) Zoomed view of glomeruli. (M-N) qPCR analysis of expression of endothelial marker *Vegf2* and anti-angiogenic *miR-210* target gene Efna3 in P2 (M) male and (N) female kidneys, normalized to *Actb* expression. Error bars ± SEM, Mann-Whitney U test. N ≥ 3 per genotype and sex. (208)

3.3.14 Nephron progenitor proliferation is normal at P2

A shift in the balance of nephron progenitor self-renewal versus differentiation results in decreased nephron number (109, 221). *miR-210* has been shown to regulate various genes involved in cell cycle regulation (148, 222). Thus, *miR-210* KO kidneys could have a nephron deficit from altered nephron progenitor proliferation. To investigate this, immunostaining for nephron progenitor marker Six2 and proliferation marker pHH3 was performed in male (**Figure 33A-B**) and female (**Figure 33D-E**) P2 kidneys. Semi-quantitative analysis of the percentage of proliferating nephron progenitors showed no differences between WT and KO males (**Figure 33C**) and females (**Figure 33F**). Western blot analysis of Six2 expression in male P2 kidneys showed no difference between WT and KO (**Figure 33G-H**). qPCR analysis of *Six2* and self-renewing nephron progenitor marker *Cited1* showed no difference in expression between WT and KO male (**Figure 33I**) and female (**Figure 33J**) P2 kidneys. Together, these data suggest that *miR-210* deletion does not impact nephron progenitor proliferation.

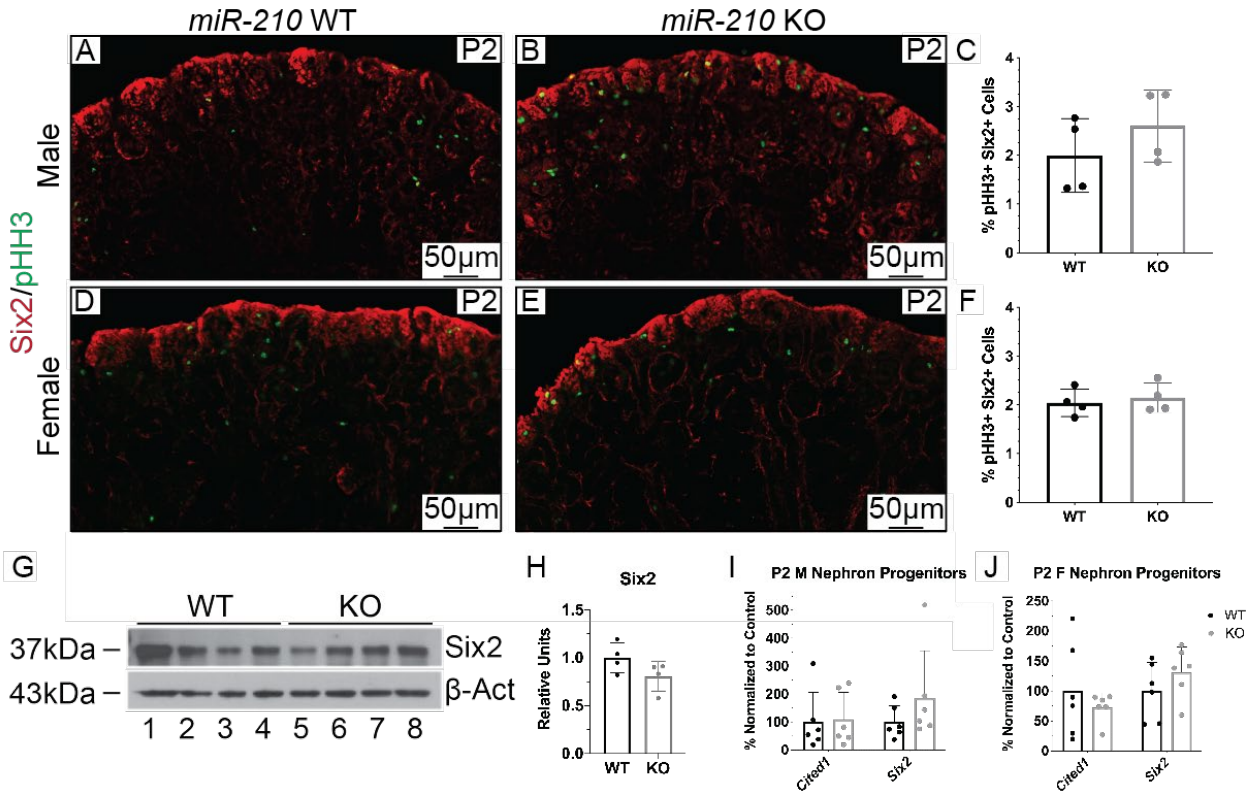

Figure 33: Nephron progenitor proliferation is normal at P2

(A-B) Immunofluorescent staining of male (A) WT and (B) KO P2 kidneys for nephron progenitor marker Six2 (red) and proliferation marker pHH3 (green). (C) Quantification of the percentage of pHH3-positive nephron progenitors in male kidneys. (D-E) Immunofluorescent staining of female (D) WT and (E) KO kidneys for Six2 (red) and pHH3 (green). (C) Quantification of the percentage of pHH3-positive nephron progenitors in female kidneys. (G-H) Western blot analysis of Six2 expression in P2 male kidneys, normalized to β-Act. (I-J) qPCR analysis of nephron progenitor markers *Cited1* and *Six2* in P2 (I) male and (J) female WT and KO kidneys, normalized to *Actb* expression. Error bars ± SEM, Mann-Whitney U test. $N \geq 4$ per genotype and sex. (208)

3.3.15 Pro-apoptotic gene expression is increased in P2 *miR-210* KO male kidneys

Apoptosis is a normal developmental process, and miRNAs are an important regulator of apoptosis during kidney development (137, 138, 143, 223, 224). *miR-210* is known to inhibit the expression of multiple pro-apoptotic genes (148). Thus, apoptotic signaling was investigated in KO mice to determine if it played a role in the nephron deficit. Immunostaining for nephron progenitor marker Six2 and active apoptotic signaling marker cleaved Casp3 (c-Casp3) (225) showed no difference in the percentage of apoptotic nephron progenitors in WT and KO male (**Figure 34A-C**) and female (**Figure 34E-G**) P2 kidneys. However, there did appear to be more apoptotic cells in KO male kidneys at the bottom of the cap mesenchyme, where nephron progenitors undergo MET to begin differentiating into the nephron (**Figure 34B**). To determine if there were more apoptotic cells in the early differentiating nephrons, immunostaining for Jag1 and c-Casp3 was performed on P2 WT and KO male kidneys (**Figure 34I-J**). Quantification of these samples showed no significant difference in the percentage of c-Casp3- and Jag1-double positive cells in the developing nephron structures between WT and KO kidneys (**Figure 34K**). It is possible that a combination of more Six2-positive and Jag1-positive cells are dying in male KO kidneys, which would contribute to the observed nephron deficit.

To assay apoptosis in the whole kidney, qPCR analysis of pro-apoptotic markers was performed. *Casp8ap2* is part of the Fas death receptor and binds pro-Casp8, which it activates upon Fas-L binding (226, 227). Activated Casp8 (p18) then activates Casp3 to transduce the pro-apoptotic signal to the cell (224, 226). qPCR analysis of pro-apoptotic and *miR-210* target *Casp8ap2* (153, 154) showed increased expression in KO male P2 kidneys (**Figure 34D**), but no difference in female kidneys (**Figure 34H**). Expression of *Casp3* was unchanged in male (**Figure 34D**) and female (**Figure 34H**) kidneys. Western blot analysis of pro-apoptotic Casp8 (225) in male P2 kidneys showed increased expression of is full-length protein pro-Casp8 but no difference in the amount of the activated p18 subunit (**Figure 34L-N**). While significantly increased expression of active apoptotic signaling was not observed, the increased expression of *Casp8ap2* and pro-Casp8 suggests that KO cells are primed for apoptotic signaling.

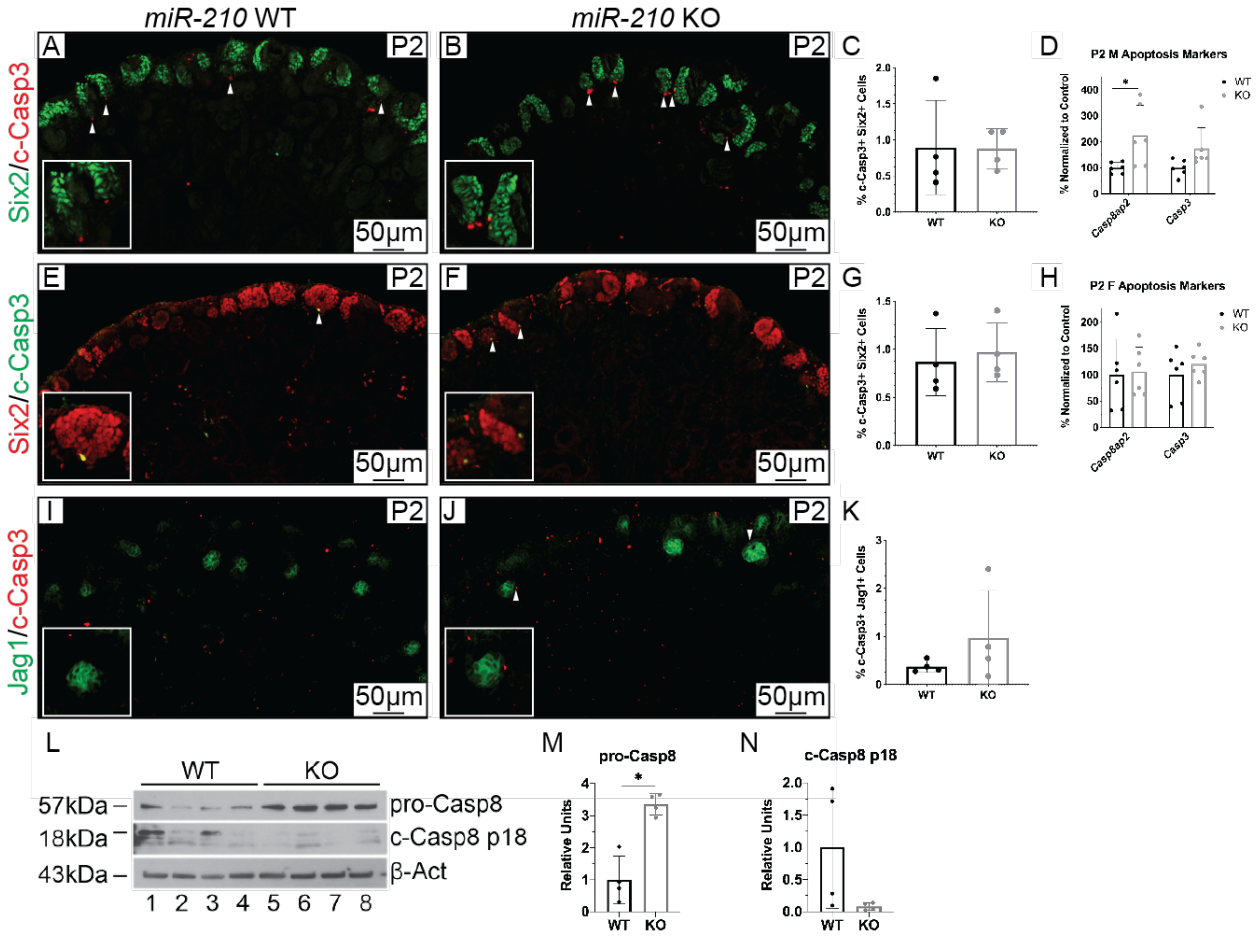

Figure 34: Increased expression of *Casp8ap2* and pro-Casp8 in P2 male KO kidneys

(A-B) Immunofluorescent staining of male (A) WT and (B) KO P2 kidneys for nephron progenitor marker Six2 (green) and apoptosis marker c-Casp3 (red). (C) Quantification of the percentage of c-Casp3-positive nephron progenitors in male kidneys. White arrows indicate c-Casp3-positive cells at the bottom of the cap mesenchyme. Inset showed magnified image of cap mesenchyme. (D,H) qPCR analysis of pro-apoptotic *miR-210* target gene *Casp8ap2* and pro-apoptotic *Casp3* in (D) male and (H) female kidneys, normalized to *Actb* expression. (E-F) Immunofluorescent staining of female (E) WT and (F) KO kidneys for Six2 (red) and c-Casp3 (green). White arrows indicate c-Casp3-positive cells at the bottom of the cap mesenchyme. Inset showed magnified image of cap mesenchyme. (G) Quantification of the percentage of c-Casp3-positive nephron progenitors in female kidneys. (I-J) Immunofluorescent staining of male (I) WT and (J) KO P2 kidneys for differentiating nephron structure marker Jag (green) and c-Casp3 (red). White arrows indicate c-Casp3-positive cells at the bottom of the cap mesenchyme. Inset showed magnified image of differentiating nephron structure. (K) Quantification of the percentage of c-Casp3-positive differentiated cells in male kidneys. (L-N) Western blot analysis of (M) inactive full length pro-Casp8 and (N) active cleaved Casp8 p18 expression in P2 male kidneys, normalized to β-Act. **P*<0.05, Error bars ± SEM, Mann-Whitney U test. $N \geq 4$ per genotype and sex. (208)

3.3.16 Cessation of nephrogenesis is normal in *miR-210* KO

About 50% of mouse nephrons form postnatally and since new nephron formation occurs exponentially, an early end to nephrogenesis could result in a significant decrease in nephron number (41, 51). To test for an early cessation of nephrogenesis, P3 and P4 kidneys were assayed. H&E staining showed no difference in tissue histology between WT and KO male P3 (**Figure 35A-B**) and P4 (**Figure 35C-D**) kidneys. Immunostaining for Six2 and Ncam showed normal expression in WT and KO in P3 (**Figure 35E-F**) and the end of Six2 expression P4 (**Figure 35G-H**) kidneys, which indicates no difference in the timing of nephrogenesis cessation. Immunostaining for Wnt/β-catenin signaling marker Lef1 showed a normal expression pattern in WT and KO P3 (**Figure 35I-J**) and P4 (**Figure 35K-L**) kidneys. Immunostaining for Notch signaling ligand Jag1 showed a normal expression pattern in WT and KO P3 (**Figure 35M-N**) and P4 (**Figure 35O-P**) kidneys. Together, these data suggest that deletion of *miR-210* does not affect the timing of the cessation of nephrogenesis, nor the localized expression pattern of Wnt and Notch signaling pathways at P3 and P4.

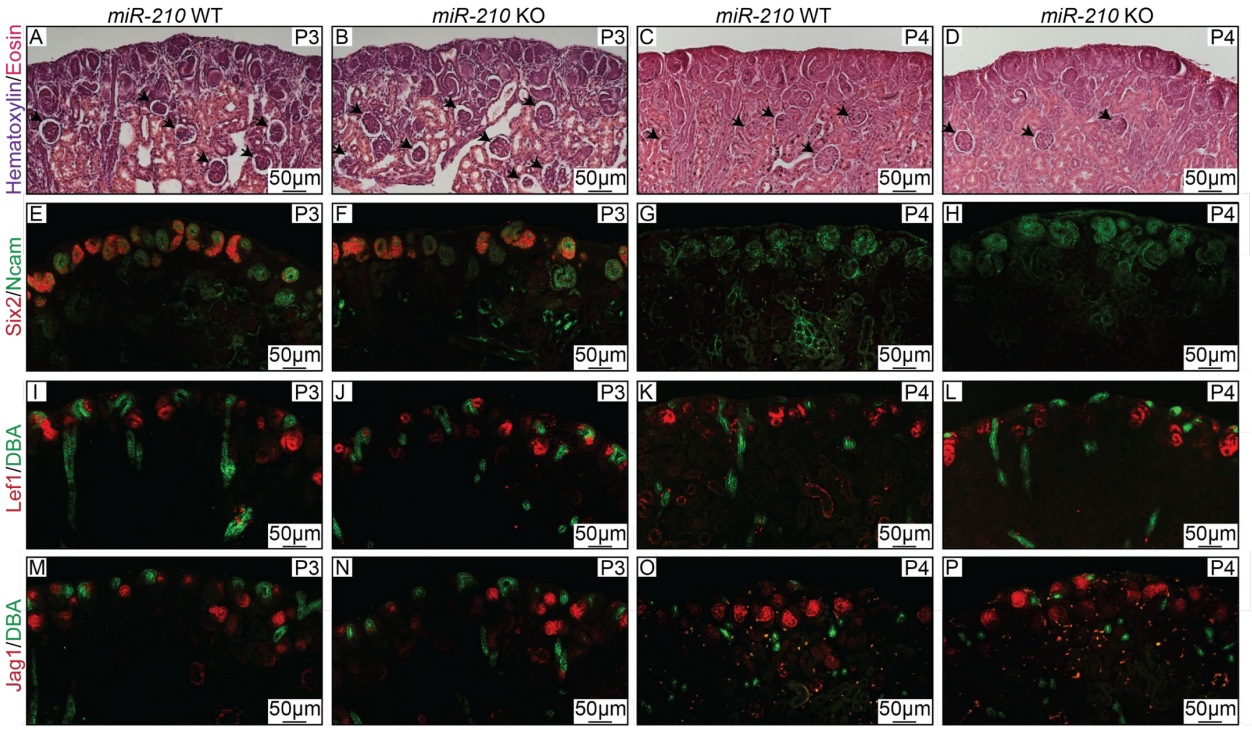

Figure 35: Nephrogenesis ends by P4 in *miR-210* WT and KO male kidneys

(A-D) H&E staining of (A-B) P3 and (C-D) P4 (A, C) WT and (B, D) KO male kidneys. Black arrowheads indicate glomeruli. (E-H) Immunofluorescent staining of nephron progenitor marker Six2 (red) and developing nephron structures marker Ncam (green) in (E-F) P3 and (G-H) P4 (E, G) WT and (F, H) KO kidneys. (I-L) Immunofluorescent staining of Wnt/β-catenin signaling marker Lef1 (red) and ureteric epithelium marker DBA (green) in (I-J) P3 and (K-L) P4 (I, K) WT and (J, L) KO kidneys. (M-P) Immunofluorescent staining of Notch signaling ligand Jag1 (red) and DBA (green) in (M-N) P3 and (O-P) P4 (M, O) WT and (N, P) KO kidneys. $N \geq 3$ per genotype. (208)

3.4 Conclusion

Global deletion of *miR-210* results in a male-specific decrease in nephron number. This observed decrease in nephron number could be due to several factors, including 1) altered nephron progenitor differentiation, 2) decreased ureteric branching, 3) decreased vasculature development, 4) decreased nephron progenitor proliferation, 5) increased apoptosis, or 6) early termination of nephrogenesis. These data suggest that the nephron deficit is due to a combination of increased Wnt signaling (i.e. increased Lef1 expression) and increased expression of the pro-apoptotic *Casp8ap2* and pro-Casp8. However, it is important to consider that some of the assays investigating other factors contributing to nephron number development may not have been sensitive enough to pick up on subtle changes.

The sex-specific difference in nephron number in wildtype animals is consistent with prior observations in both humans and mice that females have fewer nephrons compared to males (60, 76). It has been reported that there are differences in sex-related changes in nephron number in different inbred mouse strains (77). However, the observation of a nephron deficit in male, but not female, *miR-210* knockout mice may be the first description of a sex-specific functional role for a miRNA in kidney development. Deletion of *miR-210* was found to have no significant effect on mouse placental development during both normoxic and hypoxic pregnancies (202). However, this study did not analyze the sexes separately. In humans, female placentas from overweight and obese mothers had increased *miR-210* expression compared to males (166). *miR-210* has also been identified as a potential biomarker for pre-eclampsia (175, 176). Recently, a sex-specific role for a miRNA in adult kidneys was identified, where female rats with a *miR-146b-5p* deletion had exacerbated renal hypertrophy after 5/6 nephrectomy (228). Thus, it is possible that in an injurious setting (e.g. hypertension, hypoxia) *miR-210* responds in a sexually dimorphic manner.

Interestingly, a sex-specific difference in nephron number similar to that of *miR-210* deletion was observed in a model of moderate intrauterine hypoxia (which would be predicted to induce *miR-210* expression), where hypoxia-exposed males had about 25% fewer nephrons than untreated males (60). Prolonged prenatal hypoxia has also been shown to result in a male-specific disruption of collecting duct patterning through altered Wnt/β-catenin and retinoic acid signaling, which resulted in a urine concentrating defect (61). Taken together, this raises the question of whether both over- and under-expression of *miR-210* could result in a nephron deficit in a sex-

specific manner. For example, both over- and under-activity of β-catenin signaling in nephron progenitors results in fewer nephrons due to an inability to either proceed to the renal vesicle stage, or undergo mesenchymal to epithelial transition, respectively (105, 213).

Canonical Wnt signaling is necessary for the commitment of nephron progenitors to undergo a mesenchymal to epithelial transition and form the renal vesicle (229). Lef1 forms a transcriptional complex with Tcf that inhibits expression of Wnt pathway genes until β-catenin is activated, translocated to the nucleus, and complexes with Lef1/Tcf, to increase expression of target genes (230). It has previously been shown that *miR-210-3p* targets *Tcf7l2* (158) and that increased expression of *miR-210-3p* results in down-regulation of *Ctnnb1*, the β-catenin transcript (159). In the *miR-210* KO kidneys, there is increased expression of Lef1, a marker of increased β-catenin activity, and overexpression of β-catenin has previously been shown to result in early depletion of the nephron progenitor pool (105). *Lhx1*, which is downstream of Wnt signaling, acts in several steps of nephrogenesis and is important in renal vesicle patterning and tubule morphogenesis (46, 212). The increase in *Lhx1* expression in *miR-210* knockout mice is further evidence suggesting that loss of *miR-210* expression results in increased Wnt signaling. Together, this suggests that during nephrogenesis *miR-210-3p* fine-tunes Wnt/β-catenin activation to promote normal nephron number formation.

Furthermore, deletion of *miR-210* results in the increased expression of its pro-apoptotic target, *Casp8ap2*. Other studies have shown that *miR-210* targets *Casp8ap2* for degradation to promote stem cell survival after ischemic preconditioning (153) and to protect human umbilical vein endothelial cells against oxidative stress (154). Under normal conditions, Casp8ap2 promotes S-phase progression and histone biosynthesis (231-233). Upon Fas receptor activation, Casp8ap2 translocates to the cytoplasm to promote apoptosis through the Fas receptor death-inducing signaling complex (226, 234) as well as through activating the mitochondrial apoptotic pathway (235). Proper regulation of apoptosis is essential for normal kidney development (224), and part of this regulation is carried out by miRNAs (138, 223). We show a male-specific increase of *Casp8ap2* in *miR-210* KO kidneys, which has previously been reported to have increased expression in males compared to females in developing mouse lung tissue (236). These data suggest that loss of *miR-210*-mediated regulation of the pro-apoptotic *Casp8ap2* transcript is one piece of the regulatory puzzle contributing to a sex-specific decrease in nephron number; although it remains unclear in which developmental compartment this occurs.

4.0 *In Vivo* Hypoxic Kidney Development

4.1 Introduction

Intrauterine hypoxia results in impaired kidney development, but the mechanisms behind this are poorly understood (56). The previous chapters show that *miR-210* is induced in *ex vivo* pathologically hypoxic kidney development and is required for normal nephron number development in male mice. Thus, the *miR-210* knockout mouse model was used with an *in vivo* intrauterine hypoxia model to investigate the role it may play in regulating kidney development in response to intrauterine hypoxia.

4.2 Methods

4.2.1 Mouse strains

Mice heterozygous for the global *miR-210* deletion were the same as those used in (202). In collaboration with these authors, embryos were collected at E17.5 and the authors analyzed placenta, while the kidneys were collected and analyzed by myself, as described below. All other animals (*Six2-Cre-GFP; VHL*$^{flx/flx}$ mice, which have a nephron progenitor-specific deletion of the negative regulator of Hifα-subunits, as described in (75)) were housed in the vivarium at the Rangos Research Center at the UPMC Children's Hospital of Pittsburgh (Pittsburgh, PA, USA) and all animal experiments were carried out in accordance with the policies of the Institutional Animal Care and Use Committee at the University of Pittsburgh.

4.2.2 FACS-isolation of GFP-positive nephron progenitors

Kidneys were dissected from E17.5 embryos from *Six2-Cre-GFP; VHL*$^{flx/flx}$ breedings (mice as described in (75)). Kidneys were checked for fluorescent green nephron progenitors using a Leica DM 2500 microscope and Qimaging Qcam Fast 1394 camera. Fluorescent kidneys from the same embryo were pooled and placed in PBS on ice (one pair of non-fluorescent kidneys were also processed for the blank control). The kidneys were broken into small pieces with a razor and then placed in 500µL 0.3% collagenase in PBS for incubation for 10min at 37ºC with agitation. The homogenized tissue was run through 18G then 25G needles to further break up tissue. The cell suspension was transferred to a 50mL tube with 5mL of 2% FBS (fetal bovine serum) in PBS and centrifuged for 5min at 500 g. The supernatant was removed and the cells were resuspended in 500µL 2% FBS/PBS. The UPMC Children's Hospital of Pittsburgh Flow Core used a FACSAria II machine (BD Biosciences) to isolate the GFP-positive nephron progenitors into 250µL Qiazol (Qiagen). Total RNA was then isolated using the Qiagen miRNeasy Mini Kit.

4.2.3 Model of *in vivo* intrauterine hypoxia

Pregnant females heterozygous for *miR-210* deletion were housed at either 21% or 12.5% O_2, the latter to model intrauterine hypoxia, from E12.5 to E17.5. See **Figure 36** for overview.

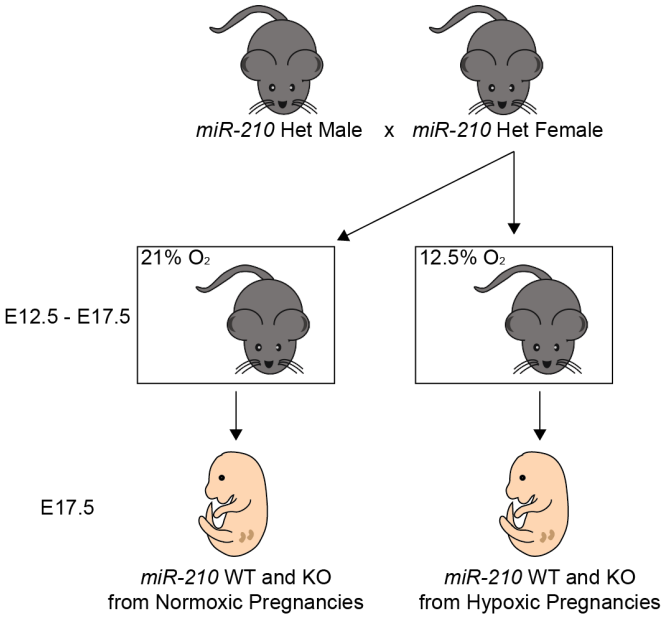

Figure 36: Overview of model of intrauterine hypoxia

Mice heterozygous for the *miR-210* deletion were bred. At E12.5, pregnant females were either placed in a hypoxia chamber with 12.5% O_2, to model intrauterine hypoxia, or kept at 21% O_2. At E17.5, embryonic kidneys were dissected for analysis. $N \geq 3$ litters per oxygen condition.

4.2.4 qPCR analysis of miRNA expression

As described in Chapter 3.2.3.

4.2.5 Paraffin-embedding of kidneys

As described in Chapter 3.2.5

4.2.6 Hematoxylin and eosin staining of kidney sections

As described in Chapter 3.2.6.

4.2.7 Immunofluorescent staining of kidney sections

As described in Chapter 3.2.10.

4.2.8 qPCR analysis of mRNA expression

As described in Chapter 2.2.4. See **Table 1**, **Table 6**, and **Table 8** for primers used.

Table 8: Primers used for qPCR (3)

Gene	Forward	Reverse	Product Size (bp)
Calb	ATGATCAGGATGGCAACGGA	GTTCGGTACAGCTTCCCTCC	160
Dpf3	TGAGAAGAGAAGTTGTAGCA	TCAAGGACACCACAGTTC	207
Foxd1	TGTGGAGAACTTTACTGCTA	AAATAGATGGACCCTCTGAG	234
Nphs1	AGGGTCGGAGGAGGATCGAA	GGGAAGCTGGGGACTGAAGT	141
Nphs2	GACCAGAGGAAGGCATCAAGC	GCACAACCTTTATGCAGAACCAG	123
Osr1	ACTGATGAGCGACCTTAC	TTGTGAGTGTAGCGTCTT	174
Pdxl	CCTCCAGGCCCCAGCA	CCCAGCTTCATGTCACTGACT	364
Raldh2	CTCACATCGGCATAGACA	GTAGTCCAAGTCAGCATCT	155
Synpo	CTCACCACGGCTATCTGCCAGA	TGGTATGGCTGCTGCTTGG	65
Vegfr1	AGAGGTATCAGAGCAGAAC	GCATCTCACTAGAGGAACT	196

4.2.9 Statistical analysis

As described in Chapter 3.2.20.

4.3 Results

4.3.1 *miR-210* expression is induced in a genetic model of pathological hypoxia

Recently, the effect of constitutive HIF expression in nephron progenitors (Six2-Cre; VHL-floxed mouse model) on kidney development was demonstrated (75). In short, overexpression of HIF (mimicking intrauterine hypoxia) resulted in decreased nephron number, mainly due to dysregulation of metabolism (75). Cargill *et al*. (75) showed that when HIF is overexpressed in nephron progenitors, there is decreased expression of *Lef1*, which matches with our finding that deletion of *miR-210* resulted in increased *Lef1* expression (**Figure 27E-F,I,J-K**). To investigate how constitutive HIF expression in nephron progenitors affects *miR-210* expression, GFP+ nephron progenitors in *Six2-VHL+/-* (Control) and *Six2-VHL-/-* (KO) kidneys were isolated using FACS. qPCR analysis showed ~20-fold increase in *miR-210* expression in HIF-overexpressing (*VHL* Knockout) nephron progenitors, compared to Control nephron progenitors (**Figure 37**).

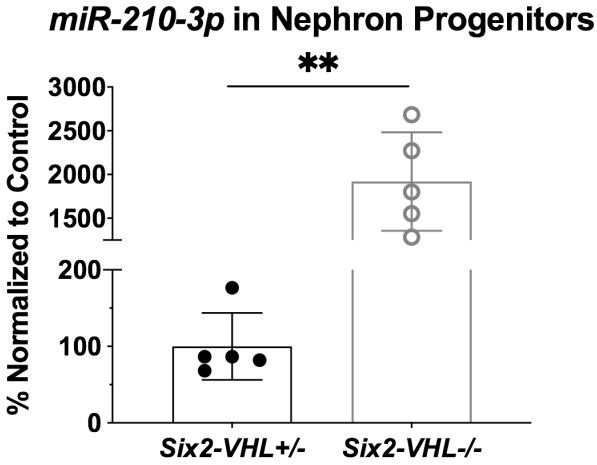

Figure 37: Upregulation of *miR-210-3p* in *Six2-VHL*$^{-/-}$ nephron progenitors

qPCR analysis of *miR-210-3p* expression, normalized to *U6* snRNA, in E17 *Six2-VHL*$^{+/-}$ (Control) and *Six2-VHL*$^{-/-}$ (Knockout) FACS-isolated GFP-positive nephron progenitors. $^{**}P<0.01$, Error bars ± SEM, Mann-Whitney U test. $N \geq 5$ per genotype. Animals provided by the Dr. Sunder Sims-Lucas Laboratory (Department of Pediatrics, University of Pittsburgh, Pittsburgh, PA).

4.3.2 *miR-210* expression is not affected by an environmental model of pathological hypoxia

To model moderate intrauterine hypoxia, pregnant dams were housed in 12.5% O_2 from E12 (two days after kidney development begins) to E17 (mid-nephrogenesis, one day before birth), at which point embryos were collected for expression analysis (**Figure 36**). qPCR analysis showed no significant increase in *miR-210* expression in whole kidneys (**Figure 38**). However, the localized expression was not analyzed, so there may be cell-specific changes in *miR-210* expression that this assay cannot detect.

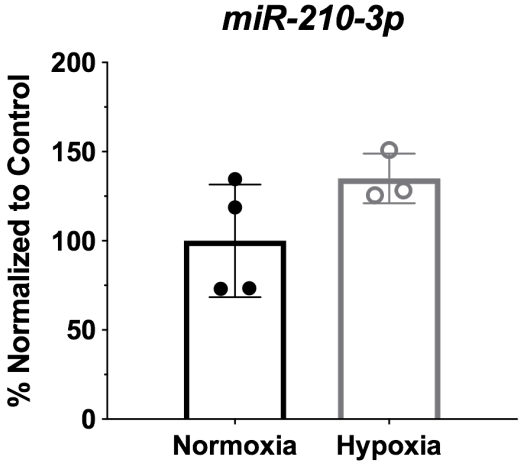

Figure 38: *miR-210-3p* expression is not affected in E17 kidneys from hypoxic pregnancies

qPCR analysis of *miR-210-3p* expression, normalized to *U6* snRNA, in E17 kidneys from normoxic and hypoxic pregnancies. Error bars ± SEM, Mann-Whitney U test. $N \geq 3$ kidneys per oxygen condition.

4.3.3 Intrauterine hypoxia induces *Six2* expression in WT kidneys at E17

H&E staining showed normal kidney histology in WT normoxic (**Figure 39A**) and hypoxic (**Figure 39C**) pregnancies. Immunostaining for nephron progenitor markers Six2 and Ncam (which also marks the developing nephron structures) showed a normal expression pattern in kidneys from normoxic (**Figure 39B**) and hypoxic (**Figure 39D**) pregnancies. qPCR analysis was performed to analyze expression of several genes involved in kidney development (**Figure 39E-H**). Of all nephron progenitor markers analyzed (*Cited1, Eya1, Osr1, Six2, Meox1, Dpf3*), only the

expression of *Six2* was increased in hypoxia (**Figure 39E**). Analysis of developing nephron structure (*Lef1, Fgfrl1, Fgf8, Wnt4, Jag1;* **Figure 39F**), glomerular (*Nphs1, Nphs2, Pdxl, Synpo* (237)*;* **Figure 39G**), ureteric (*Calb* (215); **Figure 39H**), and stromal (*Foxd1, Raldh2* (238); **Figure 39H**) markers showed no differential expression between kidneys from normoxia and hypoxic pregnancies. Thus, moderate intrauterine hypoxia has a mild effect on expression of genes involved in regulating kidney development at E17.

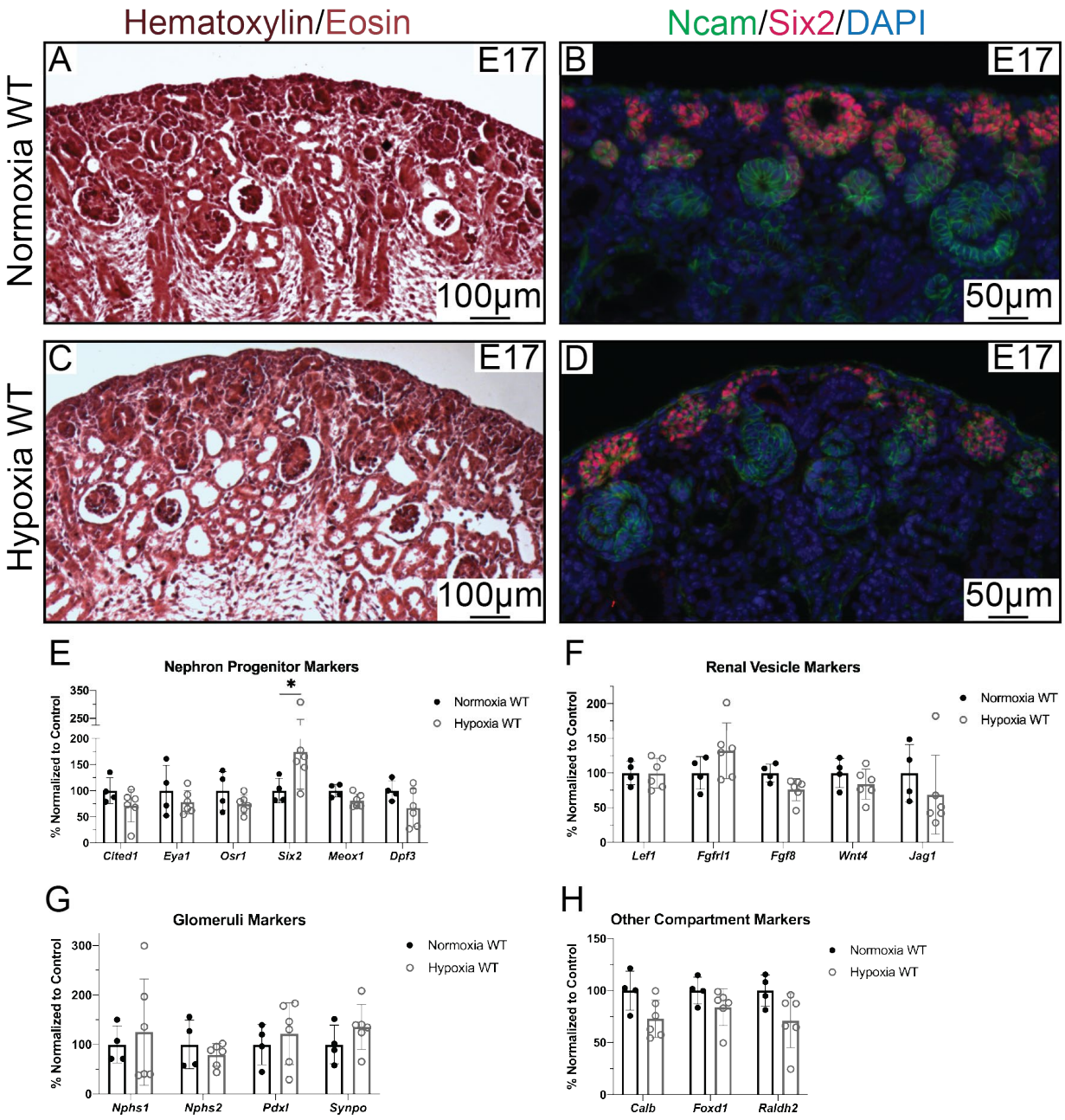

Figure 39: Kidney development at E17 from normoxic and hypoxic pregnancies

(A,C) H&E staining of E17 WT kidneys from normoxic and hypoxic pregnancies. (B,D) Immunofluorescent staining for nephron progenitors (Six2, red) and nephron progenitors and developing nephron structures (Ncam, green). (E-H) qPCR analysis of (E) nephron progenitor markers, (F) renal vesicle markers, (G) glomeruli markers, and (H) ureteric epithelium marker (*Calb*) and stroma markers (*Foxd1, Raldh2*). RNA expression was normalized to *Rn18S.* **P*<0.05, Error bars ± SEM, Mann-Whitney U test. $N \geq 4$ kidneys per oxygen condition.

4.3.4 Expression of *Vegfr2* is decreased in intrauterine hypoxia at E17

Immunostaining for endothelial cell marker Emcn (218) and podocyte marker Wt1 (239) showed a normal expression pattern in kidneys from both normoxic (**Figure 40A-B**) and hypoxic (**Figure 40C-D**) pregnancies. qPCR analysis of genes involved in renal vasculature development (*Vegfa, Vegfr1, Vegfr2, Efna3* (240)) showed decreased expression of *Vegfr2* in kidneys from hypoxic pregnancies (**Figure 40E**). These data suggest a mild effect of moderate intrauterine hypoxia on renal vasculature development at E17.

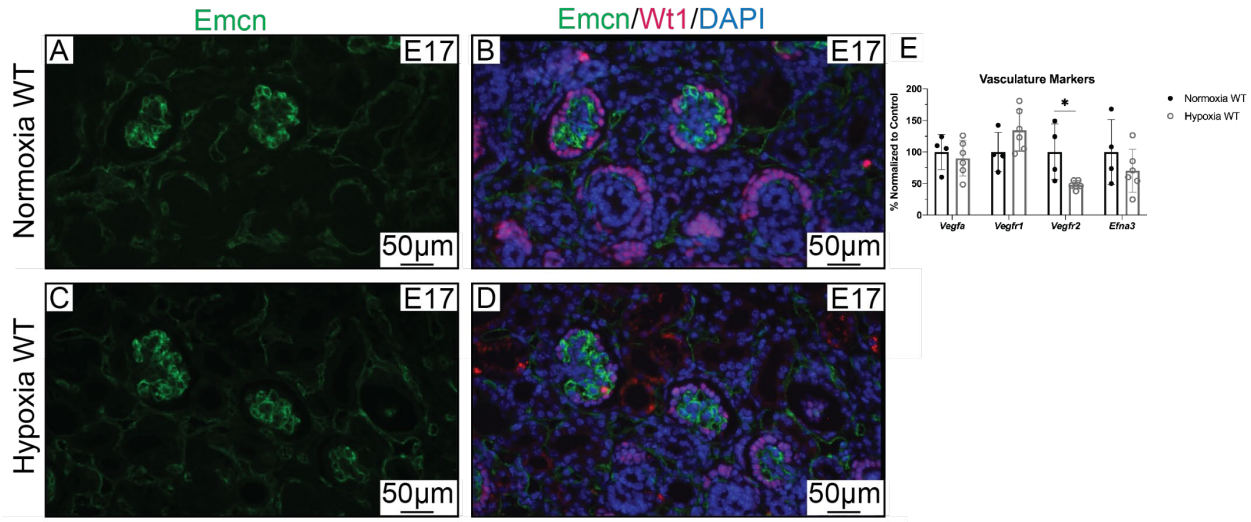

Figure 40: Renal vasculature development at E17 from normoxic and hypoxic pregnancies

(A,C) Immunofluorescent staining for microvasculature marker Emcn (green) in E17 WT kidneys from (A) normoxic and (C) hypoxic pregnancies. (B,D) Expression of podocyte marker Wt1 (red) and Emcn (green). (E) qPCR analysis of renal vasculature markers normalized to *Rn18S* expression. **P*<0.05, Error bars ± SEM, Mann-Whitney U test. $N \geq 4$ per oxygen condition.

4.3.5 Intrauterine hypoxia does not affect kidney development in *miR-210* KO by E17

After establishing how WT kidneys respond to moderate intrauterine hypoxia, how deletion of *miR-210* affects kidney development in hypoxia was next investigated. H&E staining showed normal histology in WT (**Figure 41A**) and KO (**Figure 41C**) kidneys from hypoxic pregnancies. Immunostaining for Six2 and Ncam showed a normal expression pattern in WT

(**Figure 41B**) and KO (**Figure 41D**) kidneys from hypoxic pregnancies. qPCR analysis was performed to analyze expression of several genes involved in kidney development (**Figure 41E-H**). None of the nephron progenitor markers analyzed (*Cited1, Eya1, Osr1, Six2, Meox1, Dpf3*) showed differences in expression (**Figure 41E**). Note that *Six2* expression was increased in WT hypoxic pregnancies (**Figure 39E**) and loss of *miR-210* expression did not affect *Six2* expression in hypoxia (**Figure 41E**). Analysis of developing nephron structure (*Lef1, Fgfrl1, Fgf8, Wnt4, Jag1;* **Figure 41F**), glomerular (*Nphs1, Nphs2, Pdxl, Synpo;* **Figure 41G**), and stromal (*Foxd1, Raldh2;* **Figure 41H**) markers showed no differential expression between kidneys from normoxia and hypoxic pregnancies. qPCR analysis of expression did show decreased levels of the ureteric marker *Calb* in KO kidneys exposed to intrauterine hypoxia (**Figure 41H**), suggestive of decreased ureteric branch tips. Thus, deletion of *miR-210* in the setting of moderate intrauterine hypoxia does not have much impact on expression of kidney development markers at E17.

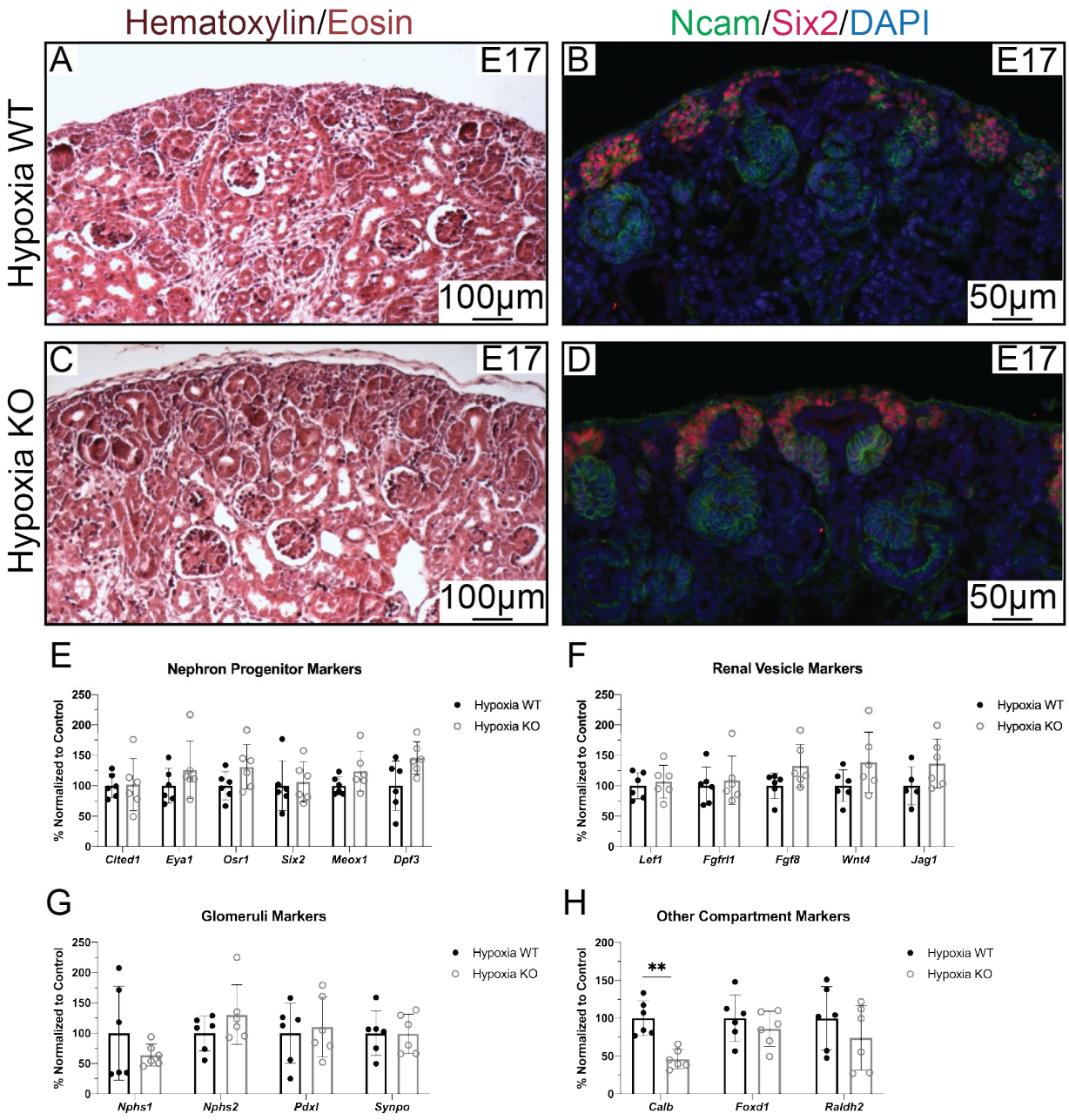

Figure 41: Hypoxic does not affect *miR-210* kidney development at E17

(A,C) H&E staining of E17 (A) WT and (C) KO kidneys from hypoxic pregnancies. (B,D) Immunofluorescent staining for nephron progenitors (Six2, red) and developing nephron structures (Ncam, green). (E-H) qPCR analysis of (E) nephron progenitor markers, (F) renal vesicle markers, (G) glomeruli markers, and (H) ureteric epithelium marker (*Cal*) and stroma markers (*Foxd1, Raldh2*). RNA expression was normalized to *Rn18S.* $^{**}P<0.01$, Error bars ± SEM, Mann-Whitney U test. $N \geq 6$ per genotype.

4.3.6 Intrauterine hypoxia does not affect *miR-210* KO renal vasculature by E17

Immunostaining for Emcn and Wt1 showed a normal expression pattern in both WT (**Figure 42A-B**) and KO (**Figure 42C-D**) hypoxic pregnancies. qPCR analysis of genes involved in renal vasculature development (*Vegfa, Vegfr1, Vegfr2, Efna3*) showed no difference in expression of *Vegfr2* in WT and KO kidneys from hypoxic pregnancies (**Figure 42E**). Thus, loss of *miR-210* does not have any further effect on *Vegfr2* expression in hypoxia.

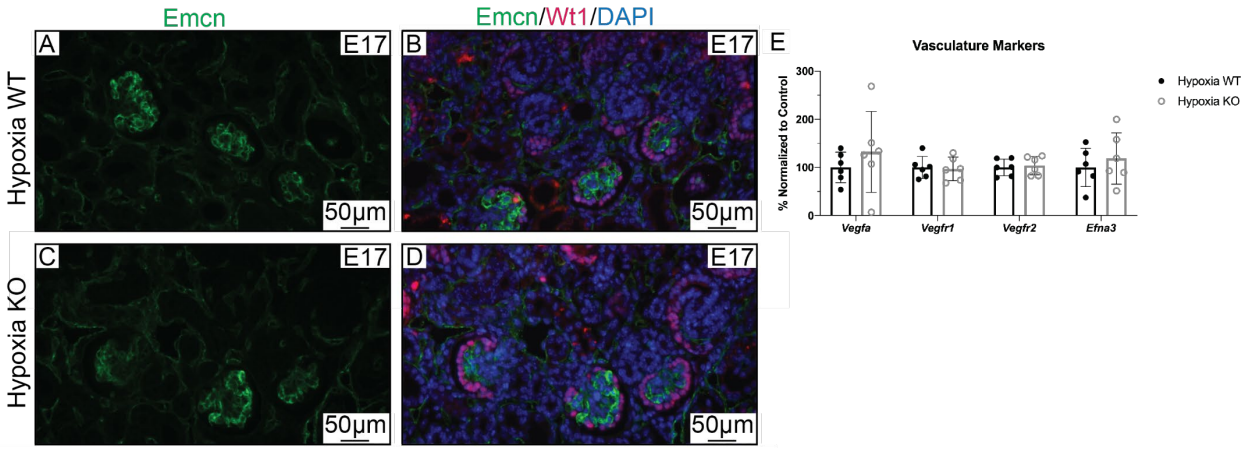

Figure 42: Hypoxia does not affect renal vasculature developmet in *miR-210* KO at E17

(A,C) Immunofluorescent staining for microvasculature marker Emcn (green) in E17 (A) WT and (C) KO kidneys from hypoxic pregnancies. (B,D) Expression of podocyte marker Wt1 (red) and Emcn (green). (E) qPCR analysis of renal vasculature markers normalized to *Rn18S* expression. **P*<0.05, Error bars ± SEM, Mann-Whitney U test. $N \geq 6$ per genotype.

4.4 Conclusion

Analysis of nephrogenesis at E17 from pregnancies complicated by moderate hypoxia (12.5% O_2) from E12.5 to E17 suggests several ways that hypoxia results in abnormal kidney development. The increased *Six2* expression suggests that there are more nephron progenitors, which could be caused by increased proliferation or their failure to differentiate, or that the nephron progenitors express higher levels of *Six2*. Overexpression of Six2 inhibits nephron progenitor

differentiation (96); and *Six2* must be down regulated for differentiation to proceed (97). Thus, increased *Six2* expression induced by moderate hypoxia during pregnancy could contribute to decreased nephron number. Decreased *Vegfr2* expression in hypoxia suggests an inhibition of proper renal vasculature development, which can contribute to decreased nephron number and abnormal glomerular development (69, 241). These data coincide with the findings in Chapter 2, suggesting a promotion of nephron progenitor self-renewal versus differentiation in pathological hypoxia.

Loss of *miR-210* expression did not change expression of these genes at this timepoint, suggesting that it does not play a role in regulating their expression in moderate intrauterine hypoxia. These data show that *in vivo* intrauterine moderate hypoxia does not result in an acceleration (i.e. observable at E17 vs P2) of the *miR-210* deletion phenotype observed in Chapter 3. Thus, *miR-210* does not appear to play a significant role in hypoxic embryonic kidney development. However, all analysis was done without separation of males and females (Chapter 4 was performed chronologically before Chapter 3); thus, there may be subtle changes in gene expression in males that are drowned out by pooled analysis with female kidneys. Males and females differ in their response to IUGR when assessing blood pressure, kidney function, and glucose homeostasis (91, 242). Future analysis of this model should be conducted with sexual dimorphism of kidney development and injury response in mind.

Pathological fetal hypoxia results in decreased blood flow to the developing kidney (64). The nephrogenic zone where the nephron progenitors reside has low vascularization (243). Blood flow and oxygenation are important drivers of nephron progenitor differentiation (69). There is likely decreased vascularization of the nephrogenic zone in pathological hypoxic pregnancies, which would inhibit differentiation, due to preferential redirection of blood flow to other organs (e.g. heart, brain) (57, 64). In the wildtype model, decreased *Vegfr2* expression was observed in the embryos from hypoxic pregnancies, indicative of impaired real vasculature development. In the setting of pathological fetal hypoxia, less development of the renal vasculature is expected to occur (56). IUGR results in endothelial dysfunction, increasing risk for development of cardiovascular and kidney disease (e.g. hypertension) (244). While nephrogenesis ends by P4 in mice, kidney vasculogenesis continues past this timepoint, to ensure that the growing nephrons receive proper vascularization (245). Impaired kidney development due to pathological hypoxia may also include impaired vascular development, contributing to lifelong risk for vascular-related

diseases. This study was not able to quantify vascular development using fluorescence microangiography (as in (69)), but would be an interesting avenue for future studies.

Expression of *Calb* is decreased in *miR-210* knockout embryos compared to wildtype littermates from hypoxic pregnancies. This is suggestive of decreased ureteric branching, which can contribute to a decrease in nephron number (47). It has been previously reported that intrauterine hypoxia results in kidney defects that are associated with suppression of ureteric β-catenin signaling (115). *Calb* is a marker of urethelium, but does not lend insight into a functional defect, as analysis of *Ret* or *Sox9* would (215). Since this study did not further investigate a branching defect, future studies could assay expression of genes regulating ureteric branching (e.g. Gdnf/Ret pathway, Wnt/β-catenin signaling) and quantify branching morphogenesis in *miR-210* KO kidneys from hypoxic pregnancies.

5.0 Future Directions and Implications

5.1 Transcriptome of hypoxic kidney development

5.1.1 Future experiments

Chapter 2 identified many mRNAs and miRNAs that are affected by pathological hypoxia during early kidney development in an unbiased fashion. Investigation of their functional roles would be the next step of this project. The DAVID analysis of the target pairs suggested several genes that would be interesting to investigate further and a literature search of these mRNAs and miRNAs would determine which would be interesting to investigate functionally for their role in hypoxic kidney development. For example, miRNAs that have been shown to regulate genes involved in pathways important in kidney development (e.g. Wnt/β-catenin, Notch, Bmp).

One aspect would be validation of miRNA-mRNA target pairs suggested by the Ingenuity Pathways Analysis (IPA). Some of these miRNA-mRNA pairs have already been validated as targets, since IPA includes experimentally validated pairs as well as databases of predicted pairs. The luciferase reporter gene assay could be used to validate the predicted binding sites of miRNA-mRNA target pairs of interest (246). Then the next step would be to perform an *ex vivo* assay for functional targeting, which would entail treating the kidney explant organ cultures with a miRNA mimic and antagomir and then measuring the expression of the target mRNA(s) as well as changes in the development of the kidney explants (247-249). This analysis could also be eventually performed *in vivo* to investigate the possibility of mimics or antagomirs in clinical applications of pathological hypoxia to correct the adverse phenotypic changes in kidney development (250, 251).

While much research has been conducted investigating the role of various protein-coding genes in kidney development and hypoxia, little is known about miRNAs in this context. Thus, further investigation of the miRNAs induced in pathologically hypoxic kidney development would be useful. *In situ* hybridization using Locked Nucleic Acid-modified oligonucleotide probes for specific miRNAs could be used to identify localized expression of the miRNAs of interest in

kidney explants cultured in different oxygen conditions (252). Functional analysis of miRNAs during kidney development could be performed using mice with specific miRNAs deleted in a global or cell-specific manner (203). Since these miRNAs are altered in conjunction with each other, it would be useful to study the effect of their loss of expression using multiple knockout models (i.e. *miR-210* and *miR-154* double knockout). This analysis would be performed in the same manner as the investigation of the effect of global deletion of *miR-210* on kidney development, as outlined in Chapter 3. In short, the first step would be to determine if there is a nephron number difference at P30, and if found, analysis of kidney development across different stages of nephrogenesis to determine the timing of the onset of changes in gene expression to cause the phenotype.

5.1.2 Global implications

Physiological hypoxia is an important process throughout development, including kidney, and pathological hypoxia poses a significant health threat (56). Thus, further understanding of the mechanisms of how pathological hypoxia adversely impacts kidney development is essential. miRNAs are increasingly being recognized as important regulators in kidney development and disease (253-257). miRNAs are being investigated as biomarkers, targets, and therapeutics for disease (258). In fact, *miR*-210 has been identified as a potential biomarker for fetal hypoxia (177), pre-eclampsia (175, 176), acute kidney injury (173), clear cell renal cell carcinoma (172), and renal transplant rejection (174). This study provides a framework for future studies to investigate the potential of these hypoxia-induced miRNAs to be used in clinical applications related to pathological hypoxia-related diseases.

5.2 *miR-210* in kidney development

5.2.1 Future experiments

Chapter 3 showed that there is a male-specific nephron deficit when *miR-210* is deleted. Analysis of the timing of this nephron deficit showed that the gene expression changes become apparent by P2, but there was no significant difference in the number of glomeruli at P2. Thus, the nephron deficit occurs between P2 and P4, which is suggested by the variance in nephron number of P2 *miR-210* male KO kidneys. Further analysis of the timing of the onset of the deficit would be useful to better understand how male mice are affected by the *miR-210* deletion as well as comparing this to the determination of nephron number in female mice. To investigate this, nephron counting (i.e. Wt1-positive glomeruli) in male and female mice at P3 and P4 could be performed as well as stereological counting of Jag1-positive structures at P2, P3, and P4, since the data reported in Chapter 3 includes stereological nephron number analysis at P2 and only semi-quantitative analysis of developing nephron structures, lacking Wt1-positive glomeruli, was performed. Analysis of the timing of cessation of nephrogenesis did not show clear differences, but there may be more subtle differences. Combined with increased apoptosis and Wnt signaling, cessation a half-day early could contribute to a 35% nephron deficit. To investigate this, samples could be collected at half-day intervals (i.e. P3, P3.5, P4) and analyzed for nephron progenitor pool depletion and developmental pathway marker expression. Another way to address the amount of nephron progenitors at P3 would be to perform whole-mount immunostaining to quantify Six2-positive nephron progenitors. Further, this whole-mount immunostaining could be performed with immunostaining for Calb-positive ureteric bud tips and analysis of the number of ureteric bud tips (i.e. branching morphogenesis deficit) as well as the number of Six2-positive cells around each Calb-positive ureteric bud tip could be performed.

Chapter 3 suggested an increase in apoptosis of differentiating nephron progenitor/pre-tubular aggregate cells in male *miR-210* KO kidneys by P2. Separate analysis of apoptotic nephron progenitors and differentiated nephron structures showed no significant differences in either cell type, but there could be a difference when analyzing cells at the point of differentiation. To investigate this finding, analysis of apoptotic cells at the bottom of the cap mesenchyme should be

conducted. Careful co-immunostaining, confocal imaging, and quantification of Six2-positive nephron progenitors, Ncam-positive nascent nephrons and nephron progenitors, and c-Casp3-positive apoptotic cells could be performed to address this question. Unlike the individual stains for Six2 and Jag1, which cannot distinguish differentiating cells and proximity to the cap mesenchyme, respectively, in this assay the amount of apoptotic cells that are Six2-positive and cells that are Six2-negative but Ncam-positive near the bottom of the cap mesenchyme would be counted. Thus, measuring the amount of apoptosis occurring during the differentiation process. Further analysis of Fas-receptor-mediated apoptosis signaling would also be useful to confirm if it is increased when *miR-210* is deleted.

The increase in Lef1 expression in male *miR-210* KO kidneys by P2 suggests increased activation of Wnt signaling pathway. Previous studies implicate *miR-210* in regulation of *Tcf7l2* as well as *Ctnnb1* (the β-catenin transcript) (158). Validation of targeting of these genes using the luciferase reporter gene assay in kidney cells (246) would shed light on the mechanism by which *miR-210* deletion affects Wnt signaling during kidney development. The *in situ* hybridization for *Wnt9b* and immunostaining for total and active β-catenin show no differences in localized expression, but these assays did not quantify expression levels. While Western blots can quantify expression changes, they cannot address cell-specific/localized expression differences. Thus, another avenue to investigate *miR-210*'s involvement in the Wnt pathway is using nephron progenitor cell cultures. Isolated *miR-210* wildtype and knockout nephron progenitors could be treated with Wnt agonists (e.g. BIO (259)) and antagonists (e.g. ICG-001 (260)) to investigate their self-renewal and differentiation potential (109, 144, 204). Treatment of the *miR-210* knockout nephron progenitors with Wnt antagonist should result in them being more like wildtype cells. Similarly, treatment of wildtype nephron progenitors with Wnt agonist should result in knockout cell-like phenotype. Further, the knockout nephron progenitors would be expected to be more susceptible to treatment with Wnt agonist, since *miR-210* is antagonistic to the pathway's activation.

The sex-specific nephron number deficit observed in *miR-210* knockout mice is similar to that observed in a model of prenatal hypoxia (60). This study found that at 12 months of age, both sexes exposed to hypoxia were more susceptible to high-salt diet-induced cardiac fibrosis, but only the hypoxia-exposed male mice were susceptible to salt-induced kidney fibrosis (60). This study and the findings in Chapter 3 match with what is known about sex-specific differences in

individuals with IUGR (91, 242). Thus, investigation of the *miR-210* knockout model in regard to decreased kidney health with aging and its response to a high-salt diet (i.e. analyzing kidney function and fibrosis at 4, 6, and 12 months) would be useful in understanding the genes involved in sex-specific differences in aging and hypertension. Further, nephron number analysis of ovariectomized (method as described in (261)) female *miR-210* wildtype and knockout mice would determine the role of sex hormones in *miR-210*-dependent regulation of kidney development. In addition, analysis of these female ovariectomized mice regarding their risk for developing hypertension would further lend insight to the role of sex-dependent *miR-210* regulation.

5.2.2 Global implications

IUGR and decreased nephron number are associated with an increased risk for developing disease, in a sex-dependent manner (76, 87, 242). However, little is known about how these sex-specific differences occur during kidney development. This study showed that hypoxia-induced *miR-210* is involved in this sex-specific regulation of kidney development, which is the first miRNA to be identified as having a sex-specific impact on nephron number. Thus, it appears that *miR-210* is important for regulating gene expression in physiologically hypoxic kidney development (i.e. normal kidney development).

Wnt/β-catenin signaling is an important regulator of the balance of nephron progenitor self-renewal versus differentiation (262), which is a major factor determining nephron number (47). Previous research has shown that nephron progenitors cultured in hypoxia had reduced Wnt signaling, disrupting their balance of self-renewal versus differentiation (197); *in utero* hypoxia suppresses ureteric β-catenin signaling (115); and *miR-210* has previously been implicated in regulating the Wnt pathway (158, 263). These data, along with this study, suggest that *miR-210* is plays a role in the hypoxic regulation of the Wnt signaling pathway during kidney development. Proper regulation of Wnt signaling is an important factor when culturing nephron progenitor cells *ex vivo* as well as in the development of kidney organoid cultures (144, 204, 264, 265). Further investigation into the mechanism of *miR-210*-mediated Wnt/β-catenin signaling regulation would increase our understanding of the complex nephrogenesis process.

Apoptosis is a normal developmental process, and miRNAs are an important regulator of apoptosis during kidney development (137, 138, 143, 223, 224). Chapter 3 adds to what is known about the role that *miR-210* plays in regulating apoptosis. *miR-210* has been shown to inhibit apoptosis during hypoxia (149, 153, 154, 266-268). The *miR-210* target *Casp8ap2*, which Chapter 3 showed is specifically increased in male *miR-210* KO kidneys, has increased expression in males compared to females in developing mouse lung tissue (236). Thus, this study shows the role that *miR-210* plays in regulating apoptosis in a sex-specific manner in the physiological hypoxia during kidney development. It has previously been shown that increased apoptosis of nephron progenitors results in a nephron deficit (138, 223). The data in Chapter 3 show that *miR-210* is another regulator of apoptosis during kidney development that is required to maintain normal nephron number development.

5.3 *In vivo* hypoxic kidney development

5.3.1 Future experiments

Chapter 4 showed no major differences in the *miR-210* knockout model to hypoxia by E17. However, Chapter 3 showed that the *miR-210* knockout mice do not exhibit changes in kidney development gene expression until P2. Thus, it is possible that there is a difference in the knockout model's response to intrauterine hypoxia at a later timepoint. To investigate this, the *in vivo* hypoxia model analysis (as in Chapter 4) could be performed at P0 and P2. Analysis of nephron number and signaling pathway activation as in Chapter 3 could also be conducted as a comparison to the normoxic *miR-210* knockout phenotype. Relatedly, the findings in Chapter 3 show a sex-specific difference during kidney development in the *miR-210* knockout model, so analysis of its response to hypoxic insult during pregnancy should be conducted with the sexes separated.

Chapter 3 showed a 35% nephron deficit in the *miR-210* knockout male mice, and a 28% nephron deficit in wildtype and knockout females, similar to that observed a model of prenatal hypoxia (60). The kidney development marker expression analysis performed in Chapter 4 suggests that the *miR-210* knockout mice from hypoxic pregnancies may have altered ureteric

branching development, which could result in a nephron deficit. Thus, analysis of nephron number at P30 in male and female *miR-210* wildtype and knockout mice from hypoxic pregnancies could be performed to address this possibility.

Recently, a mouse model with a Tet-on construct that can be used to induce overexpression of *miR-210* was created (269). This mouse could be used to determine the effect that *miR-210* overexpression has on kidney development, compared to hypoxia-induced *miR-210* overexpression, as observed in the *Six2-VHL*$^{-/-}$ and hypoxia chamber models in Chapter 4. Analysis of nephron number and expression of key genes involved in regulating kidney development in this overexpression model would lend insight to the role *miR-210* plays in the hypoxia response by comparing these results to those produced with hypoxia models. This study would also be a useful comparison to the findings of Chapter 3, to determine how loss-of-function of *miR-210* compares to its gain-of-function in the setting of kidney development.

5.3.2 Global implications

Several studies have investigated how fetal hypoxia impacts kidney development (60-62, 75, 115, 197); and *miR-210* has recently been implicated as a biomarker for acute fetal hypoxia (177). This study is the first to look at the role of *miR-210* in the kidney's response to fetal hypoxia. While few differences were identified, further investigation of the effect of *miR-210* deletion in the setting of fetal hypoxia would increase understanding of how it impacts nephron number development. Decreased expression of the ureteric bud marker *Calb* in hypoxia-exposed *miR-210* knockout embryonic kidneys suggests a link between *miR-210* and hypoxia-induced suppression of Wnt signaling (115). Studying the overexpression of *miR-210* during kidney development would also increase our understanding of what role it plays in regulating fetal responses to hypoxia.

Bibliography

1. Langmead B, Trapnell C, Pop M, Salzberg SL. Ultrafast and memory-efficient alignment of short DNA sequences to the human genome. Genome Biol. 2009;10(3):R25. Epub 2009/03/06. doi: 10.1186/gb-2009-10-3-r25. PubMed PMID: 19261174; PMCID: PMC2690996.

2. Drawz P, Rahman M. In the Clinic: Chronic Kidney Disease. Annals of Internal Medicine. 2015.

3. Tonelli M, Wiebe N, Knoll G, Bello A, Browne S, Jadhav D, Klarenbach S, Gill J. Systematic review: kidney transplantation compared with dialysis in clinically relevant outcomes. Am J Transplant. 2011;11(10):2093-109. Epub 2011/09/03. doi: 10.1111/j.1600-6143.2011.03686.x. PubMed PMID: 21883901.

4. Yoo KD, Kim CT, Kim MH, Noh J, Kim G, Kim H, An JN, Park JY, Cho H, Kim KH, Kim H, Ryu DR, Kim DK, Lim CS, Kim YS, Lee JP. Superior outcomes of kidney transplantation compared with dialysis: An optimal matched analysis of a national population-based cohort study between 2005 and 2008 in Korea. Medicine (Baltimore). 2016;95(33):e4352. Epub 2016/08/19. doi: 10.1097/MD.0000000000004352. PubMed PMID: 27537562; PMCID: PMC5370789.

5. Wolfe RA, Ashby VB, Milford EL, Ojo AO, Ettenger RE, Agodoa LY, Held PJ, Port FK. Comparison of mortality in all patients on dialysis, patients on dialysis awaiting transplantation, and recipients of a first cadaveric transplant. N Engl J Med. 1999;341(23):1725-30. Epub 1999/12/02. doi: 10.1056/NEJM199912023412303. PubMed PMID: 10580071.

6. Friedlander MR, Mackowiak SD, Li N, Chen W, Rajewsky N. miRDeep2 accurately identifies known and hundreds of novel microRNA genes in seven animal clades. Nucleic Acids Res. 2012;40(1):37-52. Epub 2011/09/14. doi: 10.1093/nar/gkr688. PubMed PMID: 21911355; PMCID: PMC3245920.

7. Newsome AD, Davis GK, Ojeda NB, Alexander BT. Complications during pregnancy and fetal development: implications for the occurrence of chronic kidney disease. Expert Rev Cardiovasc Ther. 2017;15(3):211-20. Epub 2017/03/04. doi: 10.1080/14779072.2017.1294066. PubMed PMID: 28256177; PMCID: PMC5543771.

8. Carrero JJ, Hecking M, Chesnaye NC, Jager KJ. Sex and gender disparities in the epidemiology and outcomes of chronic kidney disease. Nature reviews Nephrology. 2018. Epub 2018/01/23. doi: 10.1038/nrneph.2017.181. PubMed PMID: 29355169.

9. Sarnak MJ. Cardiovascular complications in chronic kidney disease. Am J Kidney Dis. 2003;41(5 Suppl):11-7. Epub 2003/05/31. doi: S027263860300372X [pii]. PubMed PMID: 12776309.

10. Amann K, Plank C, Dotsch J. Low nephron number--a new cardiovascular risk factor in children? Pediatric nephrology. 2004;19(12):1319-23. doi: 10.1007/s00467-004-1643-5. PubMed PMID: 15490250.

11. Horowitz B, Miskulin D, Zager P. Epidemiology of hypertension in CKD. Adv Chronic Kidney Dis. 2015;22(2):88-95. Epub 2015/02/24. doi: 10.1053/j.ackd.2014.09.004. PubMed PMID: 25704344.

12. Lumbers ER, Pringle KG, Wang Y, Gibson KJ. The renin-angiotensin system from conception to old age: the good, the bad and the ugly. Clinical and experimental pharmacology & physiology. 2013;40(11):743-52. Epub 2013/10/30. doi: 10.1111/1440-1681.12098. PubMed PMID: 24164175.

13. Yosypiv IV. Congenital anomalies of the kidney and urinary tract: a genetic disorder? Int J Nephrol. 2012;2012:909083. Epub 2012/06/12. doi: 10.1155/2012/909083. PubMed PMID: 22685656; PMCID: PMC3363415.

14. Baluarte HJ, Gruskin AB, Ingelfinger JR, Stablein D, Tejani A. Analysis of hypertension in children post renal transplantation--a report of the North American Pediatric Renal Transplant Cooperative Study (NAPRTCS). Pediatric nephrology. 1994;8(5):570-3. Epub 1994/10/01. doi: 10.1007/bf00858130. PubMed PMID: 7819003.

15. Song R, Yosypiv IV. Genetics of congenital anomalies of the kidney and urinary tract. Pediatric nephrology. 2010;26(3):353-64. doi: 10.1007/s00467-010-1629-4.

16. van der Ven AT, Vivante A, Hildebrandt F. Novel Insights into the Pathogenesis of Monogenic Congenital Anomalies of the Kidney and Urinary Tract. Journal of the American Society of Nephrology : JASN. 2018;29(1):36-50. doi: 10.1681/ASN.2017050561. PubMed PMID: 29079659.

17. Weber S. Novel genetic aspects of congenital anomalies of kidney and urinary tract. Curr Opin Pediatr. 2012;24(2):212-8. Epub 2012/01/17. doi: 10.1097/MOP.0b013e32834fdbd4. PubMed PMID: 22245908.

18. Groothoff JW, Gruppen MP, Offringa M, Hutten J, Lilien MR, Van De Kar NJ, Wolff ED, Davin JC, Heymans HS. Mortality and causes of death of end-stage renal disease in children: a Dutch cohort study. Kidney international. 2002;61(2):621-9. Epub 2002/02/19. doi: 10.1046/j.1523-1755.2002.00156.x. PubMed PMID: 11849405.

19. Sanna-Cherchi S, Ravani P, Corbani V, Parodi S, Haupt R, Piaggio G, Innocenti ML, Somenzi D, Trivelli A, Caridi G, Izzi C, Scolari F, Mattioli G, Allegri L, Ghiggeri GM. Renal outcome in patients with congenital anomalies of the kidney and urinary tract. Kidney international. 2009;76(5):528-33. Epub 2009/06/19. doi: 10.1038/ki.2009.220. PubMed PMID: 19536081.

20. Bertram JF, Douglas-Denton RN, Diouf B, Hughson MD, Hoy WE. Human nephron number: implications for health and disease. Pediatric nephrology. 2011;26(9):1529-33. Epub 2011/05/24. doi: 10.1007/s00467-011-1843-8. PubMed PMID: 21604189.

21. Hoy WE, Hughson MD, Bertram JF, Douglas-Denton R, Amann K. Nephron number, hypertension, renal disease, and renal failure. Journal of the American Society of Nephrology : JASN. 2005;16(9):2557-64. Epub 2005/07/29. doi: 10.1681/ASN.2005020172. PubMed PMID: 16049069.

22. Nyengaard JR, Bendtsen TF. Glomerular number and size in relation to age, kidney weight, and body surface in normal man. Anat Rec. 1992;232(2):194-201. Epub 1992/02/01. doi: 10.1002/ar.1092320205. PubMed PMID: 1546799.

23. Hinchliffe SA, Sargent PH, Howard CV, Chan YF, van Velzen D. Human intrauterine renal growth expressed in absolute number of glomeruli assessed by the disector method and Cavalieri principle. Lab Invest. 1991;64(6):777-84. PubMed PMID: 2046329.

24. Denic A, Lieske JC, Chakkera HA, Poggio ED, Alexander MP, Singh P, Kremers WK, Lerman LO, Rule AD. The Substantial Loss of Nephrons in Healthy Human Kidneys with Aging. Journal of the American Society of Nephrology : JASN. 2017;28(1):313-20. doi: 10.1681/ASN.2016020154. PubMed PMID: 27401688.

25. Schnaper HW. Remnant nephron physiology and the progression of chronic kidney disease. Pediatric nephrology. 2014;29(2):193-202. Epub 2013/05/30. doi: 10.1007/s00467-013-2494-8. PubMed PMID: 23715783; PMCID: PMC3796124.

26. Brenner BM, Mackenzie HS. Nephron mass as a risk factor for progression of renal disease. Kidney Int Suppl. 1997;63:S124-7. Epub 1998/01/04. PubMed PMID: 9407439.
27. Thomas DM, Coles GA, Williams JD. What does the renal reserve mean? Kidney international. 1994;45(2):411-6. doi: 10.1038/ki.1994.53.
28. Brenner BM. Nephron adaptation to renal injury or ablation. Am J Physiol. 1985;249(3 Pt 2):F324-37. Epub 1985/09/01. doi: 10.1152/ajprenal.1985.249.3.F324. PubMed PMID: 3898871.
29. Brenner BM, Lawler EV, Mackenzie HS. The hyperfiltration theory: a paradigm shift in nephrology. Kidney international. 1996;49(6):1774-7. Epub 1996/06/01. doi: 10.1038/ki.1996.265. PubMed PMID: 8743495.
30. Luyckx VA, Brenner BM. The clinical importance of nephron mass. Journal of the American Society of Nephrology : JASN. 2010;21(6):898-910. Epub 2010/02/13. doi: 10.1681/ASN.2009121248. PubMed PMID: 20150537.
31. Puelles VG, Douglas-Denton RN, Zimanyi MA, Armitage JA, Hughson MD, Kerr PG, Bertram JF. Glomerular hypertrophy in subjects with low nephron number: contributions of sex, body size and race. Nephrology, dialysis, transplantation : official publication of the European Dialysis and Transplant Association - European Renal Association. 2014;29(9):1686-95. Epub 2014/05/06. doi: 10.1093/ndt/gfu088. PubMed PMID: 24792374; PMCID: PMC4145866.
32. Seely JC. A brief review of kidney development, maturation, developmental abnormalities, and drug toxicity: juvenile animal relevancy. J Toxicol Pathol. 2017;30(2):125-33. Epub 2017/05/02. doi: 10.1293/tox.2017-0006. PubMed PMID: 28458450; PMCID: PMC5406591.
33. Hoar RM. Comparative developmental aspects of selected organ systems. II. Gastrointestinal and urogenital systems. Environ Health Perspect. 1976;18:61-6. Epub 1976/12/01. doi: 10.1289/ehp.761861. PubMed PMID: 1030401; PMCID: PMC1475310.
34. Davidson AJ. Mouse kidney development. In: Chien KR, editor. StemBook. Cambridge (MA)2008.
35. Pietila I, Vainio S. The embryonic aorta-gonad-mesonephros region as a generator of haematopoietic stem cells. APMIS. 2005;113(11-12):804-12.
36. Pole RJ, Qi BQ, Beasley SW. Patterns of apoptosis during degeneration of the pronephros and mesonephros. J Urol. 2002;167(1):269-71. Epub 2001/12/18. PubMed PMID: 11743336.

37.Vetter MR, Gibley CW, Jr. Morphogenesis and histochemistry of the developing mouse kidney. J Morphol. 1966;120(2):135-55. Epub 1966/10/01. doi: 10.1002/jmor.1051200203. PubMed PMID: 6008029.

38. Saxen L. Organogenesis of the kidney: Press Syndicate of the University of Cambridge; 1987.

39. Sainio K, Hellstedt P, Kreidberg JA, Saxen L, Sariola H. Differential regulation of two sets of mesonephric tubules by WT-1. Development. 1997;124(7):1293-9. Epub 1997/04/01. PubMed PMID: 9118800.

40. Smith C, Mackay S. Morphological development and fate of the mouse mesonephros. Journal of anatomy. 1991;174:171-84. Epub 1991/02/01. PubMed PMID: 2032933; PMCID: PMC1256053.

41. Hartman HA, Lai HL, Patterson LT. Cessation of renal morphogenesis in mice. Developmental biology. 2007;310(2):379-87. PubMed PMID: 17826763.

42. Bard JB. Growth and death in the developing mammalian kidney: signals, receptors and conversations. Bioessays. 2002;24(1):72-82. doi: 10.1002/bies.10024. PubMed PMID: 11782952.

43. Kobayashi A, Valerius MT, Mugford JW, Carroll TJ, Self M, Oliver G, McMahon AP. Six2 defines and regulates a multipotent self-renewing nephron progenitor population throughout mammalian kidney development. Cell Stem Cell. 2008;3(2):169-81. doi: 10.1016/j.stem.2008.05.020. PubMed PMID: 18682239; PMCID: PMC2561900.

44. Basson MA, Watson-Johnson J, Shakya R, Akbulut S, Hyink D, Costantini FD, Wilson PD, Mason IJ, Licht JD. Branching morphogenesis of the ureteric epithelium during kidney development is coordinated by the opposing functions of GDNF and Sprouty1. Developmental biology. 2006;299(2):466-77. doi: 10.1016/j.ydbio.2006.08.051. PubMed PMID: 17022962.

45. Costantini F, Kopan R. Patterning a complex organ: branching morphogenesis and nephron segmentation in kidney development. Developmental cell. 2010;18(5):698-712. Epub 2010/05/25. doi: 10.1016/j.devcel.2010.04.008. PubMed PMID: 20493806; PMCID: PMC2883254.

46. O'Brien LL, McMahon AP. Induction and patterning of the metanephric nephron. Semin Cell Dev Biol. 2014;36:31-8. doi: 10.1016/j.semcdb.2014.08.014. PubMed PMID: 25194660; PMCID: PMC4252735.

47. Cebrian C, Asai N, D'Agati V, Costantini F. The number of fetal nephron progenitor cells limits ureteric branching and adult nephron endowment. Cell reports. 2014;7(1):127-37. Epub

2014/03/25. doi: 10.1016/j.celrep.2014.02.033. PubMed PMID: 24656820; PMCID: PMC4049224.

48. Dziarmaga A, Eccles M, Goodyer P. Suppression of ureteric bud apoptosis rescues nephron endowment and adult renal function in Pax2 mutant mice. Journal of the American Society of Nephrology : JASN. 2006;17(6):1568-75. Epub 2006/05/05. doi: 10.1681/ASN.2005101074. PubMed PMID: 16672320.

49. Short KM, Smyth IM. The contribution of branching morphogenesis to kidney development and disease. Nature reviews Nephrology. 2016;12(12):754-67. doi: 10.1038/nrneph.2016.157. PubMed PMID: 27818506.

50. Sampogna RV, Schneider L, Al-Awqati Q. Developmental Programming of Branching Morphogenesis in the Kidney. Journal of the American Society of Nephrology : JASN. 2015;26(10):2414-22. doi: 10.1681/ASN.2014090886. PubMed PMID: 25644110; PMCID: PMC4587701.

51. Short KM, Combes AN, Lefevre J, Ju AL, Georgas KM, Lamberton T, Cairncross O, Rumballe BA, McMahon AP, Hamilton NA, Smyth IM, Little MH. Global quantification of tissue dynamics in the developing mouse kidney. Developmental cell. 2014;29(2):188-202. Epub 2014/05/02. doi: 10.1016/j.devcel.2014.02.017. PubMed PMID: 24780737.

52. Dunwoodie SL. The role of hypoxia in development of the Mammalian embryo. Developmental cell. 2009;17(6):755-73. doi: 10.1016/j.devcel.2009.11.008. PubMed PMID: 20059947.

53. Okazaki K, Maltepe E. Oxygen, epigenetics and stem cell fate. Regen Med. 2006;1(1):71-83. doi: 10.2217/17460751.1.1.71. PubMed PMID: 17465821.

54. Bernhardt WM, Schmitt R, Rosenberger C, Munchenhagen PM, Grone HJ, Frei U, Warnecke C, Bachmann S, Wiesener MS, Willam C, Eckardt KU. Expression of hypoxia-inducible transcription factors in developing human and rat kidneys. Kidney international. 2006;69(1):114-22. Epub 2005/12/24. doi: 10.1038/sj.ki.5000062. PubMed PMID: 16374431.

55. Gerosa C, Fanni D, Faa A, Van Eyken P, Ravarino A, Fanos V, Faa G. Low vascularization of the nephrogenic zone of the fetal kidney suggests a major role for hypoxia in human nephrogenesis. Int Urol Nephrol. 2017;49(9). doi: 10.1007/s11255-017-1630-y. PubMed PMID: 28573487.

56. Hemker SL, Sims-Lucas S, Ho J. Role of hypoxia during nephrogenesis. Pediatric nephrology. 2016;31(10):1571-7. doi: 10.1007/s00467-016-3333-5. PubMed PMID: 26872484; PMCID: PMC4982845.
57. Baschat AA. Fetal responses to placental insufficiency: an update. BJOG. 2004;111(10):1031-41. doi: 10.1111/j.1471-0528.2004.00273.x. PubMed PMID: 15383103.
58. Gagnon R. Placental insufficiency and its consequences. European Journal of Obstetrics & Gynecology and Reproductive Biology. 2003;110:S99-S107. doi: 10.1016/s0301-2115(03)00179-9.
59. Gonzalez-Rodriguez P, Jr., Tong W, Xue Q, Li Y, Hu S, Zhang L. Fetal hypoxia results in programming of aberrant angiotensin ii receptor expression patterns and kidney development. Int J Med Sci. 2013;10(5):532-8. Epub 2013/03/28. doi: 10.7150/ijms.5566. PubMed PMID: 23532764; PMCID: PMC3607238.
60. Walton SL, Bielefeldt-Ohmann H, Singh RR, Li J, Paravicini TM, Little MH, Moritz KM. Prenatal hypoxia leads to hypertension, renal renin-angiotensin system activation and exacerbates salt-induced pathology in a sex-specific manner. Sci Rep. 2017;7(1):8241. Epub 2017/08/16. doi: 10.1038/s41598-017-08365-4. PubMed PMID: 28811528; PMCID: PMC5557956.
61. Walton SL, Singh RR, Little MH, Bowles J, Li J, Moritz KM. Prolonged prenatal hypoxia selectively disrupts collecting duct patterning and postnatal function in male mouse offspring. The Journal of physiology. 2018;596(23):5873-89. Epub 2018/04/21. doi: 10.1113/JP275918. PubMed PMID: 29676801.
62. Figueroa H, Lozano M, Suazo C, Eixarch E, Illanes SE, Carreno JE, Villanueva S, Hernandez-Andrade E, Gratacos E, Irarrazabal CE. Intrauterine growth restriction modifies the normal gene expression in kidney from rabbit fetuses. Early Hum Dev. 2012;88(11):899-904. doi: 10.1016/j.earlhumdev.2012.07.010. PubMed PMID: 22944138.
63. Moritz KM, Mazzuca MQ, Siebel AL, Mibus A, Arena D, Tare M, Owens JA, Wlodek ME. Uteroplacental insufficiency causes a nephron deficit, modest renal insufficiency but no hypertension with ageing in female rats. The Journal of physiology. 2009;587(Pt 11):2635-46. Epub 2009/04/11. doi: 10.1113/jphysiol.2009.170407. PubMed PMID: 19359373; PMCID: PMC2714027.

64. Cosmi E, Fanelli T, Visentin S, Trevisanuto D, Zanardo V. Consequences in infants that were intrauterine growth restricted. Journal of pregnancy. 2011;2011:364381. Epub 2011/05/07. doi: 10.1155/2011/364381. PubMed PMID: 21547088; PMCID: PMC3087146.

65. Horikoshi M, Beaumont RN, Day FR, Warrington NM, Kooijman MN, Fernandez-Tajes J, Feenstra B, van Zuydam NR, Gaulton KJ, Grarup N, Bradfield JP, Strachan DP, Li-Gao R, Ahluwalia TS, Kreiner E, Rueedi R, Lyytikainen LP, Cousminer DL, Wu Y, Thiering E, Wang CA, Have CT, Hottenga JJ, Vilor-Tejedor N, Joshi PK, Boh ET, Ntalla I, Pitkanen N, Mahajan A, van Leeuwen EM, Joro R, Lagou V, Nodzenski M, Diver LA, Zondervan KT, Bustamante M, Marques-Vidal P, Mercader JM, Bennett AJ, Rahmioglu N, Nyholt DR, Ma RC, Tam CH, Tam WH, Group CCHW, Ganesh SK, van Rooij FJ, Jones SE, Loh PR, Ruth KS, Tuke MA, Tyrrell J, Wood AR, Yaghootkar H, Scholtens DM, Paternoster L, Prokopenko I, Kovacs P, Atalay M, Willems SM, Panoutsopoulou K, Wang X, Carstensen L, Geller F, Schraut KE, Murcia M, van Beijsterveldt CE, Willemsen G, Appel EV, Fonvig CE, Trier C, Tiesler CM, Standl M, Kutalik Z, Bonas-Guarch S, Hougaard DM, Sanchez F, Torrents D, Waage J, Hollegaard MV, de Haan HG, Rosendaal FR, Medina-Gomez C, Ring SM, Hemani G, McMahon G, Robertson NR, Groves CJ, Langenberg C, Luan J, Scott RA, Zhao JH, Mentch FD, MacKenzie SM, Reynolds RM, Early Growth Genetics C, Lowe WL, Tonjes A, Stumvoll M, Lindi V, Lakka TA, van Duijn CM, Kiess W, Korner A, Sorensen TI, Niinikoski H, Pahkala K, Raitakari OT, Zeggini E, Dedoussis GV, Teo YY, Saw SM, Melbye M, Campbell H, Wilson JF, Vrijheid M, de Geus EJ, Boomsma DI, Kadarmideen HN, Holm JC, Hansen T, Sebert S, Hattersley AT, Beilin LJ, Newnham JP, Pennell CE, Heinrich J, Adair LS, Borja JB, Mohlke KL, Eriksson JG, Widen E, Kahonen M, Viikari JS, Lehtimaki T, Vollenweider P, Bonnelykke K, Bisgaard H, Mook-Kanamori DO, Hofman A, Rivadeneira F, Uitterlinden AG, Pisinger C, Pedersen O, Power C, Hypponen E, Wareham NJ, Hakonarson H, Davies E, Walker BR, Jaddoe VW, Jarvelin MR, Grant SF, Vaag AA, Lawlor DA, Frayling TM, Smith GD, Morris AP, Ong KK, Felix JF, Timpson NJ, Perry JR, Evans DM, McCarthy MI, Freathy RM. Genome-wide associations for birth weight and correlations with adult disease. Nature. 2016;538(7624):248-52. doi: 10.1038/nature19806. PubMed PMID: 27680694.

66. Barker DJ, Osmond C, Golding J, Kuh D, Wadsworth ME. Growth in utero, blood pressure in childhood and adult life, and mortality from cardiovascular disease. BMJ (Clinical research ed. 1989;298(6673):564-7. Epub 1989/03/04. doi: 10.1136/bmj.298.6673.564. PubMed PMID: 2495113; PMCID: PMC1835925.

67. Dasinger JH, Davis GK, Newsome AD, Alexander BT. Developmental Programming of Hypertension: Physiological Mechanisms. Hypertension. 2016;68(4):826-31. Epub 2016/08/24. doi: 10.1161/HYPERTENSIONAHA.116.06603. PubMed PMID: 27550912; PMCID: PMC5016247.

68. Dagan A, Kwon HM, Dwarakanath V, Baum M. Effect of renal denervation on prenatal programming of hypertension and renal tubular transporter abundance. American journal of physiology Renal physiology. 2008;295(1):F29-34. Epub 2008/04/11. doi: 10.1152/ajprenal.00123.2008. PubMed PMID: 18400872; PMCID: PMC4063419.

69. Rymer C, Paredes J, Halt K, Schaefer C, Wiersch J, Zhang G, Potoka D, Vainio S, Gittes GK, Bates CM, Sims-Lucas S. Renal blood flow and oxygenation drive nephron progenitor differentiation. American journal of physiology Renal physiology. 2014;307(3):F337-45. Epub 2014/06/13. doi: 10.1152/ajprenal.00208.2014. PubMed PMID: 24920757; PMCID: PMC4121567.

70. Freeburg PB, Abrahamson DR. Hypoxia-inducible factors and kidney vascular development. Journal of the American Society of Nephrology : JASN. 2003;14(11):2723-30. doi: 10.1097/01.asn.0000092794.37534.01. PubMed PMID: 14569081.

71. Wenger RH, Stiehl DP, Camenisch G. Integration of oxygen signaling at the consensus HRE. Sci STKE. 2005;2005(306):re12. doi: 10.1126/stke.3062005re12. PubMed PMID: 16234508.

72. Freeburg PB, Robert B, St John PL, Abrahamson DR. Podocyte expression of hypoxia-inducible factor (HIF)-1 and HIF-2 during glomerular development. Journal of the American Society of Nephrology : JASN. 2003;14(4):927-38. doi: 10.1097/01.asn.0000059308.82322.4f. PubMed PMID: 12660327.

73. Hu CJ, Wang LY, Chodosh LA, Keith B, Simon MC. Differential roles of hypoxia-inducible factor 1 alpha (HIF-1 alpha) and HIF-2 alpha in hypoxic gene regulation. Molecular and cellular biology. 2003;23(24):9361-74. doi: 10.1128/Mcb.23.24.9361-9374.2003. PubMed PMID: WOS:000187040400040.

74. Liu J, Edgington-Giordano F, Dugas C, Abrams A, Katakam P, Satou R, Saifudeen Z. Regulation of Nephron Progenitor Cell Self-Renewal by Intermediary Metabolism. Journal of the American Society of Nephrology : JASN. 2017. doi: 10.1681/ASN.2016111246. PubMed PMID: 28754792.

75. Cargill K, Hemker SL, Clugston A, Murali A, Mukherjee E, Liu J, Bushnell D, Bodnar AJ, Saifudeen Z, Ho J, Bates CM, Kostka D, Goetzman ES, Sims-Lucas S. Von Hippel-Lindau Acts as a Metabolic Switch Controlling Nephron Progenitor Differentiation. Journal of the American Society of Nephrology : JASN. 2019;30(7):1192-205. Epub 2019/05/31. doi: 10.1681/ASN.2018111170. PubMed PMID: 31142573; PMCID: PMC6622426.

76. Hughson MD, Douglas-Denton R, Bertram JF, Hoy WE. Hypertension, glomerular number, and birth weight in African Americans and white subjects in the southeastern United States. Kidney international. 2006;69(4):671-8. Epub 2006/01/06. doi: 10.1038/sj.ki.5000041. PubMed PMID: 16395270.

77. Murawski IJ, Maina RW, Gupta IR. The relationship between nephron number, kidney size and body weight in two inbred mouse strains. Organogenesis. 2010;6(3):189-94. Epub 2011/01/05. doi: 10.4161/org.6.3.12125. PubMed PMID: 21197222; PMCID: PMC2946052.

78. Ransick A, Lindström NO, Liu J, Qin Z, Guo J-J, Alvarado GF, Kim AD, Black HG, Kim J, McMahon AP. Single Cell Profiling Reveals Sex, Lineage and Regional Diversity in the Mouse Kidney2019. doi: 10.1101/673335.

79. Si H, Banga RS, Kapitsinou P, Ramaiah M, Lawrence J, Kambhampati G, Gruenwald A, Bottinger E, Glicklich D, Tellis V, Greenstein S, Thomas DB, Pullman J, Fazzari M, Susztak K. Human and murine kidneys show gender- and species-specific gene expression differences in response to injury. PloS one. 2009;4(3):e4802. Epub 2009/03/12. doi: 10.1371/journal.pone.0004802. PubMed PMID: 19277126; PMCID: PMC2652077.

80. Mayne BT, Bianco-Miotto T, Buckberry S, Breen J, Clifton V, Shoubridge C, Roberts CT. Large Scale Gene Expression Meta-Analysis Reveals Tissue-Specific, Sex-Biased Gene Expression in Humans. Front Genet. 2016;7:183. Epub 2016/10/30. doi: 10.3389/fgene.2016.00183. PubMed PMID: 27790248; PMCID: PMC5062749.

81. Hutson DD, Gurrala R, Ogola BO, Zimmerman MA, Mostany R, Satou R, Lindsey SH. Estrogen receptor profiles across tissues from male and female Rattus norvegicus. Biology of Sex Differences. 2019;10(1). doi: 10.1186/s13293-019-0219-9.

82. Boddu R, Fan C, Rangarajan S, Sunil B, Bolisetty S, Curtis LM. Unique sex- and age-dependent effects in protective pathways in acute kidney injury. American journal of physiology Renal physiology. 2017;313(3):F740-F55. Epub 2017/07/07. doi: 10.1152/ajprenal.00049.2017. PubMed PMID: 28679590; PMCID: PMC5625098.

83. Kummer S, von Gersdorff G, Kemper MJ, Oh J. The influence of gender and sexual hormones on incidence and outcome of chronic kidney disease. Pediatric nephrology. 2012;27(8):1213-9. Epub 2011/07/19. doi: 10.1007/s00467-011-1963-1. PubMed PMID: 21766172.
84. Saez F, Castells MT, Zuasti A, Salazar F, Reverte V, Loria A, Salazar FJ. Sex differences in the renal changes elicited by angiotensin II blockade during the nephrogenic period. Hypertension. 2007;49(6):1429-35. Epub 2007/04/04. doi: 10.1161/HYPERTENSIONAHA.107.087957. PubMed PMID: 17404180.
85. Ikeda M, Swide T, Vayl A, Lahm T, Anderson S, Hutchens MP. Estrogen administered after cardiac arrest and cardiopulmonary resuscitation ameliorates acute kidney injury in a sex- and age-specific manner. Crit Care. 2015;19:332. Epub 2015/09/19. doi: 10.1186/s13054-015-1049-8. PubMed PMID: 26384003; PMCID: PMC4574460.
86. Davis GK, Newsome AD, Ojeda NB, Alexander BT. Effects of Intrauterine Growth Restriction and Female Sex on Future Blood Pressure and Cardiovascular Disease. Curr Hypertens Rep. 2017;19(2):13. Epub 2017/02/25. doi: 10.1007/s11906-017-0712-7. PubMed PMID: 28233240; PMCID: PMC5483947.
87. Gilbert JS, Nijland MJ. Sex differences in the developmental origins of hypertension and cardiorenal disease. Am J Physiol Regul Integr Comp Physiol. 2008;295(6):R1941-52. Epub 2008/10/31. doi: 10.1152/ajpregu.90724.2008. PubMed PMID: 18971349; PMCID: PMC2685301.
88. Baum M. Role of renal sympathetic nerve activity in prenatal programming of hypertension. Pediatric nephrology. 2018;33(3):409-19. Epub 2016/03/24. doi: 10.1007/s00467-016-3359-8. PubMed PMID: 27001053.
89. Intapad S, Tull FL, Brown AD, Dasinger JH, Ojeda NB, Fahling JM, Alexander BT. Renal denervation abolishes the age-dependent increase in blood pressure in female intrauterine growth-restricted rats at 12 months of age. Hypertension. 2013;61(4):828-34. Epub 2013/02/21. doi: 10.1161/HYPERTENSIONAHA.111.00645. PubMed PMID: 23424240; PMCID: PMC3626267.
90. Davis GK, Intapad S, Newsome AD, Coats LE, Bamrick DR, Ojeda NB, Alexander BT. Androgen Receptor Blockade Differentially Regulates Blood Pressure in Growth-Restricted Versus Ovarian Deficient Rats. Hypertension. 2019;74(4):975-82. Epub 2019/08/06. doi: 10.1161/HYPERTENSIONAHA.119.13257. PubMed PMID: 31378101; PMCID: PMC6739128.

91. Dasinger JH, Alexander BT. Gender differences in developmental programming of cardiovascular diseases. Clin Sci (Lond). 2016;130(5):337-48. Epub 2016/01/28. doi: 10.1042/CS20150611. PubMed PMID: 26814204; PMCID: PMC4912835.
92. Cuffe JS, Burgess DJ, O'Sullivan L, Singh RR, Moritz KM. Maternal corticosterone exposure in the mouse programs sex-specific renal adaptations in the renin-angiotensin-aldosterone system in 6-month offspring. Physiological reports. 2016;4(8). Epub 2016/04/29. doi: 10.14814/phy2.12754. PubMed PMID: 27122048; PMCID: PMC4848720.
93. Nishinakamura R, Matsumoto Y, Nakao K, Nakamura K, Sato A, Copeland NG, Gilbert DJ, Jenkins NA, Scully S, Lacey DL, Katsuki M, Asashima M, Yokota T. Murine homolog of SALL1 is essential for ureteric bud invasion in kidney development. Development. 2001;128(16):3105-15. PubMed PMID: 11688560.
94. Mugford JW, Sipila P, McMahon JA, McMahon AP. Osr1 expression demarcates a multi-potent population of intermediate mesoderm that undergoes progressive restriction to an Osr1-dependent nephron progenitor compartment within the mammalian kidney. Developmental biology. 2008;324(1):88-98. Epub 2008/10/07. doi: 10.1016/j.ydbio.2008.09.010. PubMed PMID: 18835385; PMCID: PMC2642884.
95. Xu J, Liu H, Park JS, Lan Y, Jiang R. Osr1 acts downstream of and interacts synergistically with Six2 to maintain nephron progenitor cells during kidney organogenesis. Development. 2014;141(7):1442-52. Epub 2014/03/07. doi: 10.1242/dev.103283. PubMed PMID: 24598167; PMCID: PMC3957368.
96. Self M, Lagutin OV, Bowling B, Hendrix J, Cai Y, Dressler GR, Oliver G. Six2 is required for suppression of nephrogenesis and progenitor renewal in the developing kidney. EMBO J. 2006;25(21):5214-28. doi: 10.1038/sj.emboj.7601381. PubMed PMID: 17036046; PMCID: PMC1630416.
97. Mugford JW, Yu J, Kobayashi A, McMahon AP. High-resolution gene expression analysis of the developing mouse kidney defines novel cellular compartments within the nephron progenitor population. Developmental biology. 2009;333(2):312-23. Epub 2009/07/14. doi: 10.1016/j.ydbio.2009.06.043. PubMed PMID: 19591821; PMCID: PMC2748313.
98. Kalatzis V, Sahly I, El-Amraoui A, Petit C. Eya1 expression in the developing ear and kidney: towards the understanding of the pathogenesis of Branchio-Oto-Renal (BOR) syndrome. Dev Dyn.

1998;213(4):486-99. doi: 10.1002/(SICI)1097-0177(199812)213:4<486::AID-AJA13>3.0.CO;2-L. PubMed PMID: 9853969.

99. Abdelhak S, Kalatzis V, Heilig R, Compain S, Samson D, Vincent C, Weil D, Cruaud C, Sahly I, Leibovici M, Bitner-Glindzicz M, Francis M, Lacombe D, Vigneron J, Charachon R, Boven K, Bedbeder P, Van Regemorter N, Weissenbach J, Petit C. A human homologue of the Drosophila eyes absent gene underlies branchio-oto-renal (BOR) syndrome and identifies a novel gene family. Nature genetics. 1997;15(2):157-64. doi: 10.1038/ng0297-157. PubMed PMID: 9020840.

100. Xu PX, Adams J, Peters H, Brown MC, Heaney S, Maas R. Eya1-deficient mice lack ears and kidneys and show abnormal apoptosis of organ primordia. Nature genetics. 1999;23(1):113-7. PubMed PMID: WOS:000082337300028.

101. Xu J, Wong EY, Cheng C, Li J, Sharkar MT, Xu CY, Chen B, Sun J, Jing D, Xu PX. Eya1 interacts with Six2 and Myc to regulate expansion of the nephron progenitor pool during nephrogenesis. Developmental cell. 2014;31(4):434-47. Epub 2014/12/03. doi: 10.1016/j.devcel.2014.10.015. PubMed PMID: 25458011; PMCID: PMC4282136.

102. Pan X, Karner CM, Carroll TJ. Myc cooperates with beta-catenin to drive gene expression in the nephron progenitor cells. Development. 2017. doi: 10.1242/dev.153700. PubMed PMID: 28993399.

103. Boyle S, Shioda T, Perantoni AO, de Caestecker M. Cited1 and Cited2 are differentially expressed in the developing kidney but are not required for nephrogenesis. Dev Dyn. 2007;236(8):2321-30. Epub 2007/07/07. doi: 10.1002/dvdy.21242. PubMed PMID: 17615577.

104. Brown AC, Muthukrishnan SD, Guay JA, Adams DC, Schafer DA, Fetting JL, Oxburgh L. Role for compartmentalization in nephron progenitor differentiation. Proc Natl Acad Sci U S A. 2013;110(12):4640-5. Epub March 4, 2013. doi: 10.1073/pnas.1213971110. PubMed PMID: 23487745; PMCID: PMC3607044.

105. Park JS, Valerius MT, McMahon AP. Wnt/beta-catenin signaling regulates nephron induction during mouse kidney development. Development. 2007;134(13):2533-9. doi: 10.1242/dev.006155. PubMed PMID: 17537789.

106. Carroll TJ, Park JS, Hayashi S, Majumdar A, McMahon AP. Wnt9b plays a central role in the regulation of mesenchymal to epithelial transitions underlying organogenesis of the mammalian urogenital system. Developmental cell. 2005;9(2):283-92. doi: 10.1016/j.devcel.2005.05.016. PubMed PMID: 16054034.

107. Kispert A, Vainio S, McMahon AP. Wnt-4 is a mesenchymal signal for epithelial transformation of metanephric mesenchyme in the developing kidney. Development. 1998;125(21):4225-34. Epub 1998/10/01. PubMed PMID: 9753677.
108. Stark K, Vainio S, Vassileva G, McMahon AP. Epithelial transformation of metanephric mesenchyme in the developing kidney regulated by Wnt-4. Nature. 1994;372(6507):679-83. Epub 1994/12/15. doi: 10.1038/372679a0. PubMed PMID: 7990960.
109. Park JS, Ma W, O'Brien LL, Chung E, Guo JJ, Cheng JG, Valerius MT, McMahon JA, Wong WH, McMahon AP. Six2 and Wnt regulate self-renewal and commitment of nephron progenitors through shared gene regulatory networks. Developmental cell. 2012;23(3):637-51. Epub 2012/08/21. doi: 10.1016/j.devcel.2012.07.008. PubMed PMID: 22902740; PMCID: PMC3892952.
110. Ramalingam H, Fessler AR, Das A, Valerius MT, Basta J, Robbins L, Brown AC, Oxburgh L, McMahon AP, Rauchman M, Carroll TJ. Disparate levels of beta-catenin activity determine nephron progenitor cell fate. Developmental biology. 2018. Epub 2018/05/01. doi: 10.1016/j.ydbio.2018.04.020. PubMed PMID: 29705331.
111. Grieshammer U, Cebrian C, Ilagan R, Meyers E, Herzlinger D, Martin GR. FGF8 is required for cell survival at distinct stages of nephrogenesis and for regulation of gene expression in nascent nephrons. Development. 2005;132(17):3847-57. Epub 2005/07/29. doi: 10.1242/dev.01944. PubMed PMID: 16049112.
112. Georgas K, Rumballe B, Valerius MT, Chiu HS, Thiagarajan RD, Lesieur E, Aronow BJ, Brunskill EW, Combes AN, Tang D, Taylor D, Grimmond SM, Potter SS, McMahon AP, Little MH. Analysis of early nephron patterning reveals a role for distal RV proliferation in fusion to the ureteric tip via a cap mesenchyme-derived connecting segment. Developmental biology. 2009;332(2):273-86. Epub 2009/06/09. doi: 10.1016/j.ydbio.2009.05.578. PubMed PMID: 19501082.
113. Perantoni AO, Timofeeva O, Naillat F, Richman C, Pajni-Underwood S, Wilson C, Vainio S, Dove LF, Lewandoski M. Inactivation of FGF8 in early mesoderm reveals an essential role in kidney development. Development. 2005;132(17):3859-71. Epub 2005/07/29. doi: 10.1242/dev.01945. PubMed PMID: 16049111.
114. Bridgewater D, Cox B, Cain J, Lau A, Athaide V, Gill PS, Kuure S, Sainio K, Rosenblum ND. Canonical WNT/beta-catenin signaling is required for ureteric branching. Developmental

biology. 2008;317(1):83-94. Epub 2008/03/25. doi: 10.1016/j.ydbio.2008.02.010. PubMed PMID: 18358465.

115. Wilkinson LJ, Neal CS, Singh RR, Sparrow DB, Kurniawan ND, Ju A, Grieve SM, Dunwoodie SL, Moritz KM, Little MH. Renal developmental defects resulting from in utero hypoxia are associated with suppression of ureteric beta-catenin signaling. Kidney international. 2015;87(5):975-83. Epub 2015/01/15. doi: 10.1038/ki.2014.394. PubMed PMID: 25587709.

116. Majumdar A, Vainio S, Kispert A, McMahon J, McMahon AP. Wnt11 and Ret/Gdnf pathways cooperate in regulating ureteric branching during metanephric kidney development. Development. 2003;130(14):3175-85. Epub 2003/06/05. PubMed PMID: 12783789.

117. Chung E, Deacon P, Park JS. Notch is required for the formation of all nephron segments and primes nephron progenitors for differentiation. Development. 2017;144(24):4530-9. doi: 10.1242/dev.156661. PubMed PMID: 29113990.

118. Cheng HT, Kim M, Valerius MT, Surendran K, Schuster-Gossler K, Gossler A, McMahon AP, Kopan R. Notch2, but not Notch1, is required for proximal fate acquisition in the mammalian nephron. Development. 2007;134(4):801-11. Epub 2007/01/19. doi: 10.1242/dev.02773. PubMed PMID: 17229764; PMCID: PMC2613851.

119. Mukherjee M, Fogarty E, Janga M, Surendran K. Notch Signaling in Kidney Development, Maintenance, and Disease. Biomolecules. 2019;9(11). Epub 2019/11/07. doi: 10.3390/biom9110692. PubMed PMID: 31690016.

120. Chung E, Deacon P, Marable S, Shin J, Park JS. Notch signaling promotes nephrogenesis by downregulating Six2. Development. 2016;143(21):3907-13. doi: 10.1242/dev.143503. PubMed PMID: 27633993.

121. Chen L, Al-Awqati Q. Segmental expression of Notch and Hairy genes in nephrogenesis. American journal of physiology Renal physiology. 2005;288(5):F939-52. doi: 10.1152/ajprenal.00369.2004. PubMed PMID: 15821257.

122. Taelman V, Van Campenhout C, Solter M, Pieler T, Bellefroid EJ. The Notch-effector HRT1 gene plays a role in glomerular development and patterning of the Xenopus pronephros anlagen. Development. 2006;133(15):2961-71. Epub 2006/07/05. doi: 10.1242/dev.02458. PubMed PMID: 16818449.

123. Borggrefe T, Lauth M, Zwijsen A, Huylebroeck D, Oswald F, Giaimo BD. The Notch intracellular domain integrates signals from Wnt, Hedgehog, TGFβ/BMP and hypoxia pathways.

Biochimica et Biophysica Acta (BBA) - Molecular Cell Research. 2016;1863(2):303-13. doi: 10.1016/j.bbamcr.2015.11.020.

124. Boyle SC, Kim M, Valerius MT, McMahon AP, Kopan R. Notch pathway activation can replace the requirement for Wnt4 and Wnt9b in mesenchymal-to-epithelial transition of nephron stem cells. Development. 2011;138(19):4245-54. Epub 2011/08/20. doi: 10.1242/dev.070433. PubMed PMID: 21852398; PMCID: PMC3171224.

125. Kasper DM, Moro A, Ristori E, Narayanan A, Hill-Teran G, Fleming E, Moreno-Mateos M, Vejnar CE, Zhang J, Lee D, Gu M, Gerstein M, Giraldez A, Nicoli S. MicroRNAs Establish Uniform Traits during the Architecture of Vertebrate Embryos. Developmental cell. 2017;40(6):552-65 e5. doi: 10.1016/j.devcel.2017.02.021. PubMed PMID: 28350988.

126. Landgraf P, Rusu M, Sheridan R, Sewer A, Iovino N, Aravin A, Pfeffer S, Rice A, Kamphorst AO, Landthaler M, Lin C, Socci ND, Hermida L, Fulci V, Chiaretti S, Foa R, Schliwka J, Fuchs U, Novosel A, Muller RU, Schermer B, Bissels U, Inman J, Phan Q, Chien M, Weir DB, Choksi R, De Vita G, Frezzetti D, Trompeter HI, Hornung V, Teng G, Hartmann G, Palkovits M, Di Lauro R, Wernet P, Macino G, Rogler CE, Nagle JW, Ju J, Papavasiliou FN, Benzing T, Lichter P, Tam W, Brownstein MJ, Bosio A, Borkhardt A, Russo JJ, Sander C, Zavolan M, Tuschl T. A mammalian microRNA expression atlas based on small RNA library sequencing. Cell. 2007;129(7):1401-14. doi: 10.1016/j.cell.2007.04.040. PubMed PMID: 17604727; PMCID: PMC2681231.

127. Phua YL, Clugston A, Chen KH, Kostka D, Ho J. Small non-coding RNA expression in mouse nephrogenic mesenchymal progenitors. Sci Data. 2018;5:180218. Epub 2018/11/14. doi: 10.1038/sdata.2018.218. PubMed PMID: 30422124; PMCID: PMC6233257.

128. Jovanovic I, Zivkovic M, Kostic M, Krstic Z, Djuric T, Kolic I, Alavantic D, Stankovic A. Transcriptome-wide based identification of miRs in congenital anomalies of the kidney and urinary tract (CAKUT) in children: the significant upregulation of tissue miR-144 expression. J Transl Med. 2016;14(1):193. doi: 10.1186/s12967-016-0955-0. PubMed PMID: 27364533; PMCID: PMC4929761.

129. Kohl S, Chen J, Vivante A, Hwang DY, Shril S, Dworschak GC, Van Der Ven A, Sanna-Cherchi S, Bauer SB, Lee RS, Soliman NA, Kehinde EO, Reutter HM, Tasic V, Hildebrandt F. Targeted sequencing of 96 renal developmental microRNAs in 1213 individuals from 980 families with congenital anomalies of the kidney and urinary tract. Nephrology, dialysis, transplantation :

official publication of the European Dialysis and Transplant Association - European Renal Association. 2016;31(8):1280-3. doi: 10.1093/ndt/gfv447. PubMed PMID: 26908769; PMCID: PMC4967727.

130. Harvey SJ, Jarad G, Cunningham J, Goldberg S, Schermer B, Harfe BD, McManus MT, Benzing T, Miner JH. Podocyte-specific deletion of dicer alters cytoskeletal dynamics and causes glomerular disease. Journal of the American Society of Nephrology : JASN. 2008;19(11):2150-8. Epub 2008/09/09. doi: 10.1681/ASN.2008020233. PubMed PMID: 18776121; PMCID: PMC2573015.

131. Ho J, Ng KH, Rosen S, Dostal A, Gregory RI, Kreidberg JA. Podocyte-specific loss of functional microRNAs leads to rapid glomerular and tubular injury. Journal of the American Society of Nephrology : JASN. 2008;19(11):2069-75. Epub 2008/10/04. doi: 10.1681/ASN.2008020162. PubMed PMID: 18832437; PMCID: PMC2573018.

132. Pastorelli LM, Wells S, Fray M, Smith A, Hough T, Harfe BD, McManus MT, Smith L, Woolf AS, Cheeseman M, Greenfield A. Genetic analyses reveal a requirement for Dicer1 in the mouse urogenital tract. Mamm Genome. 2009;20(3):140-51. Epub 2009/01/27. doi: 10.1007/s00335-008-9169-y. PubMed PMID: 19169742.

133. Phua YL, Chu JY, Marrone AK, Bodnar AJ, Sims-Lucas S, Ho J. Renal stromal miRNAs are required for normal nephrogenesis and glomerular mesangial survival. Physiological reports. 2015;3(10). doi: 10.14814/phy2.12537. PubMed PMID: 26438731; PMCID: PMC4632944.

134. Sequeira-Lopez ML, Weatherford ET, Borges GR, Monteagudo MC, Pentz ES, Harfe BD, Carretero O, Sigmund CD, Gomez RA. The microRNA-processing enzyme dicer maintains juxtaglomerular cells. Journal of the American Society of Nephrology : JASN. 2010;21(3):460-7. Epub 2010/01/09. doi: 10.1681/ASN.2009090964. PubMed PMID: 20056748; PMCID: PMC2831866.

135. Shi S, Yu L, Chiu C, Sun Y, Chen J, Khitrov G, Merkenschlager M, Holzman LB, Zhang W, Mundel P, Bottinger EP. Podocyte-selective deletion of dicer induces proteinuria and glomerulosclerosis. Journal of the American Society of Nephrology : JASN. 2008;19(11):2159-69. Epub 2008/09/09. doi: 10.1681/ASN.2008030312. PubMed PMID: 18776119; PMCID: PMC2573016.

136. Wei Q, Bhatt K, He HZ, Mi QS, Haase VH, Dong Z. Targeted deletion of Dicer from proximal tubules protects against renal ischemia-reperfusion injury. Journal of the American

Society of Nephrology : JASN. 2010;21(5):756-61. Epub 2010/04/03. doi: 10.1681/ASN.2009070718. PubMed PMID: 20360310; PMCID: PMC2865746.

137. Nakagawa N, Xin C, Roach AM, Naiman N, Shankland SJ, Ligresti G, Ren S, Szak S, Gomez IG, Duffield JS. Dicer1 activity in the stromal compartment regulates nephron differentiation and vascular patterning during mammalian kidney organogenesis. Kidney international. 2015;87(6):1125-40. Epub 2015/02/05. doi: 10.1038/ki.2014.406. PubMed PMID: 25651362; PMCID: PMC4449790.

138. Ho J, Pandey P, Schatton T, Sims-Lucas S, Khalid M, Frank MH, Hartwig S, Kreidberg JA. The Pro-Apoptotic Protein Bim Is a MicroRNA Target in Kidney Progenitors. Journal of the American Society of Nephrology : JASN. 2011;22(6):1053-63. Epub 2011/05/07. doi: 10.1681/ASN.2010080841. PubMed PMID: 21546576.

139. Nagalakshmi VK, Ren Q, Pugh MM, Valerius MT, McMahon AP, Yu J. Dicer regulates the development of nephrogenic and ureteric compartments in the mammalian kidney. Kidney international. 2011;79(3):317-30. Epub 2010/10/15. doi: 10.1038/ki.2010.385. PubMed PMID: 20944551; PMCID: PMC3214622.

140. Patel V, Hajarnis S, Williams D, Hunter R, Huynh D, Igarashi P. MicroRNAs regulate renal tubule maturation through modulation of Pkd1. Journal of the American Society of Nephrology : JASN. 2012;23(12):1941-8. Epub 2012/11/10. doi: 10.1681/ASN.2012030321. PubMed PMID: 23138483; PMCID: PMC3507362.

141. Bartram MP, Amendola E, Benzing T, Schermer B, de Vita G, Muller RU. Mice lacking microRNAs in Pax8-expressing cells develop hypothyroidism and end-stage renal failure. BMC Mol Biol. 2016;17(1):11. doi: 10.1186/s12867-016-0064-x. PubMed PMID: 27090781; PMCID: PMC4835897.

142. Bartram MP, Dafinger C, Habbig S, Benzing T, Schermer B, Muller RU. Loss of Dgcr8-mediated microRNA expression in the kidney results in hydronephrosis and renal malformation. BMC nephrology. 2015;16(1):55. Epub 2015/04/17. doi: 10.1186/s12882-015-0053-1. PubMed PMID: 25881298; PMCID: PMC4445526.

143. Marrone AK, Stolz DB, Bastacky SI, Kostka D, Bodnar AJ, Ho J. MicroRNA-17~92 is required for nephrogenesis and renal function. Journal of the American Society of Nephrology : JASN. 2014;25(7):1440-52. Epub 2014/02/11. doi: 10.1681/ASN.2013040390. PubMed PMID: 24511118; PMCID: PMC4073423.

144. Phua YL, Chen KH, Hemker SL, Marrone AK, Bodnar AJ, Liu X, Clugston A, Kostka D, Butterworth MB, Ho J. Loss of miR-17~92 results in dysregulation of Cftr in nephron progenitors. American journal of physiology Renal physiology. 2019;316(5):F993-F1005. Epub 2019/03/07. doi: 10.1152/ajprenal.00450.2018. PubMed PMID: 30838872; PMCID: PMC6580251.

145. Huang X, Le QT, Giaccia AJ. MiR-210--micromanager of the hypoxia pathway. Trends Mol Med. 2010;16(5):230-7. doi: 10.1016/j.molmed.2010.03.004. PubMed PMID: 20434954; PMCID: PMC3408219.

146. Chan SY, Loscalzo J. MicroRNA-210: a unique and pleiotropic hypoxamir. Cell Cycle. 2010;9(6):1072-83. doi: 10.4161/cc.9.6.11006. PubMed PMID: 20237418; PMCID: PMC2912143.

147. Chan YC, Banerjee J, Choi SY, Sen CK. miR-210: the master hypoxamir. Microcirculation. 2012;19(3):215-23. doi: 10.1111/j.1549-8719.2011.00154.x. PubMed PMID: 22171547; PMCID: PMC3399423.

148. Bavelloni A, Ramazzotti G, Poli A, Piazzi M, Focaccia E, Blalock W, Faenza I. MiRNA-210: A Current Overview. Anticancer Res. 2017;37(12):6511-21. Epub 2017/12/01. doi: 10.21873/anticanres.12107. PubMed PMID: 29187425.

149. Fasanaro P, D'Alessandra Y, Di Stefano V, Melchionna R, Romani S, Pompilio G, Capogrossi MC, Martelli F. MicroRNA-210 modulates endothelial cell response to hypoxia and inhibits the receptor tyrosine kinase ligand Ephrin-A3. The Journal of biological chemistry. 2008;283(23):15878-83. doi: 10.1074/jbc.M800731200. PubMed PMID: 18417479; PMCID: PMC3259646.

150. Fasanaro P, Greco S, Lorenzi M, Pescatori M, Brioschi M, Kulshreshtha R, Banfi C, Stubbs A, Calin GA, Ivan M, Capogrossi MC, Martelli F. An integrated approach for experimental target identification of hypoxia-induced miR-210. The Journal of biological chemistry. 2009;284(50):35134-43. doi: 10.1074/jbc.M109.052779. PubMed PMID: 19826008; PMCID: PMC2787374.

151. Pulkkinen K, Malm T, Turunen M, Koistinaho J, Yla-Herttuala S. Hypoxia induces microRNA miR-210 in vitro and in vivo ephrin-A3 and neuronal pentraxin 1 are potentially regulated by miR-210. FEBS Lett. 2008;582(16):2397-401. doi: 10.1016/j.febslet.2008.05.048. PubMed PMID: 18539147.

152. Huang X, Ding L, Bennewith KL, Tong RT, Welford SM, Ang KK, Story M, Le QT, Giaccia AJ. Hypoxia-inducible mir-210 regulates normoxic gene expression involved in tumor initiation. Molecular cell. 2009;35(6):856-67. doi: 10.1016/j.molcel.2009.09.006. PubMed PMID: 19782034; PMCID: PMC2782615.
153. Kim HW, Haider HK, Jiang S, Ashraf M. Ischemic preconditioning augments survival of stem cells via miR-210 expression by targeting caspase-8-associated protein 2. The Journal of biological chemistry. 2009;284(48):33161-8. doi: 10.1074/jbc.M109.020925. PubMed PMID: 19721136; PMCID: PMC2785158.
154. Li T, Song X, Zhang J, Zhao L, Shi Y, Li Z, Liu J, Liu N, Yan Y, Xiao Y, Tian X, Sun W, Guan Y, Liu B. Protection of Human Umbilical Vein Endothelial Cells against Oxidative Stress by MicroRNA-210. Oxid Med Cell Longev. 2017;2017:3565613. Epub 2017/04/04. doi: 10.1155/2017/3565613. PubMed PMID: 28367268; PMCID: PMC5359453 publication of this paper.
155. Tsuchiya S, Fujiwara T, Sato F, Shimada Y, Tanaka E, Sakai Y, Shimizu K, Tsujimoto G. MicroRNA-210 regulates cancer cell proliferation through targeting fibroblast growth factor receptor-like 1 (FGFRL1). The Journal of biological chemistry. 2011;286(1):420-8. Epub 2010/11/04. doi: 10.1074/jbc.M110.170852. PubMed PMID: 21044961; PMCID: PMC3013001.
156. Yang Y, Zhang J, Xia T, Li G, Tian T, Wang M, Wang R, Zhao L, Yang Y, Lan K, Zhou W. MicroRNA-210 promotes cancer angiogenesis by targeting fibroblast growth factor receptor-like 1 in hepatocellular carcinoma. Oncol Rep. 2016;36(5):2553-62. Epub Sep 23, 2016. doi: 10.3892/or.2016.5129. PubMed PMID: 27666683.
157. Zuo J, Wen M, Lei M, Peng X, Yang X, Liu Z. MiR-210 links hypoxia with cell proliferation regulation in human Laryngocarcinoma cancer. Journal of cellular biochemistry. 2015;116(6):1039-49. doi: 10.1002/jcb.25059. PubMed PMID: 25639884.
158. Qin L, Chen Y, Niu Y, Chen W, Wang Q, Xiao S, Li A, Xie Y, Li J, Zhao X, He Z, Mo D. A deep investigation into the adipogenesis mechanism: profile of microRNAs regulating adipogenesis by modulating the canonical Wnt/beta-catenin signaling pathway. BMC Genomics. 2010;11:320. Epub 2010/05/25. doi: 10.1186/1471-2164-11-320. PubMed PMID: 20492721; PMCID: PMC2895628.
159. Ma Q, Dasgupta C, Li Y, Huang L, Zhang L. MicroRNA-210 Suppresses Junction Proteins and Disrupts Blood-Brain Barrier Integrity in Neonatal Rat Hypoxic-Ischemic Brain Injury. Int J

Mol Sci. 2017;18(7):1356. Epub 2017/07/05. doi: 10.3390/ijms18071356. PubMed PMID: 28672801; PMCID: PMC5535849.
160. Lou YL, Guo F, Liu F, Gao FL, Zhang PQ, Niu X, Guo SC, Yin JH, Wang Y, Deng ZF. miR-210 activates notch signaling pathway in angiogenesis induced by cerebral ischemia. Mol Cell Biochem. 2012;370(1-2):45-51. doi: 10.1007/s11010-012-1396-6. PubMed PMID: 22833359.
161. Ding L, Zhao L, Chen W, Liu T, Li Z, Li X. miR-210, a modulator of hypoxia-induced epithelial-mesenchymal transition in ovarian cancer cell. Int J Clin Exp Med. 2015;8(2):2299-307. PubMed PMID: 25932166; PMCID: PMC4402813.
162. Crosby ME, Kulshreshtha R, Ivan M, Glazer PM. MicroRNA regulation of DNA repair gene expression in hypoxic stress. Cancer research. 2009;69(3):1221-9. doi: 10.1158/0008-5472.CAN-08-2516. PubMed PMID: 19141645; PMCID: PMC2997438.
163. Kulshreshtha R, Ferracin M, Wojcik SE, Garzon R, Alder H, Agosto-Perez FJ, Davuluri R, Liu CG, Croce CM, Negrini M, Calin GA, Ivan M. A microRNA signature of hypoxia. Molecular and cellular biology. 2007;27(5):1859-67. Epub 2006/12/30. doi: 10.1128/MCB.01395-06. PubMed PMID: 17194750; PMCID: PMC1820461.
164. McCormick RI, Blick C, Ragoussis J, Schoedel J, Mole DR, Young AC, Selby PJ, Banks RE, Harris AL. miR-210 is a target of hypoxia-inducible factors 1 and 2 in renal cancer, regulates ISCU and correlates with good prognosis. Br J Cancer. 2013;108(5):1133-42. doi: 10.1038/bjc.2013.56. PubMed PMID: 23449350; PMCID: PMC3619073.
165. Mutharasan RK, Nagpal V, Ichikawa Y, Ardehali H. microRNA-210 is upregulated in hypoxic cardiomyocytes through Akt- and p53-dependent pathways and exerts cytoprotective effects. Am J Physiol Heart Circ Physiol. 2011;301(4):H1519-30. doi: 10.1152/ajpheart.01080.2010. PubMed PMID: 21841015; PMCID: PMC3197368.
166. Muralimanoharan S, Guo C, Myatt L, Maloyan A. Sexual dimorphism in miR-210 expression and mitochondrial dysfunction in the placenta with maternal obesity. Int J Obes (Lond). 2015;39(8):1274-81. doi: 10.1038/ijo.2015.45. PubMed PMID: 25833255; PMCID: PMC4526386.
167. O'Brien LL, Guo Q, Lee Y, Tran T, Benazet JD, Whitney PH, Valouev A, McMahon AP. Differential regulation of mouse and human nephron progenitors by the Six family of transcriptional regulators. Development. 2016;143(4):595-608. doi: 10.1242/dev.127175. PubMed PMID: 26884396; PMCID: PMC4760318.

168. Grignon DJ, Che M. Clear cell renal cell carcinoma. Clin Lab Med. 2005;25(2):305-16. Epub 2005/04/26. doi: 10.1016/j.cll.2005.01.012. PubMed PMID: 15848738.
169. Juan D, Alexe G, Antes T, Liu H, Madabhushi A, Delisi C, Ganesan S, Bhanot G, Liou LS. Identification of a microRNA panel for clear-cell kidney cancer. Urology. 2010;75(4):835-41. doi: 10.1016/j.urology.2009.10.033. PubMed PMID: 20035975.
170. Valera VA, Walter BA, Linehan WM, Merino MJ. Regualtory effects of mircoRNA-92 (miR-92) on VHL gene expression and the hypoxic activation of miR-210 in clear cell renal cell carcinoma. Journal of Cancer. 2011;2:515-26.
171. Nakada C, Tsukamoto Y, Matsuura K, Nguyen TL, Hijiya N, Uchida T, Sato F, Mimata H, Seto M, Moriyama M. Overexpression of miR-210, a downstream target of HIF1alpha, causes centrosome amplification in renal carcinoma cells. The Journal of pathology. 2011;224(2):280-8. doi: 10.1002/path.2860. PubMed PMID: 21465485.
172. Samaan S, Khella HW, Girgis A, Scorilas A, Lianidou E, Gabril M, Krylov SN, Jewett M, Bjarnason GA, El-said H, Yousef GM. miR-210 is a prognostic marker in clear cell renal cell carcinoma. J Mol Diagn. 2015;17(2):136-44. Epub 2015/01/04. doi: 10.1016/j.jmoldx.2014.10.005. PubMed PMID: 25555365.
173. Lorenzen JM, Kielstein JT, Hafer C, Gupta SK, Kumpers P, Faulhaber-Walter R, Haller H, Fliser D, Thum T. Circulating miR-210 predicts survival in critically ill patients with acute kidney injury. Clin J Am Soc Nephrol. 2011;6(7):1540-6. Epub 2011/06/28. doi: 10.2215/CJN.00430111. PubMed PMID: 21700819.
174. Lorenzen JM, Volkmann I, Fiedler J, Schmidt M, Scheffner I, Haller H, Gwinner W, Thum T. Urinary miR-210 as a mediator of acute T-cell mediated rejection in renal allograft recipients. Am J Transplant. 2011;11(10):2221-7. Epub 2011/08/05. doi: 10.1111/j.1600-6143.2011.03679.x. PubMed PMID: 21812927.
175. Gan L, Liu Z, Wei M, Chen Y, Yang X, Chen L, Xiao X. MiR-210 and miR-155 as potential diagnostic markers for pre-eclampsia pregnancies. Medicine (Baltimore). 2017;96(28):e7515. doi: 10.1097/MD.0000000000007515. PubMed PMID: 28700503.
176. Nejad RMA, Saeidi K, Gharbi S, Salari Z, Saleh-Gohari N. Quantification of circulating miR-517c-3p and miR-210-3p levels in preeclampsia. Pregnancy Hypertens. 2019;16:75-8. Epub 2019/05/06. doi: 10.1016/j.preghy.2019.03.004. PubMed PMID: 31056162.

177. Vonkova B, Blahakova I, Hruban L, Janku P, Pospisilova S. MicroRNA-210 expression during childbirth and postpartum as a potential biomarker of acute fetal hypoxia. Biomed Pap Med Fac Univ Palacky Olomouc Czech Repub. 2018. Epub 2018/12/20. doi: 10.5507/bp.2018.075. PubMed PMID: 30565568.

178. Liu LL, Li D, He YL, Zhou YZ, Gong SH, Wu LY, Zhao YQ, Huang X, Zhao T, Xu L, Wu KW, Li MG, Zhu LL, Fan M. miR-210 protects renal cell against hypoxia-induced apoptosis by targeting HIF-1 alpha. Mol Med. 2017;23. Epub 2018/02/02. doi: 10.2119/molmed.2017.00013. PubMed PMID: 29387863; PMCID: PMC5653737.

179. Liu F, Lou YL, Wu J, Ruan QF, Xie A, Guo F, Cui SP, Deng ZF, Wang Y. Upregulation of microRNA-210 regulates renal angiogenesis mediated by activation of VEGF signaling pathway under ischemia/perfusion injury in vivo and in vitro. Kidney Blood Press Res. 2012;35(3):182-91. doi: 10.1159/000331054. PubMed PMID: 22123256.

180. Nakada C, Hijiya N, Tsukamoto Y, Yano S, Kai T, Uchida T, Kimoto M, Takahashi M, Daa T, Matsuura K, Shin T, Mimata H, Moriyama M. A transgenic mouse expressing miR-210 in proximal tubule cells shows mitochondrial alteration: possible association of miR-210 with a shift in energy metabolism. The Journal of pathology. 2020. Epub 2020/02/20. doi: 10.1002/path.5394. PubMed PMID: 32073141.

181. Akimoto T, Hammerman MR, Kusano E. Low ambient O2 enhances ureteric bud branching in vitro. Organogenesis. 2005;2(1):17-21.

182. Tufro-McReddie A, Norwood VF, Aylor KW, Botkin SJ, Carey RM, Gomez RA. Oxygen regulates vascular endothelial growth factor-mediated vasculogenesis and tubulogenesis. Developmental biology. 1997;183(2):139-49. doi: 10.1006/dbio.1997.8513. PubMed PMID: 9126290.

183. Aresh B, Peuckert C. Dissection and Culture of Mouse Embryonic Kidney. J Vis Exp. 2017(123). Epub 2017/06/02. doi: 10.3791/55715. PubMed PMID: 28570550; PMCID: PMC5607993.

184. Livak KJ, Schmittgen TD. Analysis of relative gene expression data using real-time quantitative PCR and the 2(-Delta Delta C(T)) Method. Methods. 2001;25(4):402-8. Epub 2002/02/16. doi: 10.1006/meth.2001.1262. PubMed PMID: 11846609.

185. Andrews S. Babraham Bioinformatics - FastQC A Quality Control tool for High Throughput Sequence Data 2010 [cited 2017 January 1, 2017]. Available from: http://www.bioinformatics.babraham.ac.uk/projects/fastqc/.
186. Lab B. Trim Galore 2014 [cited 2017]. Available from: http://www.bioinformatics.babraham.ac.uk/projects/trim_galore.
187. Church DM, Schneider VA, Graves T, Auger K, Cunningham F, Bouk N, Chen HC, Agarwala R, McLaren WM, Ritchie GR, Albracht D, Kremitzki M, Rock S, Kotkiewicz H, Kremitzki C, Wollam A, Trani L, Fulton L, Fulton R, Matthews L, Whitehead S, Chow W, Torrance J, Dunn M, Harden G, Threadgold G, Wood J, Collins J, Heath P, Griffiths G, Pelan S, Grafham D, Eichler EE, Weinstock G, Mardis ER, Wilson RK, Howe K, Flicek P, Hubbard T. Modernizing reference genome assemblies. PLoS Biol. 2011;9(7):e1001091. Epub 2011/07/14. doi: 10.1371/journal.pbio.1001091. PubMed PMID: 21750661; PMCID: PMC3130012 married to the deputy editor of PLoS Medicine, Melissa Norton. Evan Eichler is on the board of Pacific Biosciences.
188. Dobin A, Davis CA, Schlesinger F, Drenkow J, Zaleski C, Jha S, Batut P, Chaisson M, Gingeras TR. STAR: ultrafast universal RNA-seq aligner. Bioinformatics. 2013;29(1):15-21. doi: 10.1093/bioinformatics/bts635. PubMed PMID: 23104886; PMCID: PMC3530905.
189. Lawrence M, Huber W, Pages H, Aboyoun P, Carlson M, Gentleman R, Morgan MT, Carey VJ. Software for computing and annotating genomic ranges. PLoS Comput Biol. 2013;9(8):e1003118. Epub 2013/08/21. doi: 10.1371/journal.pcbi.1003118. PubMed PMID: 23950696; PMCID: PMC3738458.
190. Zerbino DR, Achuthan P, Akanni W, Amode MR, Barrell D, Bhai J, Billis K, Cummins C, Gall A, Giron CG, Gil L, Gordon L, Haggerty L, Haskell E, Hourlier T, Izuogu OG, Janacek SH, Juettemann T, To JK, Laird MR, Lavidas I, Liu Z, Loveland JE, Maurel T, McLaren W, Moore B, Mudge J, Murphy DN, Newman V, Nuhn M, Ogeh D, Ong CK, Parker A, Patricio M, Riat HS, Schuilenburg H, Sheppard D, Sparrow H, Taylor K, Thormann A, Vullo A, Walts B, Zadissa A, Frankish A, Hunt SE, Kostadima M, Langridge N, Martin FJ, Muffato M, Perry E, Ruffier M, Staines DM, Trevanion SJ, Aken BL, Cunningham F, Yates A, Flicek P. Ensembl 2018. Nucleic Acids Res. 2018;46(D1):D754-D61. Epub 2017/11/21. doi: 10.1093/nar/gkx1098. PubMed PMID: 29155950; PMCID: PMC5753206.

191. Love MI, Huber W, Anders S. Moderated estimation of fold change and dispersion for RNA-seq data with DESeq2. Genome Biol. 2014;15(12):550. Epub 2014/12/18. doi: 10.1186/s13059-014-0550-8. PubMed PMID: 25516281; PMCID: PMC4302049.
192. Martin M. Cutadapt removes adapter sequences from high-throughput sequencing reads. EMBnetjournal. 2011;17(1):10-2. doi: 10.14806/ej.17.1.200.
193. Kozomara A, Griffiths-Jones S. miRBase: integrating microRNA annotation and deep-sequencing data. Nucleic Acids Res. 2011;39(Database issue):D152-7. Epub 2010/11/03. doi: 10.1093/nar/gkq1027. PubMed PMID: 21037258; PMCID: PMC3013655.
194. Bates CM, Kegg H, Grady S. Expression of somatostatin in the adult and developing mouse kidney. Kidney international. 2004;66(5):1785-93. Epub 2004/10/22. doi: 10.1111/j.1523-1755.2004.00953.x. PubMed PMID: 15496149.
195. Liao Y, Smyth GK, Shi W. The R package Rsubread is easier, faster, cheaper and better for alignment and quantification of RNA sequencing reads. Nucleic Acids Res. 2019;47(8):e47. Epub 2019/02/21. doi: 10.1093/nar/gkz114. PubMed PMID: 30783653; PMCID: PMC6486549.
196. Dennis GJ, Sherman BT, Hosack DA, Yang J, Gao W, Lane HC, Lempicki RA. DAVID: Database for Annoation, Visualization, and Integrated Discovery. Genome Biol. 2003;4(5):P3. Epub Apr 3.
197. Liu S, Song N, He J, Yu X, Guo J, Jiao X, Ding X, Teng J. Effect of Hypoxia on the Differentiation and the Self-Renewal of Metanephrogenic Mesenchymal Stem Cells. Stem Cells Int. 2017;2017:7168687. doi: 10.1155/2017/7168687. PubMed PMID: 28194187.
198. Lacedonia D, Scioscia G, Pia Palladino G, Gallo C, Carpagnano GE, Sabato R, Foschino Barbaro MP. MicroRNA expression profile during different conditions of hypoxia. Oncotarget. 2018;9(80):35114-22. Epub 2018/11/13. doi: 10.18632/oncotarget.26210. PubMed PMID: 30416683; PMCID: PMC6205556.
199. Schanza LM, Seles M, Stotz M, Fosselteder J, Hutterer GC, Pichler M, Stiegelbauer V. MicroRNAs Associated with Von Hippel-Lindau Pathway in Renal Cell Carcinoma: A Comprehensive Review. Int J Mol Sci. 2017;18(11). doi: 10.3390/ijms18112495. PubMed PMID: 29165391.
200. Shen G, Li X, Jia YF, Piazza GA, Xi Y. Hypoxia-regulated microRNAs in human cancer. Acta Pharmacol Sin. 2013;34(3):336-41. Epub February 4, 2013. doi: 10.1038/aps.2012.195. PubMed PMID: 23377548; PMCID: PMC3587916.

201. Weiss JB, Eisenhardt SU, Stark GB, Bode C, Moser M, Grundmann S. MicroRNAs in ischemia-reperfusion injury. Am J Cardiovasc Dis. 2012;2(3):237-47. PubMed PMID: 22937493; PMCID: PMC3427975.
202. Krawczynski K, Mishima T, Huang X, Sadovsky Y. Intact feto-placental growth in microRNA-210 deficient mice. Placenta. 2016;47:113-5. doi: 10.1016/j.placenta.2016.09.007. PubMed PMID: 27780532.
203. Park CY, Jeker LT, Carver-Moore K, Oh A, Liu HJ, Cameron R, Richards H, Li Z, Adler D, Yoshinaga Y, Martinez M, Nefadov M, Abbas AK, Weiss A, Lanier LL, de Jong PJ, Bluestone JA, Srivastava D, McManus MT. A resource for the conditional ablation of microRNAs in the mouse. Cell reports. 2012;1(4):385-91. Epub 2012/05/10. doi: 10.1016/j.celrep.2012.02.008. PubMed PMID: 22570807; PMCID: PMC3345170.
204. Brown AC, Muthukrishnan SD, Oxburgh L. A synthetic niche for nephron progenitor cells. Developmental cell. 2015;34(2):229-41. doi: 10.1016/j.devcel.2015.06.021. PubMed PMID: 26190145; PMCID: PMC4519427.
205. Nyengaard JR. Stereologic methods and their application in kidney research. Journal of the American Society of Nephrology. 1999;10(5):1100-23. PubMed PMID: WOS:000079923000023.
206. Yang Y, Jeanpierre C, Dressler GR, Lacoste M, Niaudet P, Gubler MC. WT1 and PAX-2 podocyte expression in Denys-Drash syndrome and isolated diffuse mesangial sclerosis. Am J Pathol. 1999;154(1):181-92. PubMed PMID: 9916932.
207. Cullen-McEwen LA, Armitage JA, Nyengaard JR, Bertram JF. Estimating nephron number in the developing kidney using the physical disector/fractionator combination. Methods Mol Biol. 2012;886:109-19. doi: 10.1007/978-1-61779-851-1_10. PubMed PMID: 22639255.
208. Hemker SL, Cerqueira DM, Bodnar AJ, Cargill KR, Clugston A, Anslow MJ, Sims-Lucas S, Kostka D, Ho J. Deletion of hypoxia-responsive microRNA-210 results in a sex-specific decrease in nephron number. Faseb J. 2020. Epub 2020/03/07. doi: 10.1096/fj.201902767R. PubMed PMID: 32141129.
209. Klein G, Langegger M, Goridis C, Ekblom P. Neural cell adhesion molecules during embryonic induction and development of the kidney. Development. 1988;102(4):749-61. Epub 1988/04/01. PubMed PMID: 3048972.
210. Chang W, Lee CY, Park JH, Park MS, Maeng LS, Yoon CS, Lee MY, Hwang KC, Chung YA. Survival of hypoxic human mesenchymal stem cells is enhanced by a positive feedback loop

involving miR-210 and hypoxia-inducible factor 1. Journal of Veterinary Science. 2013;14(1):69-76. doi: 10.4142/jvs.2013.14.1.69. PubMed PMID: WOS:000317373400010.

211. Wang H, Zhao Y, Luo R, Bian X, Wang Y, Shao X, Li YX, Liu M, Wang YL. A positive feedback self-regulatory loop between miR-210 and HIF-1alpha mediated by CPEB2 is involved in trophoblast syncytiolization: implication of trophoblast malfunction in preeclampsia. Biology of reproduction. 2019. Epub 2019/10/17. doi: 10.1093/biolre/ioz196. PubMed PMID: 31616934.

212. Kobayashi A, Kwan KM, Carroll TJ, McMahon AP, Mendelsohn CL, Behringer RR. Distinct and sequential tissue-specific activities of the LIM-class homeobox gene Lim1 for tubular morphogenesis during kidney development. Development. 2005;132(12):2809-23. Epub 2005/06/03. doi: 10.1242/dev.01858. PubMed PMID: 15930111.

213. Bridgewater D, Di Giovanni V, Cain JE, Cox B, Jakobson M, Sainio K, Rosenblum ND. beta-catenin causes renal dysplasia via upregulation of Tgfbeta2 and Dkk1. Journal of the American Society of Nephrology : JASN. 2011;22(4):718-31. doi: 10.1681/ASN.2010050562. PubMed PMID: 21436291; PMCID: PMC3065227.

214. Shah MM, Sampogna RV, Sakurai H, Bush KT, Nigam SK. Branching morphogenesis and kidney disease. Development. 2004;131(7):1449-62. doi: 10.1242/dev.01089. PubMed PMID: 15023929.

215. Rutledge EA, Benazet JD, McMahon AP. Cellular heterogeneity in the ureteric progenitor niche and distinct profiles of branching morphogenesis in organ development. Development. 2017;144:3177-88. doi: 10.1242/dev.149112. PubMed PMID: 28705898.

216. Alaiti MA, Ishikawa M, Masuda H, Simon DI, Jain MK, Asahara T, Costa MA. Up-regulation of miR-210 by vascular endothelial growth factor in ex vivo expanded CD34+ cells enhances cell-mediated angiogenesis. J Cell Mol Med. 2012;16(10):2413-21. doi: 10.1111/j.1582-4934.2012.01557.x. PubMed PMID: 22360314; PMCID: PMC3823435.

217. Arif M, Pandey R, Alam P, Jiang S, Sadayappan S, Paul A, Ahmed RPH. MicroRNA-210-mediated proliferation, survival, and angiogenesis promote cardiac repair post myocardial infarction in rodents. J Mol Med (Berl). 2017. doi: 10.1007/s00109-017-1591-8. PubMed PMID: 28948298.

218. Ekblom P. Formation of basement membranes in the embryonic kidney: an immunohistological study. J Cell Biol. 1981;91(1):1-10. PubMed PMID: 6795211; PMCID: PMC2111945.

219. Natoli TA, Gareski TC, Dackowski WR, Smith L, Bukanov NO, Russo RJ, Husson H, Matthews D, Piepenhagen P, Ibraghimov-Beskrovnaya O. Pkd1 and Nek8 mutations affect cell-cell adhesion and cilia in cysts formed in kidney organ cultures. American journal of physiology Renal physiology. 2008;294(1):F73-83. doi: 10.1152/ajprenal.00362.2007. PubMed PMID: 17928412.

220. Robert B, St John PL, Hyink DP, Abrahamson DR. Evidence that embryonic kidney cells expressing flk-1 are intrinsic, vasculogenic angioblasts. Am J Physiol. 1996;271(3 Pt 2):F744-53. PubMed PMID: 8853438.

221. Nishinakamura R, Uchiyama Y, Sakaguchi M, Fujimura S. Nephron progenitors in the metanephric mesenchyme. Pediatric nephrology. 2011;26(9):1463-7. doi: 10.1007/s00467-011-1806-0. PubMed PMID: 21336811.

222. Ivan M, Huang X. miR-210: fine-tuning the hypoxic response. Adv Exp Med Biol. 2014;772:205-27. doi: 10.1007/978-1-4614-5915-6_10. PubMed PMID: 24272361; PMCID: PMC4515752.

223. Cerqueira DM, Bodnar AJ, Phua YL, Freer R, Hemker SL, Walensky LD, Hukriede NA, Ho J. Bim gene dosage is critical in modulating nephron progenitor survival in the absence of microRNAs during kidney development. Faseb J. 2017;31(8):3540-54. doi: 10.1096/fj.201700010R. PubMed PMID: 28446592; PMCID: PMC5503708.

224. Ho J. The regulation of apoptosis in kidney development: implications for nephron number and pattern? Frontiers in pediatrics. 2014;2:128. Epub 2014/12/06. doi: 10.3389/fped.2014.00128. PubMed PMID: 25478553; PMCID: PMC4235295.

225. Yi CH, Yuan J. The Jekyll and Hyde functions of caspases. Developmental cell. 2009;16(1):21-34. Epub 2009/01/22. doi: 10.1016/j.devcel.2008.12.012. PubMed PMID: 19154716; PMCID: 2850564.

226. Imai Y, Kimura T, Murakami A, Yajima N, Sakamaki K, Yonehara S. The CED-4-homologous protein FLASH is involved in Fas-mediated activation of caspase-8 during apoptosis. Nature. 1999;398(6730):777-85. Epub 1999/05/11. doi: 10.1038/19709. PubMed PMID: 10235259.

227. Krieghoff-Henning E, Hofmann TG. Role of nuclear bodies in apoptosis signalling. Biochim Biophys Acta. 2008;1783(11):2185-94. Epub 2008/08/06. doi: 10.1016/j.bbamcr.2008.07.002. PubMed PMID: 18680765.

228. Paterson MR, Geurts AM, Kriegel AJ. miR-146b-5p has a sex-specific role in renal and cardiac pathology in a rat model of chronic kidney disease. Kidney international. 2019. doi: 10.1016/j.kint.2019.07.017.

229. Halt K, Vainio S. Coordination of kidney organogenesis by Wnt signaling. Pediatric nephrology. 2014;29(4):737-44. doi: 10.1007/s00467-013-2733-z. PubMed PMID: 24445433; PMCID: PMC3928513.

230. Steinhart Z, Angers S. Wnt signaling in development and tissue homeostasis. Development. 2018;145(11). Epub 2018/06/10. doi: 10.1242/dev.146589. PubMed PMID: 29884654.

231. Alm-Kristiansen AH, Saether T, Matre V, Gilfillan S, Dahle O, Gabrielsen OS. FLASH acts as a co-activator of the transcription factor c-Myb and localizes to active RNA polymerase II foci. Oncogene. 2008;27(34):4644-56. Epub 2008/04/15. doi: 10.1038/onc.2008.105. PubMed PMID: 18408764.

232. Barcaroli D, Bongiorno-Borbone L, Terrinoni A, Hofmann TG, Rossi M, Knight RA, Matera AG, Melino G, De Laurenzi V. FLASH is required for histone transcription and S-phase progression. Proc Natl Acad Sci U S A. 2006;103(40):14808-12. Epub 2006/09/28. doi: 10.1073/pnas.0604227103. PubMed PMID: 17003125; PMCID: PMC1578501.

233. Kiriyama M, Kobayashi Y, Saito M, Ishikawa F, Yonehara S. Interaction of FLASH with arsenite resistance protein 2 is involved in cell cycle progression at S phase. Molecular and cellular biology. 2009;29(17):4729-41. Epub 2009/06/24. doi: 10.1128/MCB.00289-09. PubMed PMID: 19546234; PMCID: PMC2725714.

234. Krieghoff E, Milovic-Holm K, Hofmann TG. FLASH meets nuclear bodies: CD95 receptor signals via a nuclear pathway. Cell Cycle. 2007;6(7):771-5. Epub 2007/03/23. doi: 10.4161/cc.6.7.4046. PubMed PMID: 17377497.

235. Milovic-Holm K, Krieghoff E, Jensen K, Will H, Hofmann TG. FLASH links the CD95 signaling pathway to the cell nucleus and nuclear bodies. EMBO J. 2007;26(2):391-401. Epub 2007/01/25. doi: 10.1038/sj.emboj.7601504. PubMed PMID: 17245429; PMCID: PMC1783462.

236. Simard M, Provost PR, Tremblay Y. Sexually dimorphic gene expression that overlaps maturation of type II pneumonocytes in fetal mouse lungs. Reprod Biol Endocrinol. 2006;4:25. Epub 2006/05/06. doi: 10.1186/1477-7827-4-25. PubMed PMID: 16674826; PMCID: PMC1513230.

237. Reiser J, Altintas MM. Podocytes. F1000Res. 2016;5. Epub 2016/02/27. doi: 10.12688/f1000research.7255.1. PubMed PMID: 26918173; PMCID: PMC4755401.
238. Levinson RS, Batourina E, Choi C, Vorontchikhina M, Kitajewski J, Mendelsohn CL. Foxd1-dependent signals control cellularity in the renal capsule, a structure required for normal renal development. Development. 2005;132(3):529-39. doi: 10.1242/dev.01604. PubMed PMID: 15634693.
239. Gao X, Chen X, Taglienti M, Rumballe B, Little MH, Kreidberg JA. Angioblast-mesenchyme induction of early kidney development is mediated by Wt1 and Vegfa. Development. 2005;132(24):5437-49. doi: 10.1242/dev.02095. PubMed PMID: 16291795.
240. Mohamed T, Sequeira-Lopez MLS. Development of the renal vasculature. Semin Cell Dev Biol. 2019;91:132-46. Epub 2018/06/08. doi: 10.1016/j.semcdb.2018.06.001. PubMed PMID: 29879472; PMCID: PMC6281798.
241. Sison K, Eremina V, Baelde H, Min W, Hirashima M, Fantus IG, Quaggin SE. Glomerular structure and function require paracrine, not autocrine, VEGF-VEGFR-2 signaling. Journal of the American Society of Nephrology : JASN. 2010;21(10):1691-701. Epub 2010/08/07. doi: 10.1681/ASN.2010030295. PubMed PMID: 20688931; PMCID: PMC3013545.
242. Intapad S, Dasinger JH, Johnson JM, Brown AD, Ojeda NB, Alexander BT. Male and Female Intrauterine Growth-Restricted Offspring Differ in Blood Pressure, Renal Function, and Glucose Homeostasis Responses to a Postnatal Diet High in Fat and Sugar. Hypertension. 2019;73(3):620-9. Epub 2019/01/15. doi: 10.1161/HYPERTENSIONAHA.118.12134. PubMed PMID: 30636548; PMCID: PMC6374157.
243. Gerosa C, Fanni D, Faa A, Van Eyken P, Ravarino A, Fanos V, Faa G. Low vascularization of the nephrogenic zone of the fetal kidney suggests a major role for hypoxia in human nephrogenesis. Int Urol Nephrol. 2017. doi: 10.1007/s11255-017-1630-y. PubMed PMID: 28573487.
244. Yzydorczyk C, Armengaud JB, Peyter AC, Chehade H, Cachat F, Juvet C, Siddeek B, Simoncini S, Sabatier F, Dignat-George F, Mitanchez D, Simeoni U. Endothelial dysfunction in individuals born after fetal growth restriction: cardiovascular and renal consequences and preventive approaches. J Dev Orig Health Dis. 2017:1-17. doi: 10.1017/S2040174417000265. PubMed PMID: 28460648.

245. Daniel E, Azizoglu DB, Ryan AR, Walji TA, Chaney CP, Sutton GI, Carroll TJ, Marciano DK, Cleaver O. Spatiotemporal heterogeneity and patterning of developing renal blood vessels. Angiogenesis. 2018. Epub 2018/04/09. doi: 10.1007/s10456-018-9612-y. PubMed PMID: 29627966.

246. Jin Y, Chen Z, Liu X, Zhou X. Evaluating the microRNA targeting sites by luciferase reporter gene assay. Methods Mol Biol. 2013;936:117-27. Epub 2012/09/26. doi: 10.1007/978-1-62703-083-0_10. PubMed PMID: 23007504; PMCID: PMC3646406.

247. van Solingen C, Seghers L, Bijkerk R, Duijs JM, Roeten MK, van Oeveren-Rietdijk AM, Baelde HJ, Monge M, Vos JB, de Boer HC, Quax PH, Rabelink TJ, van Zonneveld AJ. Antagomir-mediated silencing of endothelial cell specific microRNA-126 impairs ischemia-induced angiogenesis. J Cell Mol Med. 2009;13(8A):1577-85. Epub 2009/01/06. doi: 10.1111/j.1582-4934.2008.00613.x. PubMed PMID: 19120690; PMCID: PMC3828868.

248. Yuan XP, Liu LS, Chen CB, Zhou J, Zheng YT, Wang XP, Han M, Wang CX. MicroRNA-423-5p facilitates hypoxia/reoxygenation-induced apoptosis in renal proximal tubular epithelial cells by targeting GSTM1 via endoplasmic reticulum stress. Oncotarget. 2017. doi: 10.18632/oncotarget.18289. PubMed PMID: 28614065.

249. Davies JA, Ladomery M, Hohenstein P, Michael L, Shafe A, Spraggon L, Hastie N. Development of an siRNA-based method for repressing specific genes in renal organ culture and its use to show that the Wt1 tumour suppressor is required for nephron differentiation. Hum Mol Genet. 2004;13(2):235-46. Epub 2003/12/03. doi: 10.1093/hmg/ddh015. PubMed PMID: 14645201.

250. Wang J, Gao Y, Ma M, Li M, Zou D, Yang J, Zhu Z, Zhao X. Effect of miR-21 on renal fibrosis by regulating MMP-9 and TIMP1 in kk-ay diabetic nephropathy mice. Cell Biochem Biophys. 2013;67(2):537-46. Epub 2013/02/28. doi: 10.1007/s12013-013-9539-2. PubMed PMID: 23443810.

251. Merhautova J, Demlova R, Slaby O. MicroRNA-Based Therapy in Animal Models of Selected Gastrointestinal Cancers. Front Pharmacol. 2016;7:329. Epub 2016/10/13. doi: 10.3389/fphar.2016.00329. PubMed PMID: 27729862; PMCID: PMC5037200.

252. Kloosterman WP, Wienholds E, de Bruijn E, Kauppinen S, Plasterk RH. In situ detection of miRNAs in animal embryos using LNA-modified oligonucleotide probes. Nature methods. 2006;3(1):27-9. Epub 2005/12/22. doi: 10.1038/nmeth843. PubMed PMID: 16369549.

253. Badal SS, Danesh FR. MicroRNAs and their applications in kidney diseases. Pediatric nephrology. 2015;30(5):727-40. Epub June 14, 2014. doi: 10.1007/s00467-014-2867-7. PubMed PMID: 24928414; PMCID: PMC4265577.
254. Kota SK, Kota SB. Noncoding RNA and epigenetic gene regulation in renal diseases. Drug Discov Today. 2017;22(7):1112-22. Epub 2017/05/11. doi: 10.1016/j.drudis.2017.04.020. PubMed PMID: 28487070; PMCID: PMC5709041.
255. Petrillo F, Iervolino A, Zacchia M, Simeoni A, Masella C, Capolongo G, Perna A, Capasso G, Trepiccione F. MicroRNAs in Renal Diseases: A Potential Novel Therapeutic Target. Kidney Dis (Basel). 2017;3(3):111-9. Epub 2018/01/19. doi: 10.1159/000481730. PubMed PMID: 29344506; PMCID: PMC5757617.
256. Ichii O, Horino T. MicroRNAs associated with the development of kidney diseases in humans and animals. J Toxicol Pathol. 2018;31(1):23-34. Epub 2018/02/27. doi: 10.1293/tox.2017-0051. PubMed PMID: 29479137; PMCID: PMC5820100.
257. Baker MA, Davis SJ, Liu P, Pan X, Williams AM, Iczkowski KA, Gallagher ST, Bishop K, Regner KR, Liu Y, Liang M. Tissue-Specific MicroRNA Expression Patterns in Four Types of Kidney Disease. Journal of the American Society of Nephrology : JASN. 2017;28(10):2985-92. doi: 10.1681/ASN.2016121280. PubMed PMID: 28663230; PMCID: PMC5619963.
258. Hanna J, Hossain GS, Kocerha J. The Potential for microRNA Therapeutics and Clinical Research. Front Genet. 2019;10:478. Epub 2019/06/04. doi: 10.3389/fgene.2019.00478. PubMed PMID: 31156715; PMCID: PMC6532434.
259. Meijer L, Skaltsounis AL, Magiatis P, Polychronopoulos P, Knockaert M, Leost M, Ryan XP, Vonica CA, Brivanlou A, Dajani R, Crovace C, Tarricone C, Musacchio A, Roe SM, Pearl L, Greengard P. GSK-3-selective inhibitors derived from Tyrian purple indirubins. Chem Biol. 2003;10(12):1255-66. Epub 2004/01/01. doi: 10.1016/j.chembiol.2003.11.010. PubMed PMID: 14700633.
260. Emami KH, Nguyen C, Ma H, Kim DH, Jeong KW, Eguchi M, Moon RT, Teo JL, Kim HY, Moon SH, Ha JR, Kahn M. A small molecule inhibitor of beta-catenin/CREB-binding protein transcription [corrected]. Proc Natl Acad Sci U S A. 2004;101(34):12682-7. Epub 2004/08/18. doi: 10.1073/pnas.0404875101. PubMed PMID: 15314234; PMCID: PMC515116.

261. Souza VR, Mendes E, Casaro M, Antiorio ATFB, Oliveira FA, Ferreira CM. Description of Ovariectomy Protocol in Mice. In: Guest PC, editor. Pre-Clinical Models: Techniques and Protocols. New York, NY: Springer New York; 2019. p. 303-9.
262. Karner CM, Das A, Ma Z, Self M, Chen C, Lum L, Oliver G, Carroll TJ. Canonical Wnt9b signaling balances progenitor cell expansion and differentiation during kidney development. Development. 2011;138(7):1247-57. Epub 2011/02/26. doi: 10.1242/dev.057646. PubMed PMID: 21350016; PMCID: PMC3050658.
263. Li X, Peng B, Zhu X, Wang P, Sun K, Lei X, He H, Tian Y, Mo S, Zhang R, Yang L. MiR-210-3p inhibits osteogenic differentiation and promotes adipogenic differentiation correlated with Wnt signaling in ERalpha-deficient rBMSCs. J Cell Physiol. 2019. Epub 2019/06/14. doi: 10.1002/jcp.28916. PubMed PMID: 31190372.
264. Tan Z, Shan J, Rak-Raszewska A, Vainio SJ. Embryonic Stem Cells Derived Kidney Organoids as Faithful Models to Target Programmed Nephrogenesis. Sci Rep. 2018;8(1):16618. Epub 2018/11/11. doi: 10.1038/s41598-018-34995-3. PubMed PMID: 30413738; PMCID: PMC6226521.
265. Morizane R, Bonventre JV. Kidney Organoids: A Translational Journey. Trends Mol Med. 2017;23(3):246-63. Epub 2017/02/12. doi: 10.1016/j.molmed.2017.01.001. PubMed PMID: 28188103; PMCID: PMC5442988.
266. Bao Q, Jia H, A R, Cao Z, Zhang Y. MiR-210 inhibits hypoxia-induced apoptosis of smooth muscle cells via targeting MEF2C. Int J Clin Exp Pathol. 2019;12(5):1846-58. Epub 2020/01/15. PubMed PMID: 31934008; PMCID: PMC6947104.
267. Diao H, Liu B, Shi Y, Song C, Guo Z, Liu N, Song X, Lu Y, Lin X, Li Z. MicroRNA-210 alleviates oxidative stress-associated cardiomyocyte apoptosis by regulating BNIP3. Biosci Biotechnol Biochem. 2017:1-9. doi: 10.1080/09168451.2017.1343118.
268. Luan Y, Zhang X, Zhang Y, Dong Y. MicroRNA-210 Protects PC-12 Cells Against Hypoxia-Induced Injury by Targeting BNIP3. Front Cell Neurosci. 2017;11:285. doi: 10.3389/fncel.2017.00285. PubMed PMID: 29018330; PMCID: PMC5614931.
269. Zaccagnini G, Maimone B, Fuschi P, Maselli D, Spinetti G, Gaetano C, Martelli F. Overexpression of miR-210 and its significance in ischemic tissue damage. Sci Rep. 2017;7(1):9563. doi: 10.1038/s41598-017-09763-4. PubMed PMID: 28842599; PMCID: PMC5573334.